

**SAND MOBILITY IN A RIFFLE-POOL SECTION OF A REGULATED GRAVEL BED  
RIVER: A CASE STUDY OF A SALMON SPAWNING REACH OF THE SAN  
JOAQUIN RIVER, CALIFORNIA**

A Thesis submitted to the faculty of  
San Francisco State University  
In partial fulfillment of  
the requirements for  
the Degree

Master of Science

In

Geoscience

by

Trent Michael Sherman

San Francisco, California

May 2024

Copyright by  
Trent Michael Sherman  
2024

## Certification of Approval

I certify that I have read SAND MOBILITY IN A RIFFLE-POOL SECTION OF A REGULATED GRAVEL BED RIVER: A CASE STUDY OF A SALMON SPAWNING REACH OF THE SAN JOAQUIN RIVER, CALIFORNIA by Trent Michael Sherman, and that in my opinion this work meets the criteria for approving a thesis submitted in partial fulfillment of the requirement for the degree Master of Science in Geoscience at San Francisco State University.

---

Dr. Erin Bray, Ph.D.  
Assistant Professor,  
Thesis Committee Chair

---

Yadira Ibarra, Ph.D.  
Associate Professor

---

Matthew Meyers, Ph.D.  
Researcher

## Abstract

The San Joaquin River extends almost 400 miles. It begins in the Sierra Nevada mountain range, flows through the low-land Central Valley, and drains into the San Francisco Bay. The San Joaquin River has a tortuous history of channel modifications, including in-channel and floodplain gravel mining, hydroelectric power operations, and water resources related diversions and dams. In 1942, Friant Dam was constructed near Fresno, California, by the U.S. Bureau of Reclamation. Friant Dam provided operators the ability to regulate flows in the San Joaquin River to provide societal benefits such as flood control, drought resilience, and recreation; however, it also altered the river's hydrologic regime, sediment conveyance, and ability to support the riverine ecosystem that existed before the dam. These changes, in part with other passage barriers downstream, resulted in the extirpation of Chinook salmon within the low-land gravel bedded reach. A lawsuit was settled in 2006 that created the San Joaquin River Restoration Program and required federal and state agencies to reintroduce a self-sustaining spring-run Chinook salmon population between Friant Dam and the Merced River confluence. That mission is plagued by significant challenges, such as the sediment conveyance barrier imposed by Friant Dam between the upper watershed and lowland reaches. Additionally, the current salmon spawning reach contains an abundance of sand that inhibits salmon egg incubation and fry emergence. The source of this sand is unknown, and it is not clear if the sand content is changing with time. These characteristics of the San Joaquin River provide ample opportunity for researching morphological and sediment transport processes.

This thesis encompasses three chapters that describe how sand (defined herein as sediment smaller than or equal to 2 mm) moves through California's San Joaquin River within a nine-mile study reach directly downstream Friant Dam. Chapter 1 introduces the problem statement and field area, states my research question, then describes methods, results, and a discussion of bedload sampling within the mainstem San Joaquin River at flows ranging between 220 and 6,900 cfs. Chapter two discusses bedload sampling in the ephemeral Cottonwood Creek, the upstream-most tributary downstream of Friant Dam, marking what is believed to be the upstream-most sediment source in the reach. The sand supplied to the mainstem San Joaquin River from a large storm in March 2023 is estimated and compared to the mainstem bedload transport rates discussed in chapter 1. This provides a basis to investigate if the sand is stored within or transported through the study reach. Chapter 3 describes in-channel sand presence and extent within the study reach and tracks the erosion of a bank at Ledger Island. Surficial sand storage volumes are estimated for fall of 2021, 2022, and 2023, which mark the baseline in a low water year, after several months of approximately bankfull flow releases (up to 1,800 cfs), and after several months of flood flow releases (up to ~10,400 cfs), respectively. Chapter 3 then ties each of the chapters together by providing a discussion and my conclusions on the bedload transport of sand through this river in three consecutive years of low flows, moderate flows, and high flows.

Bedload transport within the study reach varies spatially and with stream discharge. Wadable low flows produced negligible sand transport when measured with a Helley-Smith bedload sampler. Bankfull flows occur at approximately 1,500 cfs in this reach (2-year recurrence) and were measured for bedload transport at two sites in the reach (Ledger Island, 4.7 miles downstream of Friant Dam and Owl Hollow, 9 miles downstream of Friant Dam) when

Friant Dam released two pulse flows of 1,500 cfs in February of 2022. Bedload transport rates were measured with a cataraft-based sampling platform and Tuttle River - 2 bedload sampler, allowing the cataraft to collect equal-interval bedload samples laterally across the channel. Moderate flows transported trace amounts of sand in bedload, along with large amounts of organic debris. Sand transport at moderate flows is likely discontinuous throughout the reach due to low shear stress zones where the sand deposits on the bed, typically in pools. Bedload transport rates were measured at the same sites with the same methods at high flows (about 6-to-8-year-recurrence), which confirmed that a 6,000 to 7,000 cfs flow release is capable of mobilizing the size ranges of sand that we measured in storage on the bed.

Sand bedload transport rates at Ledger Island at 6,430 cfs ranged between 1.3 and 8.7 tons/day, with a mean of 5.1 tons/day and trace amounts of gravel present with a maximum grain size of 40 mm. At flows of 6,900 cfs at Owl Hollow, sand bedload transport rates ranged between 32.7 and 95.6 tons/day, with a mean of 64.4 tons/day. The largest particle found in transport was 21 mm in diameter through its intermediate axis. Bedload transport rates at these sites show that more sand is exiting the study reach than passing through the halfway point, thus suggesting increasing sediment supply downstream. Additionally, an existing HEC-RAS model predicts that bed shear stress is higher at Owl Hollow than at Ledger Island, such that it has the capacity to transport more sediment.

Bedload transport sampling on ephemeral Cottonwood Creek during a storm confirmed that the creek is a source of sand to the San Joaquin River and showed that it delivers sand (and trace amounts of gravel) at the top of the study reach during infrequent flows as low as 160 cfs. We estimate that Cottonwood Creek supplied about 50 tons of sand to the San Joaquin River during a storm in March 2023, and about 450 tons throughout the study period. Average sand bedload transport rate was 20.1 tons/day with a maximum of 59 tons/day and minimum of 0.1 tons/day.

Between 2021 and 2023, a bank at Ledger Island eroded an average of 13.9 feet laterally and a volume of about 2,700 cubic yards (about 4,000 tons). Because more sediment eroded from the bank than was measured in storage in the pool below, it is evident that sand is being mobilized downstream.

The sand supplied by Cottonwood Creek, the eroding bank at Ledger Island, and other minor near-channel sediment sources was flushed through the study reach with a 37 percent decrease in sand content between 2021 and 2023. I estimate that in-channel surficial sand content was as high as 170,000 tons in August 2021, and then decreased after an extended bankfull flow event in 2022 and a 12.5-year recurrence high flow (10,400 cfs) to 107,000 tons in August 2023. The results of this thesis indicate from multiple methods that in-channel sand storage within the study reach is decreasing, despite episodic sand contributions from tributaries and near-channel sources.

## Acknowledgements

This thesis could not have been completed without countless hours of help and support from so many wonderful people in my life. This project showed me that it “takes a village” to cultivate great things. Starting is the hardest part, so I’ll just jump right in.

My family is the first and foremost reason that I’ve been able to accomplish great things. They taught me to aim high, and they are my cheer leaders when I struggle. They give me a solid foundation to stem from. They are also remarkably patient and supportive of me with my wacky interests. Mom, Dad, Kaita, Alex, Gramma, and Lacey – where would I be without you? Not here. Dad – the best part of this entire thing was building the cataraft with you. I’ll hold those memories forever.

My friends are wonderful humans. They humor me when I rant about rocks and rivers and get frustrated that these things don’t bother them. “So, you just wake up and go about your lives without worrying about this stuff? Really?” Yes, apparently so. Thank you all for listening to my [spectacular] field lectures. I’ve also dragged you to the field on multiple occasions to help me collect data. It ain’t easy work, but you don’t know how much I appreciated your company and help. Thank you Steve Barton, Charity David, Joseph Haas, Lacey, Evver Gonzales, Jennifer and Anthony Moralez, Chad and Christa Collins, Honey and Joey Krueger, and Mila.

I would not have fallen in love with rivers in the same way if I hadn’t met Matt Meyers. Thank you for bringing me into your river issues at such a young academic age, and never failing to stoke my fire on river processes. Our conversations have been islands of paradise amid endless seas of bureaucracy. Thank you for challenging me, advocating for me, and being my friend as well as a mentor.

Erin Bray – thank you for guiding me through this difficult process that we call “research.” You’ve opened my eyes to the power of science and have taught me how to use it as a tool. Thank you for being patient with me and slowing me down when I get too ambitious. I did not consider myself a scientist before I met you.

Scott McBain and Smokey Pittman – you two welcomed me into the world of geomorphology with open arms and I cannot thank you enough for that. I tend to find strange hobbies, and this one is just as niche as my others. Thank you for taking my phone calls when you had better things to do, and thank you for your insights and guidance when I had no clue what to do next. I think I still owe you a beer... probably a case by now!

Mila – you’re the best research assistant I could ever ask for. Thank you for staying up late at night with me and encouraging me to get outside and watch you climb trees. You’re my cat, you’re also my friend.

Thank you also to Tom Johnson and the U.S. Bureau of Reclamation for your help with flow release scheduling. I can only hope that my research and results help you in a similar magnitude. White Water Voyages – thank you for loaning me river equipment to get out there and make measurements! This is getting at the heart of river science, and you helped make it possible. Thank you also to Ed Sullivan and Shaun Simon at NV5 for letting me use your sieve lab; this was an integral piece of the analysis at a time when I had no other options.

Lastly, to my partner, adventure buddy, and my love. How do I thank you enough, Lacey? You've been a part of every step along the way. You're my family, my friend, my [ridiculously good looking] field assistant, and ardent critic. Nothing gets past you, and I admire you endlessly. Thank you for being my rock, and so much more.

I have no doubt that there are others I'm forgetting to list, and thank you if you are one of these people. I should buy you a beer sometime.

## Table of Contents

<b>List of Tables</b>	<b>x</b>
<b>List of Figures</b>	<b>xi</b>
<b>Chapter 1: Mainstem San Joaquin River Bedload Sampling</b>	<b>1</b>
Introduction	1
Research Question	3
Methods	4
Site Selection	4
Handheld Helley-Smith Bedload Transport Measurement Method	5
Handheld Helley-Smith Sample Processing and Analysis	6
Tutle River – 2 Bedload Collection Method	7
Tutle River – 2 bedload sample processing and analysis	7
Water Surface Slope	8
Calculated Shear Stress from HEC-RAS	8
Results	10
Bedload at Low Flows	10
Bedload at Moderate Flows	11
Bedload at High Flows	11
HEC-RAS Shear Stress and Meyer-Peter Muller Bedload Transport Rates	12
Discussion	12
Bedload at Low Flows	12
Bedload at Moderate Flows	13
Bedload at High Flows	15
Bedload Flux Through the Study Reach	17
<b>Chapter 2: Cottonwood Creek Bedload Sampling</b>	<b>19</b>
Introduction	19
Methods	19
TR-2 Bedload Sampling	19
Stream Discharge Measurements	20
Estimating Total Sand Supply	20
Bed Scour Stakes	20
Results	21
Discussion	22
Bedload Flux Through the Study Reach	23
<b>Chapter 3: Facies Mapping and Bank Erosion</b>	<b>24</b>
Introduction	24
Methods	24
Facies Mapping	24
In-channel Sand Volume	25
Sand Grab Samples	26
Bank Erosion	26

<b>Results</b>	<b>27</b>
Cottonwood Creek confluence to Friant Cove	27
Friant Cove	28
North Fork Bridge to Lower Lost Lake	29
In-channel Gravel Pits	29
Ledger Island and Sumner Peck Ranch	30
Eroding Bank	30
Ledger Island to Riffle 40	31
Riffle 40 to Riffle 38	32
Little Dry Creek Confluence	32
Donaghy/Rank Island	33
Vulcan Chute	33
Owl Hollow	34
Total In-channel Sand Storage	34
Grain Size Distribution	35
<b>Discussion</b>	<b>35</b>
Bedload Flux Through the Study Reach	35
<b>Conclusions</b>	<b>36</b>
<b>Figures and Tables</b>	<b>37</b>
<b>Appendices</b>	<b>77</b>
<b>Appendix A: Flood Frequency Analysis</b>	<b>78</b>

## List of Tables

<b>Table A- 1: Flow recurrence intervals as calculated from peak flow data from 2000 to 2023 at USGS stream gage 11251000.</b>	<b>110</b>
	<b>xiv</b>
<b>Table 1. Significant features within the study reach and their distance downstream of Friant Dam.</b>	<b>72</b>
<b>Table 2. Summary of bedload transport rates sampled at Owl Hollow, Ledger Island, and Cottonwood Creek between March 13 and 17, 2023.</b>	<b>73</b>
<b>Table 3. Ledger Island modeled values for channel shear stress and associated Meyer-Peter Muller bedload transport rates. Observed bedload transport rates are provided for comparison.</b>	<b>74</b>
<b>Table 4. Owl Hollow modeled channel shear stress and associated Meyer-Peter Muller bedload transport rates. Observed bedload transport rates are provided for comparison.</b>	<b>75</b>
<b>Table 5. Calculated in-channel sand storage along 9-mile study reach between Friant Dam and Owl Hollow. The top section presents values in tons and the bottom section presents values in cubic yards. Values correspond with Figure 19.</b>	<b>76</b>

## List of Figures

- Figure 1. Map of the 9-mile study reach of the San Joaquin River between Friant Dam and Owl Hollow, in Fresno and Madera counties, near the city of Friant California. Blue markers indicate the number of miles downstream from Friant Dam. The inset map shows the San Joaquin River’s westward flow to the Pacific Ocean and its highlighted drainage area. The star marks the approximate study reach near Fresno, California. 38**
- Figure 2. Hydrograph of the San Joaquin River at USGS stream gauge 11251000 San Joaquin River below Friant (SJF) showing hydrology during the study period. The blue boxes indicate the approximate time of bed sand storage mapping. The pink box shows the approximate time of increased flows for San Joaquin River Exchange Contractor deliveries, and the red circles show the approximate timing of bedload transport sampling events at bankfull (moderate flows) and high flow events. 39**
- Figure 3. Helley-Smith bedload sampling at low flows within sandy gravel substrate at the downstream Owl Hollow riffle. The cobble was placed on top to ensure that the sampler entrance remained flush on the bottom plate. River flow is from right to left, and sand is present on the bed. 40**
- Figure 4. Low-flow bedload transport rates measured with Helley-Smith bedload sampler, organized by downstream location. 41**
- Figure 5. Mean low-flow bedload transport rates, organized by downstream location. 42**
- Figure 6. Hydrograph from California Data Exchange Center stream gage San Joaquin River Below Friant (SJF), illustrating two pulse flow releases from Friant Dam. The red squares indicate the approximate times when bedload samples were collected. Because this stream gage is several miles upstream of the sample locations, peak flows during sampling were lower than shown on the hydrograph. Acoustic Doppler Channel Profiler data confirmed that river discharge was about 1,500 cfs during sampling. 43**
- Figure 7. Large amounts of organic debris and trace amounts of sand were collected in bedload transport sampling at 1,500 cfs during the pulse flows in February 2022. 44**
- Figure 8. Trace amounts of sand were collected in bedload transport sampling during the pulse flows of 1,500 cfs in February 2022. The mesh size of the TR-2 sampler is 0.5 mm. 45**
- Figure 9. Stream flow hydrograph and associated timing of bedload transport sampling during high flows of spring 2023. 46**
- Figure 10. Calculated bedload transport rates from samples collected by San Francisco State University in March 2023. The majority of sediment in transport at flows of 6,400 cfs and 6,900 cfs at Ledger Island and Owl Hollow, respectively, is comprised of sand sized**

particles. Gravel was measured in transport; however, it made up a small fraction of the bedload samples. Bedload transport rates were about an order of magnitude higher at Owl Hollow than at Ledger Island. 47

Figure 11. Box and whisker plot comparing grain sizes between bedload samples (blue boxes) and bed material (brown boxes). Samples were collected from Cottonwood Creek, the mainstem San Joaquin river at Ledger Island and Owl Hollow, the eroding bank at Ledger Island, and the mouth of Little Dry Creek. 48

Figure 12. Bedload transport rates measured on the San Joaquin River from multiple studies at different locations. All measurements were conducted within my study reach except for U.S. Geological Survey which were about 12 miles downstream of Friant Dam. The top panel shows that the ranges of bedload transport rates measured in my thesis are within the rates measured by other studies. The bottom panel shows modeled estimates of bed shear stress at corresponding bedload measurement sites. SFSU = San Francisco State University. 49

Figure 13. HEC-RAS model transect locations near the bedload sampling locations at Ledger Island. The model transect locations in the aerial image correspond with the predicted shear stresses (color corresponding) across a range of flows shown in the inset plot. 50

Figure 14. HEC-RAS model transect locations near the bedload sampling locations at Owl Hollow. The model transect locations in the aerial image correspond with the predicted shear stresses (color corresponding) across a range of flows shown in the inset plot. 51

Figure 15. Bedload rating curve at Ledger Island. The green data, trendline, and function represent data collected by Graham Mathews Associates in 2011, and the pink data represent bedload transport measurements collected by SFSU and McBain Associates at Ledger Island during high flows in 2023. The brown data, trendline, and function are representative of the average bedload transport rate at each corresponding stream flow rate. 52

Figure 16. Subsurface sand content shown as a percentage of substrate bulk composition in riffles downstream of Friant Dam, data from (Resources 2010). 53

Figure 17. Cottonwood Creek sedigraph showing the measured bedload transport rates and the estimated continuous transport rates during the sampling period in spring 2023. 54

Figure 18. Index map showing the locations of mapping areas with significant in-channel sand storage. 55

Figure 19. Study period changes of in-channel sand storage content by site and date. The three years of data presented below represent dry and wet year conditions. The top panel presents sand storage in tons and the bottom panel presents sand storage in cubic yards.

<b>The values correspond with Table 5. Vertical dashed lines correspond to locations of interest in my study reach.</b>	<b>56</b>
<b>Figure 20. Sand storage at the confluence of Cottonwood Creek and the San Joaquin River, approximately 1,000 feet downstream of Friant Dam.</b>	<b>58</b>
<b>Figure 21. Bed substrate of the San Joaquin River deep channel downstream of the Cottonwood Creek confluence. Top image shows trace amounts of sand present in 2021. Bottom image shows no sand present in 2023.</b>	<b>59</b>
<b>Figure 22. Sand storage at the Friant Cove area.</b>	<b>60</b>
<b>Figure 23. Sand storage at the Friant Riffle.</b>	<b>61</b>
<b>Figure 24. Sand storage between Lost Lake Park and Ledger Island.</b>	<b>62</b>
<b>Figure 25. Sand storage at the south end of Ledger Island.</b>	<b>63</b>
<b>Figure 26. Eroding bank at Ledger Island. Top left image shows the bank height relative to the author (6 feet/1.8 meters); the paddle is 5 feet (1.5 meters) long. The top right image shows a fissured block of bank material in a slow calving process; the rod is 2 meters long, graduated in 0.1 meter intervals. The bottom image shows sluff at the base of the eroding bank, pipes (1.5 inch/3.8 cm outside diameter) emanating from the vertical bank face, and multicolored strata indicating the individual lifts this bank was constructed in.</b>	<b>64</b>
<b>Figure 27. Bank edge delineations showing erosion propagation at Ledger Island. The top image shows conditions in 2011 during flood flows and projections of future bank edges in 2021 and 2023. The bottom image shows conditions in 2023 and the previous extents of the bank edge. The bank edge is defined here as the crest at the top of the vertical face. Erosion is propagating toward the abandoned mine pit.</b>	<b>65</b>
<b>Figure 28. Sand storage between Ledger Island and Riffle 40.</b>	<b>66</b>
<b>Figure 29. Sand storage between Riffle 40 and Riffle 38.</b>	<b>67</b>
<b>Figure 30. Sand storage near the confluence of Little Dry Creek and the San Joaquin River.</b>	<b>68</b>
<b>Figure 31. Sand storage at Rank Island near a large mansion.</b>	<b>69</b>
<b>Figure 32. Sand storage at a narrow chute near the Vulcan property and at Owl Hollow.</b>	<b>70</b>
<b>Figure 33. Cumulative grain size distributions of grab samples collected in 2021 and 2023.</b>	<b>71</b>

## **List of Appendices**

**Figure A- 1: annual peak flows on San Joaquin River as measured at the USGS stream gauge 11251000 for the entire period of record (1908 – 2023, count = 114 years).**

**79**

**Figure A- 2: Flood frequency analysis plot using post-dam peak flow data from 1950 to 2024 at USGS stream gauge 11251000 San Joaquin River below Friant. The horizontal lines show the flows that were sampled for bedload transport rates by the Bray Rivers Lab at San Francisco State University. The statistics and figure were generated using USGS PeakFQ software. 80**

**Table A- 1: Flood frequency analysis results at San Joaquin River Below Friant stream gauge (11251000) using USGS PeakFQ software package for years 1950 to 2024. These results correspond to actual annual peak flows measured and do not represent the Log-Pearson Type-III distribution fitted curve in Figure A- 2. The Estimated Moments Analysis (EMA) method was used. Study period years are highlighted in yellow. 83**

## Chapter 1: Mainstem San Joaquin River Bedload Sampling

### Introduction

Rivers convey water and sediment. Dams benefit society by regulating the flow of water in rivers, but they also affect sediment transport regimes, which inevitably will impact a river's morphology by changing the channel's vertical gradient distribution and horizontal expressions. This has occurred in several California rivers (Willis and Griggs 2003), and the San Joaquin River is no exception. The San Joaquin River extends almost 400 miles from the high Sierra Nevada mountain range, through the low-land Central Valley, and drains into the San Francisco Bay. The construction of Friant Dam in 1940, in addition to historic in-channel gravel mining, altered the San Joaquin River's hydrologic and sediment regimes, with an unintended consequence of eliminating Chinook salmon within 150 miles downstream. A lawsuit was settled in 2006 that created the San Joaquin River Restoration Program (SJRRP) and required federal and state agencies to reintroduce a self-sustaining spring-run Chinook salmon population between Friant Dam and the Merced River confluence. At the time of settlement, the river conditions needed for self-sustaining salmon populations were unknown and current river conditions were not well characterized. The requirements of the Settlement created a unique purpose for investigating sediment transport within a dam regulated, lowland, gravel bedded reach of the San Joaquin River.

Salmonid spawning habitat can be characterized in part by the streambed sediment, or substrate, that comprises it (Bjornn and Reiser 1991). Suitable spawning substrate is usually a combination of pebbles and gravel that contain low concentrations of sand and smaller grains that would otherwise infiltrate the gravel framework (Bjornn 1969). The presence of sand in the streambed is controlled by the available sand supply and the river's hydraulic power to transport it. Sand accumulates in areas where its supply is greater than the river's ability to remove it, typically in low-energy pools or backwater areas. Excessive sand content within the riverbed has been shown to inhibit salmon spawning production on the San Joaquin River (Nelson and Reed 2011, Resources 2019). Spring-run Chinook salmon spawning is now limited to riffles within the upper seven miles downstream of Friant Dam; this area is known as the spring-run spawning reach and spans between river miles 260.6 and 267.6 (between Friant Dam and the confluence of Little Dry Creek) (Program 2017).

It is well documented that rivers with dams and diversions lose their balance of fine sediment input and transport capacity, leading to fine sediment accumulation that can impact riverine biota (Milhous (1994). The sediment imbalance can become pronounced during times of high tributary flows and low mainstem flows, resulting in sediment deposition near their confluences. River managers have proposed solutions that include flushing flows, or brief periods of planned elevated dam releases with the intent of transporting sediment and performing other geomorphic work within the river corridor. Flushing flows require an understanding of the sediment yield and a hydraulic analysis within a specified reach (Milhous 1994). Furthermore, the objectives of the flushing flow must be defined and evaluated before designing flushing flow magnitude, duration, and frequency. This introduces the challenge of conflicting objectives, such

that a single flushing flow cannot satisfy all channel and sediment maintenance processes (Kondolf and Wilcock 1996). Additionally, selective sediment transport of specific grain size fractions are controlled by not only hydraulic conditions, but also the gradation of grain sizes present on the bed (Curran and Wilcock 2005). Whereas many river management actions target the removal of sand and transport of gravel with flushing flows (Milhous 1994, Kondolf and Wilcock 1996), Curran and Wilcock (2005) found that the rate of gravel transport increases with sand content in the bed. Overall, the presence of sand creates complex interactions between bed stability and ecological integrity, but neither can be improved without a sound understanding of the sediment balance within a given reach.

Multiple groups have measured sand mobility downstream of Friant Dam (Associates 2011, Tetra Tech 2012, Reclamation 2014, Marinuea, Wright and Minear 2015, Tetra Tech 2018) by quantifying sand inputs, transport, or storage between different points. Because of complications with equipment, spatial extent of sample sites, available flow conditions, or other data gaps, they each concluded more measurements were needed to understand sand mobility across a broader range of conditions. Similarly, a sediment budget (an accounting system of sediment flux between two points) was produced by the U.S. Bureau of Reclamation for river miles 267.6 – 182.0 for the water years 2010 through 2012 (Reclamation 2014). While this work contributed to the knowledge of sediment mobility across several reaches of the San Joaquin River, it was constructed at a coarse spatial resolution with limited detail of the spring-run Chinook spawning reach. It is evident that the sand budget within this reach is not completely closed and that knowledge gaps remain (Reclamation 2014, Tetra Tech 2018). To manage the river for salmon production, the sand content and mobility within the spawning reach needs to be better understood.

Previous investigations on the San Joaquin River show that in-channel sand has a few potential sources that include eroding banks, tributaries, gravel-mining pit waste, and sediment remnant from Friant Dam construction (Tetra Tech 2012, Tetra Tech 2018). In one study of the spring-run spawning reach, sand volume was measured at six locations in 2010 during moderate flows of 1200 cubic feet per second (cfs) (Tetra Tech 2012). At this flow, sand was transported across riffles in bedload, but change in sand storage volumes were not reported over a range of flows and few repeat surveys have been conducted since. There is only one location within the spring-run spawning reach where sand from localized erosion of the riverbank was shown to be a significant contributor to the sand budget (Tetra Tech 2018). That bank, located at river mile 262.1, has an average annual sand contribution that represents 4% of the total sand storage 19 miles downstream (Tetra Tech 2018). While these studies account for sand contributions from near and within the river, they do not directly account for sand contribution from other areas of the watershed.

The mainstem San Joaquin River has two tributaries within the spring-run spawning reach, Cottonwood Creek (river mile 267.4) and Little Dry Creek (river mile 260.6) (Figure 1). Both tributaries are potential sand sources to the reach. Sediment transport was measured in these creeks by the US Geological Survey during an eight-year study to collect suspended sediment load (Marinuea, Wright and Lopez 2016). They reported that low rates of bedload transport likely occurred on Cottonwood Creek of particles smaller than gravel, but did not provide a quantitative estimate of sand bedload transport rates. They also reported that Little Dry

Creek showed evidence of sand transport during that period, however, the channel is modified from mining activities that could disrupt the flow of water and sediment through that portion of the creek. Sediment transport within these creeks occur only in episodic events because they are intermittent streams that are dry most of the year. Furthermore, (Haught, Marinuea et al. 2023) investigated suspended sediment transport rates in these tributaries between 2011 and 2019, which estimated annual sediment loads up to  $2.68 \times 10^3$  tons in Little Dry Creek and  $1.98 \times 10^3$  tons in Cottonwood Creek. Additionally, (Cain 1997) estimated the total annual sediment supply from Cottonwood Creek of 740 tons and Little Dry Creek of 4,500 tons (with 10 percent of those values assumed to be gravel and larger sediment). Each study noted that these values do not reflect sediment contribution to the mainstem San Joaquin River, but instead reflect transport values upstream of hydraulic features that might capture large (and unquantified) amounts of that sediment. While these studies do not contribute direct information about sand mobility within or supply to the San Joaquin River, they provide sand transport values that can be assumed as maximum quantities supplied from the tributaries.

Several questions remain to be answered to fully describe sand storage and mobility within the spring-run spawning reach, some of which include: 1) how much of the tributary sand reaches the San Joaquin River?, 2) how is sand transported and stored in the San Joaquin River at low, moderate, and high flows? and 3) is sand content within the Spring-run spawning reach depleting, increasing, or stable? The answers will inform how much sand is moving into the system compared to how much is leaving the system and will inform management actions regarding salmon spawning habitat. Resolving all of these questions is beyond the scope of this thesis because it is depended on monitoring across a range of water year types whose schedule is uncertain and as a result would require investigation over many more years; however, each one can be assessed independently under limited conditions.

## **Research Question**

How is sand transported and stored within a 9-mile reach of the San Joaquin River (Figure 1), directly downstream of Friant dam at flows ranging between 220 and 10,000 cfs? The goal of this thesis is to answer the question above by describing the changes in sand presence and extent, storage volume, and transport rates before, after, and during significant flow changes within my study period between April 2021 through November 2023 (Figure 2). I refer to my study area as the “study reach” of the San Joaquin River between Friant Dam and Owl Hollow (Figure 1).

I approached my research question by distilling the study reach into three primary perspectives. Chapters 1 and 2 describe my investigations of sand transport in bedload. In these chapters, I use pronouns “we,” and “our” to acknowledge the contributions from McBain Associates, who helped me perform these investigations. Chapter 3 describes my investigation of sand presence on the riverbed through facies mapping, while also investigating the volume of sand stored throughout the study reach. Each chapter builds upon the previous to tell the story of sand transport within the dam-regulated reach of this lowland river.

In this thesis, I classified the upper size limit of sand as 2 millimeters (mm) in diameter for consistency with other studies on the San Joaquin River. I chose not to investigate how sand is transported in suspended load due to the complexity of sample processing. I limited the scope

of this study to surficial sand content and did not investigate subsurface sand (interstitial sand content between gravel and cobbles that form the framework of the riverbed). Similarly, my considerations of sand sources are limited to in-channel, near channel, and tributaries in modern times and do not consider lithologic or mineralogic origin of the sand. Within these limitations, the three perspectives of bedload transport rate, sand presence, and sand volume, offered methods that are robust, within my skillset and budget, and were appropriate to answer my research question for the flow conditions that I expected to encounter.

## **Methods**

A timeline of the study period is presented as a hydrograph of the San Joaquin River in Figure 2. The hydrograph shows the dates when measurements were collected to give the reader a sense of the hydrologic conditions present before, during, and after measurements were collected. I performed a flood frequency analysis to define the approximate recurrence interval of the flows encountered during this study. Appendix A provides the results of the flood frequency analysis, including a flood frequency plot and a recurrence interval table containing some approximate key flow rates. The analysis used annual peak flows at stream gauge San Joaquin River below Friant (SJF) between 1950 and 2024. I chose this period because it provides a long-term flow record since the construction of Friant Dam in 1942 and the formation of the SJRRP in 2006, who provides flow recommendations for the river. Results show that low flows in this study (below 600 cfs and typically wadable) are released most years, moderate flows in this study ranged between 700 and 1,800 cfs and recur about every other year, and peak high flows in this study reached the 12.5-year recurrence interval.

We measured bedload transport rate at 11 locations across flows ranging between 220 and 6,900 cfs in the mainstem San Joaquin River between November 2019 and March 2023. Samples were collected using two types of samplers, which we chose according to the flow conditions present during the time of sampling. Sampling during wadable flows below 700 cfs was performed using a handheld Helley-Smith bedload sampler, and samples from higher flows were collected using a Toutle River 2 (TR-2) bedload sampler. The site selection, sample collection, and sample processing methods are described in the following sections.

In this thesis, we classify the upper size limit of sand as 2 mm in diameter for consistency with other studies on the San Joaquin River (Associates 2011, Reclamation 2014, Tetra Tech 2018); however, we do not apply a lower size limit to sand because quantities of silt and clay were negligible in the samples collected. It is worth noting that while Resources (2010) did not specify grain types by size, a review of their data shows that they most likely classified the upper size limit of sand to be less than 6.35 mm, with particles 6.35 mm and larger classified as gravel.

### ***Site Selection***

I selected ten low flow sample sites based on the ability to wade there safely, their having a gravel bed, and their distribution throughout the nine-mile study reach. Low flow sample sites were generally at the downstream end of a pool (pool tail-out) on the upstream limb of a riffle crest, where flow is relatively shallow and swift. These areas generally lack sand at the bed

surface and were selected to prevent the sampler from vacuuming sand directly from the bed (Bunte and Abt 2009, Bunte, Swingle et al. 2019). I also expected these areas to have a high sand transport capacity compared to their sand supply, meaning that sand will be transported through that area if it is supplied to it. Sample sites satisfying these conditions are most likely to transport sand that is moving through the riffle-pool system, because it would have required that the sand be transported from a sand source upstream with potentially lower transport capacity, such as the next pool upstream.

I selected two moderate and high flow sites at Ledger Island and Owl Hollow, 4.68 and 9 miles downstream of Friant Dam, respectively. Ledger Island was chosen because Graham Matthews & Associates had performed bedload sampling there in 2011 (Associates 2011) across a range of high flows (about 4,000 – 8,000 cfs), and sampling there between moderate and high flows would provide a more complete understanding of sediment mobility through that site. Furthermore, it is upstream of two potential major sand sources: the eroding bank at the southern end of Ledger Island, and Little Dry Creek. Constraining sand transport at Ledger Island will help identify how much sand from Cottonwood Creek or the mainstem San Joaquin Riverbed transports through this reach. The sample site at Ledger Island is a straight section with a low water surface slope, is downstream of a riffle, has a gravel bed, and provides ample vehicle access and cable-way anchors.

Owl Hollow was chosen to be the downstream boundary of the study reach because it provides ample vehicle and sampling access downstream of the Ledger Island eroding bank and Little Dry Creek. Constraining sand transport here can help identify the amount of sand leaving the reach compared to the amount entering the reach and transporting through Ledger Island. Owl Hollow has a wide pool bounded by riffles and has bed substrates consisting of sand, gravel, and combinations of both. The upstream riffle shows signs of growing gravel flood deposits, indicating high transport capacity and competency upstream of the site. Owl Hollow is surrounded by abandoned historic gravel mining pits, and appears to have been altered by in-channel gravel extraction activities based on maps produced by Cain (1997).

Table 1 lists significant features and sites throughout the 9-mile study reach, and their respective number of river-miles downstream of Friant Dam.

### ***Handheld Helley-Smith Bedload Transport Measurement Method***

Low-flow samples (samples collected below 700 cfs) were collected using a Helley-Smith bedload sampler with an aperture 3-inches tall and 3-inches wide. To install the sampler on the bed, a rectangular aluminum bottom plate was secured to the bed horizontally, and the sampler was placed on top. In some cases, the bed was uneven and needed to be leveled by moving cobbles to provide a flat surface for the plate. In these cases where bed substrate was rearranged to accommodate the plate, several minutes were waited to allow the new bed surface to equilibrate before installing the sampler in an attempt to minimize the sampling of sand that would not have been in transport otherwise. To secure the sampler to the plate, it was either staked in place with rebar driven into the bed, or held in place with a heavy cobble on top of the sampler. While both techniques prevented the sampler from shifting or being pushed

downstream by current, the cobble technique was preferred to using rebar stakes because it caused less disturbance of the bed.

Sampling locations were chosen based on safe and reasonable wading access at the pool tail-out (the upstream limb of the riffle crest) and where bed substrate was not primarily sand. The bottom plate and sampler were not placed directly on a sand bed because the Helley-Smith sampler was designed to have a strong hydraulic efficiency, which can oversample sand when deployed improperly (Bunte and Abt, 2009). Sampling time intervals varied from 30 to 60 minutes, which began when the sampler was placed on the plate and able to collect bedload in an attached 0.25-millimeter (mm) mesh bag. At the end of the sampling interval, the sampler was removed from the bed, replaced with a clean mesh bag, and then replaced at a different location for another measurement. During this next measurement, the bedload sample from the previous measurement was rendered from the mesh bag, or the mesh bag was placed into a sealed plastic bag to be processed later.

To render the bedload sample from the mesh bag, a spray bottle was used to push water from the outside of the bag into the bag, which allowed sediment to collect in a bottom corner of the mesh bag. Once all bedload material collected in a corner, the mesh bag was turned inside out and flushed into the 1-gallon bag. At this point, the mesh bag was ready to be used for another measurement and the gallon bag was labeled with the date, time, sample duration, sample collection method, location, and people present, and then stored until it was processed.

### ***Handheld Helley-Smith Sample Processing and Analysis***

Bedload sample materials included organic material, trace amounts of sand, and water. The total sample mass was measured, and then vegetation was removed by hand (when possible). To separate the water from the sand, the bag contents were poured into a metal cooking pan and heated in an oven until the water evaporated. The oven was set at about 95 degrees Celsius to evaporate the water. The sample remaining in the cooking tray was then scraped out, collected, and weighed with a scale sensitive to 0.01g. This material was then returned to its original bag and stored.

Bedload samples collected in the Helley-Smith were too small to perform grain size analysis by sieving, so instead, samples were measured for total mass and described by their soil characteristics. A bedload unit transport rate (such that the “unit” is the river’s bedload load transport rate normalized to 1-meter width of the channel) was calculated to estimate the amount of bedload passing the sample location in grams per meter per hour with the equation

$$Q_{ub} = \frac{M}{0.0762} \cdot \frac{60}{T} \quad (1)$$

where:

$Q_{ub}$  = unit bedload transport (grams/meter/hour)

$M$  = sample mass (grams)

$T$  = sample time interval

0.0762 = conversion factor for 3 inches to 1 meter

60 = conversion factor to normalize the sample time interval to hours.

This transport rate is useful when comparing the amount of sand moving in bedload to the width of a typical Chinook salmon redd. This value was then extrapolated to estimate the amount of bedload moving across the entire river channel at the sample location in tons/day (tons/day), using the equation

$$Q_b = Q_{ub} \cdot 0.00000147 \cdot W \cdot 24 \quad (2)$$

where:

$Q_b$  = bedload transport rate (tons/day)

$Q_{ub}$  = unit bedload transport rate (grams/meter/hour)

0.00000147 = conversion factor for grams to tons

$W$  = river width (meters)

24 = conversion factor to normalize the sample time interval to days

### ***Tuttle River – 2 Bedload Collection Method***

Bedload was collected from a cataraft-based sampling platform at Ledger Island and Owl Hollow during moderate and high flows. The cataraft was deployed at both sites during moderate flows of 1,500 cfs, and during flood releases at 6,430 and 6,900 cfs at Ledger Island and Owl Hollow, respectively. The cataraft was attached to a cableway tensioned perpendicular to flow, allowing the cataraft to traverse laterally across the river. A TR-2 bedload sampler was lowered from the cataraft to the bed, collecting samples within a 0.5mm mesh bag. The TR-2 sampler has a 6 x 12-inch entrance nozzle and a low expansion ratio, providing low hydraulic efficiency to minimize the suction effect and over-sampling of sand.

Standard bedload sampling methods were used (Edwards and Glysson 1999), such that each sample consists of a single “pass” across the channel with several TR-2 deployments at even spacing intervals across the channel and specified down-times.

### ***Tuttle River – 2 bedload sample processing and analysis***

Bedload at moderate and high flows were sampled using the TR-2 sampler with an entrance aperture 12-inches wide and 6-inches tall, and a collection bag with 0.5 mm mesh. Samples were dried, weighed, and sieved to determine the grain size distribution following California Test 202 (Transportation 2010) methods. Large samples were run through a sample splitter prior to sieving to prevent overloading sieves and biasing the size distribution. Sieve size classes included 12.5, 9.5, 4.75, 2.36, 1.18, 0.600, 0.300, 0.150, and 0.075 mm. Grain size statistics were calculated by interpolating the cumulative percent passing percentiles between the relevant sieves. Bedload transport rate (tons/day) was calculated for each sample using Edwards and Glysson (1999) equation

$$Q_b = K \cdot \left( \frac{W_T}{t_T} \right) \cdot M_T \quad (3)$$

where:

$Q_b$  = bedload transport rate (tons/day)

$K$  = conversion factor (0.095 for a 12-inch sampler)

$W_T$  = sampled width of the river (feet)

$t_T$  = total time the sampler was on the bed (seconds)

$M_T$  = sample mass (grams)

Note that bedload transport rates for size fractions smaller than the mesh size of the bedload sampler (0.5 mm) should be considered an estimate because the sampler is not designed to capture them; it is likely that size fraction is underrepresented.

### ***Water Surface Slope***

The slope of the water surface was measured at Owl Hollow and Ledger Island when conditions and time constraints allowed. The slope was measured by surveying a distance of approximately 150 feet upstream and downstream of the transect locations, using a TopCon autolevel and a telescoping survey rod. The survey was conducted according to methods specified by Harrelson, Rawlins and Potyondy (1994).

### ***Calculated Shear Stress from HEC-RAS***

Sediment is mobilized in rivers by the force of flowing water acting against the bed and banks. The flow force is represented by the stress acting at the boundary between the water and sediment, called the boundary shear stress, and is defined as the flow force acting per unit area of stream bed (Wilcock, Pitlick and Cui 2009). Shear stress cannot be measured directly. It must be estimated from channel geometry, channel roughness, and hydraulics. Nonetheless, shear stress is difficult to estimate in alluvial channels because there is great variation across and along the bed (as compared to engineered concrete channels). Having an understanding of shear stress at various stream discharges, along with the minimum shear stress required to mobilize sediment (critical shear stress), can help produce estimates of bedload transport rates when accompanied with an empirically-based sediment transport equation. I ran this analysis to see how our observed bedload transport rates compare to a model's estimate.

To estimate shear stress at my bedload sampling sites, I acquired a surface water flow model from California's Department of Water Resources, which had previously been calibrated across a range of flows between 100 and 8,000 cfs. The model platform is a free open-source software designed by the Army Corps of Engineers to perform one-dimensional steady flow calculations, called Hydraulic Engineering Center-River Analysis System (HEC-RAS). Because the model was calibrated across a range of flows that encompass my bedload measurements, I felt that it was reasonable to use the model's flow scenarios to obtain channel shear stress values

in the vicinity of my bedload sampling sites. I used the model's calculated channel shear stress values as input for a bedload transport equation (equation 6) to estimate bedload transport rates at the flows present during my bedload sampling. However, before I could do this, I also had to estimate the critical shear stress at each site.

Critical shear stress is described by the Shields' flume derived equation (Shields 1936):

$$\tau_{cr} = \tau_{cr}^* \times g(\rho_s - \rho_w)d \quad (4)$$

where:

$\tau_{cr}$  = dimensional critical shear stress,

$\tau_{cr}^*$  = dimensionless critical shear stress,

$g$  = acceleration due to gravity,

$\rho_s$  = density of sediment,

$\rho_w$  = density of water, and

$d$  = size of the particle of interest.

Equation (4) solves for the dimensional critical shear stress,  $\tau_{cr}$ , which is the force required to *begin* mobilizing bed sediment with diameter  $d$ . The dimensionless critical shear stress,  $\tau_{cr}^*$ , also known as the Shields Parameter, Shields number, or Shields Criterion, represents a ratio of fluid force against a particle to the weight of the particle (Wilcock, Pitlick and Cui 2009). Equation 4 requires a value for the Shield's Parameter, a contentious value that Shields (1936) proposed to be 0.06. Since Shields' original flume experiment, research has suggested it is smaller than Shield's originally proposed value for mixed gravel and sand bedded rivers (Andrews 1983), and largely depends on the gradation of sediment sizes. I calculated a range of Shield's Parameter values using Andrews (1983) (equation 5), whose research showed that the Shield's Parameter can be approximated using the equation:

$$\tau_{*ci} = 0.0834 * \left( \frac{d_i}{d_{s50}} \right)^{-0.872} \quad (5)$$

Where:

$\tau_{*ci}$  = dimensionless critical shear stress (Shield's Parameter)

$\tau_i$  = sediment grain size of interest

$\tau_{s50}$  = median sediment grain size of the sub-surface

I used 2 mm as the grain size of interest because it marks the upper threshold of sand sizes used in several sediment studies on the San Joaquin River. I used multiple values for the median subsurface grain size, which were either from my Cottonwood Creek and Owl Hollow grab samples and Resources (2010). The range of Shield's Parameter values that I calculated from equation 5 were between 0.034 and 0.047, which were within the range of Shield's Parameter values listed by the U.S. Geological Survey (Survey 2008) for fine to coarse sands (ranging between 0.029 and 0.109).

I then used these values as input for the Meyer-Peter and Muller bedload transport rate equation (Meyer-Peter and Muller 1948). The Meyer-Peter Muller equation is simple in form,

however, it provides a dimensionless bedload transport rate, which and can be rewritten for a dimensional rate in the following form:

$$q_s = \left( \frac{8}{(s-1)g\rho^{1.5}} \right) (\tau - \tau_c)^{1.5} \quad (6)$$

Where:

$q_s$  = sediment bedload transport rate per unit widths = sediment density

$\rho$  = fluid density

$g$  = acceleration of gravity

$\tau$  = shear stress

$\tau_c$  = critical shear stress for incipient grain mobility

Then, I multiplied the output from the Meyer-Peter Muller equation by the river width at my bedload sampling transect to produce an estimate of the bedload transport rate. These calculations show the respective amounts of 2 mm sand expected to transport through these areas across various flow scenarios, and served as a first order approximation to show me if the bedload transport values I measured were limited by either the river's ability to mobilize sediment, or the river's supply of sand.

## Results

### *Bedload at Low Flows*

I collected thirty-seven bedload samples with a handheld Helley-Smith sampler (Figure 3) between Friant Dam and Owl Hollow at flows ranging between 215 and 685 cfs. Daily bedload transport rates ranged between undetectable amounts and 0.374 tons/day (748 pounds/day) with a mean of 0.057 tons/day (114 pounds/day) and standard deviation of  $\pm 0.095$  tons/day (190.6 pounds/day). Sieve analysis was not performed on these samples because individually, their total mass did not meet the minimum threshold for sieve analysis (Transportation 2010).

Bedload transport rates at Owl Hollow ranged between undetectable and 0.344 tons/day (687 pounds/day) with a mean of 0.113 tons/day (225.6 pounds/day) and a standard deviation of  $\pm 0.154$  tons/day (307 pounds/day).

Bedload transport rates at the upstream-most end of Ledger Island ranged between 0.007 tons/day (14.5 pounds/day) and 0.018 tons/day (36.8 pounds/day) with a mean of 0.013 tons/day (25.94 pounds/day) and a standard deviation of  $\pm 0.005$  tons/day (9.52 pounds/day).

Figure 4 and Figure 5 show the bedload transport rates at low flows arranged from left to right in ascending order of miles downstream from Friant Dam. Riffle 38 accounts for the highest transport rate measured (0.374 tons/day), the highest average rate (0.138 tons/day), and

the broadest range of transport rates. Riffle 38 is 6.83 miles downstream of Friant Dam, about 800 feet upstream of the confluence of Little Dry Creek with the mainstem San Joaquin River. The second highest low-flow bedload transport rate was at Owl Hollow, almost 9 miles downstream of Friant Dam. Owl Hollow bedload also showed the second broadest range of transport rates.

### ***Bedload at Moderate Flows***

On February 24 and 25, 2022, pulse flows were released from Friant Dam that increased the river discharge from base flow (350 cfs) to 1500 cfs. The hydrograph at California Data Exchange Center San Joaquin at Friant (CDEC SJF) stream gauge is shown in Figure 6. Bedload sampling at both Ledger Island and Owl Hollow captured large amounts of organic debris (Figure 7), consisting mostly of a green slimy material resembling moss and algae. While trace amounts of fine-to-medium grained sand were observed in the samples (Figure 8), the sand was not able to be separated from organic debris, and therefore an accurate measurement of sand content was not rendered from these samples. No gravel was observed in these samples.

### ***Bedload at High Flows***

During high flows of March 2023, Owl Hollow total bedload measurements at 6,900 cfs ranged between 41.8 and 109.1 tons/day, with a mean of 77.0 tons/day and standard deviation of  $\pm 29.9$  tons/day. Transport rates for the fraction greater than 2 mm ranged between 9.0 and 14.1 tons/day, with a mean of 12.4 tons/day; the transport rate for the fraction smaller than 2mm ranged between 32.7 and 95.6 tons/day, with a mean of 64.4 tons/day. The largest particle found in transport was 21 mm in diameter through its intermediate axis. The  $D_{50}$  for sediment in transport was 1.0 mm, and the mean uniformity coefficient ( $D_{60}/D_{10}$ ) for all samples was 2.17. The water surface slope of the pool through the transect was 0.0006.

During the same high flow event, Ledger Island total bedload measurements at 6,700 cfs ranged between 1.7 and 10.8 tons/day, with a mean of 6.9 tons/day and standard deviation of  $\pm 3.6$  tons/day. Transport rates for the fraction greater than 2 mm ranged between 0.4 and 2.4 tons/day, with a mean of 1.8 tons/day; the transport rate for the fraction smaller than 2 mm ranged between 1.3 and 8.7 tons/day, with a mean of 5.1 tons/day. The largest particle found in transport was 40 mm in diameter through the intermediate axis. The  $D_{50}$  of sediment collected in bedload transport was 1.3 mm, and the mean uniformity coefficient for all samples was 2.91. The water surface slope of the pool through the transect was 0.0003. Figure 9 shows the timing of bedload transport sampling at Ledger Island and Owl Hollow with respect to the hydrograph at SJF. Note that Owl Hollow had flow contributions from Little Dry Creek, and therefore includes an approximated combined hydrograph during that sampling period. Figure 10 shows the calculated bedload transport rates during these sampling events. The bedload transport rates are shown for all size classes, the size fraction finer than 2mm, and the size fraction greater than 2mm.

Figure 10 shows that sand sized particles comprise the majority of sediment in transport at the flows sampled at both Ledger Island and Owl Hollow. Table 2 shows the bedload transport rate statistics, and Figure 11 compares grain sizes of sediment in transport during the high flow sampling events at Ledger Island and Owl Hollow relative to the size of bed material at select

sites. For the two sites where both bed material and bedload transport was measured (Cottonwood Creek and Owl Hollow), there was not a substantial difference in the median grain size of sand in transport at high flows compared to sand stored on the bed during low flows. Figure 11 also shows that the largest sediment in bedload transport was measured at Ledger Island, while the coarsest sand bed material was found at the mouth of Little Dry Creek. Conversely, the finest sand in the study reach was found at the eroding bank at Leger Island.

### ***HEC-RAS Shear Stress and Meyer-Peter Muller Bedload Transport Rates***

The HEC-RAS channel shear stress analyses are shown at Ledger Island in Table 3 and at Owl Hollow in Table 4. I present the values for stream flow discharges at 1,500 cfs, 6,000 cfs, and 7,000 cfs because they most closely resemble the moderate and high flows that bedload was collected at. At Ledger Island, Shields's values between 0.032 and 0.034 most closely reflect the observed bedload transport rates when used with the Peter-Meyer Muller equation. The calculated bedload transport rates are 0 tons/day at moderate flows and about 4 to 8 tons/day during the high flows. At Owl Hollow, however, the range of Shields values calculated using Andrews (1983) return very high bedload transport rates when used with the Peter-Meyer Muller equation, between 47 and 170 tons/day during moderate flows and 6,000 to 8,000 tons/day during high flows. For comparison, we observed 0 tons/day during moderate flows and 64 tons/day at high flows during bedload sampling.

While these Shields values seem reasonable based on Andrews (1983), they do not inform us about sediment that is actually being supplied from upstream. The Meyer-Peter Muller equation only reflects the river's *capacity* to transport sediment that is supplied.

## **Discussion**

### ***Bedload at Low Flows***

Bedload transport rates at low flows have high variance compared to their mean, and as a result makes it difficult to develop a strong correlation with low stream flow rates. It is possible that low flows do not apply enough shear stress to the bed to mobilize a constant supply of sediment downstream. It is likely that spikes in shear stress occur locally due to flow perturbations around larger grains that comprise the bed's framework, thus mobilizing sand in amounts commensurate with the shear stress spike. Because much of the bed substrate has a sand matrix filling the interstices between gravel and cobbles, sand is usually present (even if in trace amounts) and available for transport. While this would also be expected at higher flows, sediment transporting at low flows might not be lifted high enough into the water column to transport smoothly across the bed, and could be captured within the interstices of larger particles, thereby being hidden from the flow's forces. Future studies could investigate if longer sampling periods reduce the bedload transport rate variance.

Bedload transport rates at low flows remain relatively low throughout the reach until Riffle 38, 6.8 miles downstream of Friant Dam, where the highest transport rates were measured. Downstream of Riffle 38, transport rates remain high compared to the other sites. Furthermore,

there were no distinct differences in the characteristics of bedload material upstream of Little Dry Creek compared to samples collected downstream. One possible explanation for the noticeable increase in bedload at and downstream of Riffle 38 is sand availability; if it is assumed that sand does not pass through Friant Dam (Reclamation 2014), then sand supply increases downstream as more sand sources accumulate (from banks, gullies, land use operations, etc.). Resources (2010) characterized riffle surface and subsurface sediment grain sizes within this study area. Although they classified sand sized particles as less than 6.4 mm, over three-times larger than the 2 mm grainsize threshold we consider, Resources (2010) data shows that surface bulk sand content was at most 5% of any sample (by mass) and did not increase noticeably downstream between Friant Dam and Owl Hollow. Furthermore, sand that is stored in the bed below the armored gravel layer could be a source of bedload if the overlying gravel mobilizes and exposes the sand. Bray and Dunne (2017) observed gravel transport in riffles at flows as low as 700 cfs, however, it is unlikely that the subsurface sand is a primary source of bedload at low flows because no gravel was observed in transport or sampled during our sampling efforts, even at the highest end of the low flows. While in-channel sand storage is a topic that is explored in Chapter 3, it is not apparent that the in-channel surficial sand plumes are the culprit of higher bedload rates at these sites. It is likely that the wide variance of bedload transport rates at low flows represents the tendency for sand to mobilize where it is available and where shear stress is ample, and thus infrequently.

### ***Bedload at Moderate Flows***

Bedload transport rates during the 1,500 cfs pulse flows were significantly lower than expected. Prior to sampling, I made estimates of bedload transport at Owl Hollow using the Meyer-Peter Muller equation (equation 6). At discharge scenarios of 350 and 1,200 cfs, I calculated average bedload transport estimates of 0 and 153 tons/day, respectively. The incipient transport was expected to occur at some point between 350 and 1,200 cfs, but I did not have data resolution to discern the flow of incipient sand transport. Although 153 tons/day seemed like an unreasonably high estimate for 1,200 cfs, I reasoned that the equation is a reflection of the river's capacity to transport sediment, not the amount of sediment that would be supplied and transported through the site. Therefore, I expected bedload transport rates at 300 cfs above the highest model scenario to be higher than the trace amounts of sand that we measured. Additionally, given the large sand supply within the Owl Hollow pool, I felt that the bedload sampling system was positioned in the ideal location to capture any sand mobilizing from or through the pool, since it was about 100 feet downstream of the bed substrate transition between sand and sandy gravel. I have three hypotheses to explain the difference between my expected and measured bedload transport values:

1. Only trace amounts of sand mobilize at Owl Hollow and Ledger Island at 1,500 cfs.
2. The peak sand transport rate at these flows and locations had already occurred by the time that sampling began; therefore, at moderate flow conditions, the bed adjusts and equilibrates quickly on the rising limb of the hydrograph.

3. The bedload sample collection bag filled with mossy organic debris transporting high in the water column as the sampler was being lowered to the bed; the organic debris created a “seal” against the bag’s mesh which created backpressure within the bag, therefore directing flow and bedload around the bag and not through it.

GMA 2011 provides a bedload transport power function for sediment smaller than 2 mm at flows between 4,500 and 8,000 cfs. Extrapolating this trend line to 3,000 cfs suggests that sand would transport at about 1 ton/day. If this is true, then hypothesis 1 above is false and hypotheses 2 and 3 are likely. If bedload transport does not behave as depicted by the power function at 3,000 cfs, then hypothesis 1 is most likely and hypotheses 2 and 3 would not have affected our sampling results. More on this topic is explored in Chapter 3, where the presence and extent of sand plumes was shown to change (and decrease in most locations) after long-term contractor flows of 1,500 cfs.

Tetra Tech (2018b) measured bedload transport in 2014 at three riffles within this study reach at 1,300 cfs. They sampled from a cataraft with a TR-2 bedload sampler in the same manner as conducted in this thesis, except that their sample transects were located at the downstream end of each riffle, instead of on the upstream limb of a riffle or a glide as was conducted in this thesis. Tetra Tech had trouble sampling bedload and concluded that their sampler had scooped bed material, however, they adjusted the data to provide bedload estimates. They concluded while there is evidence that the riffle surfaces are mobile at 1,300 cfs, their bedload estimates of sand and gravel of a “few tons per day” (ranging between about 0.5 and 6 tons/day) were likely bias high and subject to “considerable uncertainty.” Similarly, Tetra Tech’s sand study (Tetra Tech 2018a) shows that 1,200 cfs provides ample capacity to transport sand at approximately 5.2 and 6.8 miles downstream of Friant Dam. Furthermore, they conclude that long duration flows “probably exceeding 2,000 cfs” are capable of eroding sand deposited in pools.

Although I was not able to collect sufficient bedload samples at moderate flows to constrain a transport rate, Figure 12 shows bedload transport rates collected from several studies on the San Joaquin River at several locations. The upper panel of this figure includes bedload transport rates measured by Tetra Tech and the U.S. Geological Survey, which can provide estimates (or ranges) of bedload transport rates at moderate flows. Tetra Tech collected these data from within my study reach, but not at any of my bedload sampling sites. The U.S. Geological Survey collected their data about 300 feet downstream of Highway 41, which is about 3 miles downstream of my study area, however, is still within the gravel bedded reach of the San Joaquin River and at a spot showing alluvial processes such as gravel bar formation and migration. Figure 12 shows that there are sites in the vicinity of my study reach where sand is mobilized in bedload at or below 1,500 cfs, however, the lower panel provides model predicted bed shear stress at each of those sites. Results show that the sampling locations at Ledger Island and Owl Hollow experience very low bed shear stress at 1,500 cfs, and therefore probably do not experience much bedload transport at those flows. I conclude that hypothesis 1 above is the most likely explanation for the low bedload transport rates observed during the 1,500 cfs pulse flows, however, it is plausible that a combination of all three hypotheses apply to some extent. Future studies could investigate if algal mats covering the bed capture sand in bedload at low flows, and at what flows they are scoured from the bed.

### ***Bedload at High Flows***

Bedload material at high flows includes sand and gravel at both Ledger Island and Owl Hollow sites. Total bedload transport rates at Owl Hollow were on average 11-times greater than at Ledger Island, and were higher for both grain size classes greater-than and less-than 2 mm (Figure 10). This could be due to sediment availability, such that there is more sediment available upstream of or within the Owl Hollow pool to be mobilized through the site, or from higher shear stresses at Owl Hollow. While both of these possibilities are likely, the water surface slope at Owl Hollow (0.0006) is twice as steep as at Ledger Island (0.0003), which suggests that shear stresses are significantly higher. It is reasonable to expect that a 2x increase in slope can result in a 2x shear stress application from the river against the bed substrate, and thus capable of mobilizing at least 2x the amount of sediment in bedload if it is available to be mobilized. Alternatively, if sediment availability is the factor controlling sediment transport at these sites, then this brings into question if there is a higher sediment supply to Owl Hollow than to Ledger Island. The question of sediment supply can be investigated from multiple sources, being either from:

- 1) in-channel (surficial and subsurface) sediment sources mobilized to each site;
- 2) near-channel sediment sources mobilized to each site;
- 3) proximity to the Little Dry Creek confluence, which could be delivering sediment to the mainstem San Joaquin River during high flows;

I used the HEC-RAS hydraulic model to see how channel shear stress differed at the two sample sites. Model results show that during sampling, the Ledger Island site had a channel shear of about  $1.17 \text{ N/m}^2$  (at 6,400 cfs and slope of 0.0003), while Owl Hollow had a channel shear stress of about  $9.3 \text{ N/m}^2$  (at 6,900 cfs and slope of 0.0006). This comparison is illustrated by Figure 12, which shows that measured sediment transport rates were about 10-times higher at Owl Hollow, which experienced channel shear stresses about 10-times greater than at Ledger Island. This figure also shows no clear correlation between channel shear stress and bedload transport rate (bottom panel), therefore suggesting that bedload transport rates are not easily compared between sites without applying normalization factors (because it is well documented that bed shear stress drives sediment transport). It may also suggest that sediment supply is a limiting factor of sediment transport in this reach. This is supported by the fact that channel shear stress at Ledger Island increases minimally between 4,000 and 8,000 cfs, however, sediment transport rates increase by an order of magnitude; because sediment is not being scoured from the bed at this site, it must be sourced from upstream. Additionally, Figure 12 shows that the bedload transport rates measured in this thesis are reasonable and within the expected range of rates as shown by other studies.

Figure 13 and Figure 14 also demonstrate the difference in bed shear stresses at Ledger Island and Owl Hollow across ranges of flow. More notable, however, is how the bed shear stress varies within each of those sites across a short distance even at a constant stream flow. Figure 13 and Figure 14 demonstrate the importance of understanding the bed shear stress at bedload sampling locations, especially if sediment transport modeling will be employed. Sand

bedload transport rates were about an order of magnitude at Ledger Island than at Owl Hollow, which agrees with expectations from calculated bed shear stress from the HEC-RAS model.

A bedload rating curve is provided in Figure 15. It shows bedload transport data collected at Leger Island (Associates 2011) across a range of flows. The brown trendline and regression represent a bedload transport function of the average bedload transport rates at each stream flow rate. I used this function in conjunction with the 3-year hydrograph of my study period (Figure 2) to determine the total sediment load that would have transported past this site, which I estimate to be 5,750 tons of sand. I could not create a bedload rating curve at Owl Hollow because I have transport rates at only one flow rate, so I estimated the sediment load from my study period at that site by multiplying the Ledger Island function by the difference in average bedload transport rates at 6,400 cfs (Table 1). This estimate implies that about 46,000 tons of sand exited the downstream end of my study reach in the 3 years that I studied it.

Little Dry Creek is a potential major source of fine sediment to the San Joaquin River (Reclamation 2014). (Cain 1997) estimates that Little Dry Creek transports a total annual sediment supply of 4,500 tons of sand/year; however, the amount that makes it beyond flow barriers to the San Joaquin River is unknown and unquantified (Reclamation 2014). During high flows of approximately 3,000 cfs in 2017, California Department of Water Resources staff attempted to measure bedload transporting across a weir in Little Dry Creek 0.3 miles upstream of its confluence with the San Joaquin River; while no formal report was made describing this work, staff stated via phone conversation in March of 2023 that no sediment was measured and that the water passing the weir was about 1-foot deep and clear, lacking turbidity. I visited this site in September 2021 and noted that the substrate downstream of the weir was gravel and cobble with sparse sand deposited on the leeside of in-channel large woody vegetation. A large plume of sand (about 300 cubic meters) is located immediately upstream of the weir that appears to have deposited instead of flowing past the weir. Local researchers stated that this channel is also a diversion canal from the San Joaquin River, which is routinely excavated of sand by the nearby mining company to maintain flow diversions. From these observations, it is likely that much of the sand being transported in Little Dry Creek is captured upstream of the weir, possibly in abandoned gravel mine pits or removed mechanically.

While the amount of surficial in-channel and near-channel sand storage is discussed in Chapter 3 of this thesis, subsurface sand storage is a source that can be potentially released during high flows as the coarser, armored gravel and cobble layers are mobilized (Meyers 2021). Data included from DWR's riffle particle composition study (Resources 2010) were investigated to see if subsurface sand composition increases downstream between Friant Dam and Owl Hollow (Resources 2010); Figure 16 shows that while the  $R^2$  value of this linear regression is not very strong ( $R^2 = 0.1096$ ), it appears that the trend is mostly driven by four samples having high subsurface sand contents between 7-8 miles downstream of Friant Dam. Figure 16 shows that the amount of subsurface sand increases to between 14-27% about 1.5 miles upstream of the Owl Hollow bedload sampling transect (9 miles downstream of Friant Dam), but that subsurface sand content at the next riffle upstream of the Ledger Island bedload sampling transect (4.68 miles downstream of Friant Dam) is between 7-11%. If high flows are capable of mobilizing the armor layer of gravel and cobbles in these vicinities, then the potential exists that more sand is exposed upstream of Owl Hollow and could be mobilized through the sampling location. To be explored

further in Chapter 3 of this thesis, is the two large sand bedded pools upstream of the Ledger Island sampling site.

In 2017, Tetra Tech performed bedload sampling during high flows of about 5,500 cfs (Tetra Tech 2018b) using methods similar to those in this thesis. Although they measured sand, gravel, and cobbles transporting in bedload, they encountered difficulty sampling under high flows and report a high likelihood of having inadvertently scooped cobble bed substrate with the sampler, instead of capturing sediment transporting along the bed. They adjusted their bedload calculations to account for this and estimated 9.7 tons/day of sand and gravel at the Friant riffle (about 1 mile downstream of Friant Dam), and 5.8 tons/day of sand and gravel at Riffle 40 (about 6.2 miles downstream of Friant Dam and about 0.8 miles upstream of Little Dry Creek confluence). Our results indicate similar rates of transport, having sampled at flows about 1,000 cfs higher and measuring an average of  $6.9 \pm 3.6$  tons/day at Ledger Island. Tetra Tech did not sample bedload downstream of Little Dry Creek, however, our results show substantially higher sediment transport rates at Owl Hollow, indicating either the flushing of in-channel sand or supply from Little Dry Creek. Chapter 3 investigates the movement of in-channel sand before and after the high flows.

### ***Bedload Flux Through the Study Reach***

Multiple empirical studies have investigated bedload transport within the study reach and concluded that bedload transport likely contains sand at moderate (bankfull, about 1,400 cfs) and high flows. Sand transport is likely discontinuous throughout the reach as it encounters areas of low bed shear stress and deposits on the bed, such as in pools with low hydraulic slope. Although subject to large variability, I measured sand transport in the range of 1 to 10 tons/day upstream of Little Dry Creek. This seems like a reasonable estimate when considering the bedload transport rates of other nearby studies and that there are not many sediment sources between there and Friant Dam. Additionally, bedload contributions from Cottonwood Creek are currently unquantified and if present, they are infrequent (explored in Chapter 2). For scale, a medium size dump truck has an approximate load capacity of 10 tons. If transport rates are much higher than these estimates, then we should expect to see significant geomorphic changes to the river planform or bed elevation, which is a topic explored in chapter 3.

Bedload transport rates during high flows at Owl Hollow were about an order of magnitude higher than rates upstream. This indicates that more sediment is leaving the downstream end of the study area than is transporting through the middle and upper end (at about 2 and 5.5 miles downstream of Friant Dam). The sand transport function (Figure 15), when applied to the hydrograph in Figure 2 suggests that about 5,750 tons of sand transported through Ledger Island throughout my study period. While I was not able to make a sand rating curve for Owl Hollow, a simple estimate can be provided by multiplying the Ledger Island function by the difference in transport rate averages measured in March 2023, estimates that about 46,000 tons of sand could have transported through Owl Hollow in my study period. The bottom panel of Figure 12 shows that bed shear stress varies significantly throughout the reach, which is likely dependent on the geomorphic setting of the sample sites. Figure 13 and Figure 14 show that bed shear stress can vary significantly across a single sampling site. Bed shear stress is known to drive sediment transport (where there is ample supply), thus suggesting that sediment transport

rates in this reach are largely controlled by sediment supply. Chapter 2 investigates sediment supply entering the upstream end of the study area, and then Chapter 3 investigates whether that sediment transports through the study area.

## Chapter 2: Cottonwood Creek Bedload Sampling

### Introduction

Cottonwood Creek is an ephemeral stream that meets the San Joaquin River about 1,000 feet downstream of Friant Dam. It is a likely sediment source to the San Joaquin River below Friant Dam, however, its sediment yield is unknown. Its drainage area is about 37 square miles (95 square kilometers) (Survey 2019) and can have long periods of no flow (Haught, Marinuea et al. 2023). Cottonwood Creek is very responsive to rainfall events and exhibits flashy hydrographs with flows rising quickly and receding flows decreasing more gradually (McBain & Trush 2002). There is an inactive stream gage on Cottonwood Creek about 0.5 miles upstream of the San Joaquin River. Stream flow data collected between November 1997 and July 2019 shows about 20 flow events occurred within that period up to 1,600 cfs. Pre-Friant Dam gaging was conducted by the USGS in the 1940s and early 1950s for 10 years, which show that the creek did not flow every year and peaked below 150 cfs. Based on my experience with this drainage, it seems to flow only during high intensity rainstorms when the ground has been previously saturated.

The watershed consists of rolling hills with granitic outcrops of the Sierra Nevada foothills, ranches, and open grassland. Two miles upstream of the San Joaquin River confluence, Cottonwood Creek becomes channelized as it incises through a steep walled and narrow canyon. The canyon contains multiple lithologies including pumice, granite, and metasedimentary outcrops. Although Cottonwood Creek is heavily vegetated with grass and willow trees, it is mostly sand bedded with some sections scoured to bedrock. The bed substrate is coarse subangular sand. Cottonwood Creek's steep slope and narrow confining walls indicate high transport capacity, however, the thick vegetation indicates an infrequency of flow events that are not able to completely scour the bed.

### Methods

We sampled bedload at Cottonwood Creek during a storm in March 2023 to determine its sediment supply to the Mainstem San Joaquin River. We sampled throughout a two-day period during flood flows produced by the storm. The methods were similar to those described in Chapter 1 and are listed below.

#### *TR-2 Bedload Sampling*

We attempted to use a handheld Helley-Smith bedload sampler at Cottonwood Creek, however, flows were too deep and too swift to deploy it safely or properly. We performed bedload sampling from a cataraft platform using the same methods previously described in Chapter 1. The cataraft was deployed across a cableway located about 100 feet downstream of the US Bureau of Reclamation bridge, or about 400 feet upstream of the low-flow confluence of Cottonwood Creek and the San Joaquin River. We considered deploying the sampler from the downstream end of the bridge, however, we were deterred by large woody debris, a fence, rebar,

and concrete structures that are known to be below the water surface in that area. For sample processing, we used the same methods as described in Chapter 1.

### ***Stream Discharge Measurements***

Stream discharge was measured with an Acoustic Doppler Channel Profiler (ADCP) and current meter. When deploying the ADCP, the sensing instrument was housed in a floating vessel and pulled across the channel by rope to measure flow in each direction to account for the possibility of directional bias. When measuring stream flow with the current meter, flow was measured at the sixty-percent depth across the channel (Harrelson, Rawlins and Potyondy 1994). In areas where flow was too deep to measure by wading with the current meter, or where the channel was too wide to pull the ADCP by rope, the devices were deployed from a cataraft that would traverse a cableway across the channel. Stage measurements were taken from a fixed monument at the beginning and end of each stream discharge and bedload transport measurement.

### ***Estimating Total Sand Supply***

Sand supply from Cottonwood Creek is difficult to estimate because there is not an active stream gage to provide a long-term flow record, and the bedload sampling site we chose was strongly affected by backwater from the San Joaquin River. When we sampled bedload in March 2023, the backwater effect made it impossible to create a rating curve between Cottonwood Creek stream discharge and bedload transport because we observed decreasing stage with increasing stream discharge. Instead, we estimated the volume of sediment supplied over the two-day sampling period by plotting daily averaged bedload transport rate for each sample in time-series and estimating the area beneath the curve (Figure 17).

To estimate bedload supplied from Cottonwood Creek throughout my study period, we needed to develop or estimate a hydrograph for it. We did this by using the Little Dry Creek hydrograph as a starting point. We compared the peak flow at Little Dry Creek during the March 2023 storm (when we sampled bedload on Cottonwood Creek) to our highest stream discharge measurement on Cottonwood Creek. This provided a peak flow ratio between the two tributaries, with our highest stream discharge measurement at Cottonwood Creek being 38 percent of the peak at Little Dry Creek. We used this ratio to assume that Cottonwood Creek produced flows that were 38 percent of Little Dry Creek's flows across the entire study period. Then, we estimated the sediment supplied during each peak flow on the "Cottonwood Creek assumed hydrograph" (38 percent of the Little Dry Creek hydrograph) by linearly scaling the difference from the March 2023 peak discharge and associated sand supply.

This is a conservative method that likely underestimates Cottonwood Creek sediment supply because bedload typically increases exponentially with flows, not linearly as we applied in this method. Additionally, we did not account for the duration of flows, only the peak magnitudes.

### ***Bed Scour Stakes***

I installed four metal stakes vertically into the bed of Cottonwood Creek to measure scour or deposition after a flood. I installed the stakes in October of 2021 when the bed was dry. They were placed approximately 150 feet upstream of the bridge, 50 feet upstream of the bridge, 50 feet downstream of the bridge, and 100 feet downstream of the bridge. Each stake was about 3 feet long, and I drove them into the bed about 1.5 – 2 feet deep angled upstream about 5 degrees. I then measured the distance of each rod exposed above the bed surface.

If flows were produced in Cottonwood Creek, I would return to the stakes to measure if the distance of above the bed had changed; an increase in rod length would imply scour, a decrease in rod length would imply deposition, and an absence of rods would imply great magnitudes of either scour or deposition based on other context clues.

## Results

During the flood flow sampling event of March 2023, stream discharge ranged from 160 to 470 cfs. We collected 14 bedload samples consisting mostly of sand with fine gravel. The gravel consisted mostly of pumice, and sand consisted of pumice, lithics, and quartz. The median bedload grain size was 0.72 mm, with 90.2 percent finer than 2 mm. Grab samples after the flood revealed that bed material was slightly coarser than the bedload, which had a median grain size diameter of 0.83 mm, with 85.3 percent finer than 2 mm.

The average (mean) bedload transport rate was 22 tons/day, with a maximum of 67 tons/day and a minimum of 0.1 tons/day. For sediment smaller than 2 mm, the average bedload rate was 20.1 tons/day, with a maximum of 59 tons/day and minimum of 0.1 tons/day. During the sampling period, bedload delivery from Cottonwood Creek to the mainstem San Joaquin River is estimated to be 51.6 tons (37.4 cubic yards). Figure 17 shows a sedigraph of the measured sediment transport rates during the sampling period. A bedload transport rate summary is provided in Table 2.

Hysteresis was observed in Cottonwood Creek bedload transport, and therefore a rating curve was not established between stream discharge and bedload discharge. Similarly, stream discharge did not correlate with stage in Cottonwood Creek; stage was falling during times when discharge was constant or increasing. This appears to have been influenced by the stage in the mainstem San Joaquin River, where reductions in flow release from Friant Dam reduced backwater at the mouth of Cottonwood Creek. This is illustrated in Figure 9, where a sharp decrease in San Joaquin River flows appears to correspond to an increase in bedload transport rate on Cottonwood Creek. Note that because the SJF stream gauge is about 1.5 miles downstream of Friant Dam, the effects of hysteresis at Cottonwood Creek would have initiated earlier than depicted by the hydrograph in Figure 9.

We estimate from the Little Dry Creek hydrograph proxy, that Cottonwood Creek had several flow events throughout the spring of 2023 that were capable of mobilizing bedload. We estimate that number to be about 300 cubic yards (450 tons) of sand and fine gravel.

In August 2023 after flows ceased, only the two stakes immediately upstream and downstream of the bridge remained. The upstream stake was leaning downstream about 25 degrees and indicated a stable bed with no difference in exposed rod length. The downstream stake was leaning downstream about 5 degrees and indicated that 1.15 feet of deposition had occurred there. Grass cover was no longer on the bed, but bushes and willow trees remained. It is

likely that the upstream stake was scoured out and buried nearby, based on photograph observations indicating that sand had been scoured away from now-exposed boulders in that area. It is likely that the downstream-most stake was buried, as it appears to be in a depositional environment.

## **Discussion**

Several lines of evidence indicate that Cottonwood Creek supplies sand to the mainstem San Joaquin River, discussed below.

Bedload discharge was not correlated with streamflow discharge during Cottonwood Creek sampling. It is likely that a backwater effect from the mainstem San Joaquin River affected sediment transport in Cottonwood Creek by changing the hydraulic gradient at the interface of the two systems. Most Cottonwood Creek bedload samples were collected during the rising limb of the San Joaquin River hydrograph, during which the total mass of each bedload sample gradually increased. After the Friant Dam flow releases sharply decreased, bedload samples from Cottonwood Creek showed a noticeable increase in total volume. This suggests that sediment load moving through the sampling zone was largely dependent on the hydraulic gradient produced by interference from the mainstem San Joaquin River.

This is not to say that bedload transport through the sampling zone does not depend on flows draining from Cottonwood Creek. It is possible that bedload was depositing on the bed at the upstream end of the backwater-affected area (presumably upstream of the bridge), and remobilized when the hydraulic gradient increased as San Joaquin River flows dropped. This would have produced biased bedload transport rates until the depositional environment equilibrated to the hydraulics.

The confluence of Cottonwood Creek and the San Joaquin River did not feature a sandy delta that would indicate an obvious high sediment supply from Cottonwood Creek, however, that is not ample evidence to reject the possibility of it. At the upstream end of this backwater area, there is a dense wall of willow trees and other woody vegetation that take root in sandy substrate. This vegetative wall extends at least 100 feet upstream, and might act as a protective curtain to retain the sandy riverbed at the mouth of Cottonwood Creek, but it does not preclude sediment load from passing through to the San Joaquin River. Sand mapping in April and August of 2021 revealed a thin sand veneer covering bedrock and boulders in the shallow backwatered mouth of Cottonwood Creek. The creek was known to have flowed in February of 2021, and personal accounts by operators of Friant Dam stated that the flows were turbid like the color of chocolate milk, indicating sediment entrainment. Because Friant Dam releases never exceeded 334 cfs (typical low base flow condition) in that time period, it is likely that entrained sediment would have encountered the confluence and deposited within the backwater area, or shortly downstream. It is probable that sediment in this area is routinely washed out when dam releases are increased. Additional sand presence in this area and its extent is covered in Chapter 3.

Scour stakes that were placed in the bed near the bridge showed that there was enough sediment conveyance in the system to either remove or bury two stakes, and deposit 1.15 feet of sand near another one. These stakes do not provide certain evidence of channel baseline movement because they are only a few discrete sample points which may have affected hydraulics enough to have induced sediment scour or deposition around them. However, the

remaining two stakes provide evidence that 1) the bed did not scour beyond their burial depth, 2) there is a depositional environment downstream of the bridge, and 3) the thalweg immediately upstream of the bridge is relatively stable.

We estimate that Cottonwood Creek supplied about 300 cubic yards (450 tons) of sand to the San Joaquin River in 2023 (for reference, 300 cubic yards is the approximate volume of a full-size school bus). This is a crude estimate and is likely an underestimate because it estimates bedload transport linearly with peak flows, not exponentially. However, based on the Ledger Island bedload rates measured in 2023 (discussed in Chapter 1), this amount of sand would take 43 days to flush beyond Ledger Island at consistent flows of 6,400 cfs. For a conservative estimate based again on the Little Dry Creek hydrograph, it is likely that flows ceased in Cottonwood Creek by May 1<sup>st</sup>. After that date, flows in the San Joaquin River remained above 6,400 cfs for 40 days, but were as high as 10,400 cfs. This provides ample reason to believe that the San Joaquin River was capable of flushing more than 300 cubic yards of sand beyond the Ledger Island sampling site. Additionally, Associates (2011) found that bedload transport rate increases exponentially with flow increase, such that 10,000 cfs could transport 90 tons of sand per day. In May of 2023, San Joaquin River flows remained above 10,000 cfs for 13 days. Even if our estimate of sand supply from Cottonwood Creek is low by 50 percent, it appears that the San Joaquin River still had ample sediment conveyance in 2023 at the Ledger Island to flush more than Cottonwood Creek's supplied sand volume downstream.

### ***Bedload Flux Through the Study Reach***

Chapter 1 showed that sand transports through the study reach in bedload at high flows and is likely mobilized during moderate flows. Chapter 2 investigated sediment inputs at the upstream-most end of the study reach, showing conclusive evidence that Cottonwood Creek contributes sand and fine gravel to the reach during intermittent flow events. From this, we understand that mainstem San Joaquin River bedload is not limited to in-channel or bank sand sources, and that bedload transport processes at moderate flow should not be expected to cause significant geomorphic changes. Chapter 1 shows that high flows were capable of flushing the sand supplied by Cottonwood Creek throughout the study reach, however, intermittent Cottonwood Creek flows occur independently of Friant Dam operations. This suggests that sediment supplied from Cottonwood Creek could be stored in the San Joaquin River channel until moderate or high flows are released from Friant Dam. Next, chapter 3 describes the presence and extent of in-channel sand storage before and after moderate and high flow events.

## Chapter 3: Facies Mapping and Bank Erosion

### Introduction

This chapter presents the spatial mapping and characterization of the presence and extent of sand within my study reach. My goal was to describe where sand is, how much sand is in each area, if sand size changes substantially throughout the reach, and how the presence and extent of sand changed between 2021, 2022, and 2023. My curiosity to answer this question springs from the concept that while no sand is known to pass through Friant Dam, there is still relatively large sand storage within the study reach. If no sand is passing through the dam, then sand content should be decreasing with time unless there is a substantial sand source downstream of the dam. It is possible that sand could be coming from either Cottonwood Creek, nearby banks, gullies, and hill slopes, or from the bed itself (primarily the subsurface below the armored gravel layer). Two long standing questions I have had since working on the San Joaquin River are:

- is sand mobilized from pools during contractor flow releases of moderate magnitude (about 1,500 cfs)?
- is sand is stored at the bottom of the deep channel immediately downstream of the Cottonwood Creek confluence?

Contractor flow releases are a specifically allocated volume and flow rate that is released from Friant Dam when downstream water rights holders cannot have their water demand met by other water sources. These flows occur primarily on dry years during irrigation season. Water is released at the bottom of Friant Dam and flows through and beyond my study reach, where it is diverted dozens of miles downstream for beneficial uses. I am curious if these flows are capable of mobilizing in-channel sand during a flow release magnitude of 1,500 cfs or higher.

The San Joaquin River is confined by bedrock for 0.45 miles between Friant Dam and Friant Pool. This reach is between 25 and 30 feet deep for about 1,000 feet immediately downstream of the confluence where Cottonwood Creek meets the San Joaquin River. It has previously been unclear if this zone is a depositional environment where sediment supplied from Cottonwood Creek comes to rest, or if it is scoured clean by high flows. Whereas Chapter 2 of this thesis shows that Cottonwood Creek does supply sand and fine gravel to the San Joaquin River, Chapter 3 provides insight to its downstream fate.

To answer these questions, I performed field reconnaissance in the late summer of each year when flows were low (between 200 and 400 cfs). These conditions provided long days of overhead sunlight that penetrated to water column for optimal visibility of the bed. My reconnaissance was performed by wading and floating the river in inflatable rafts and kayaks.

### Methods

#### *Facies Mapping*

I mapped riverbed substrate from a boat to identify the extent of sand storage compared to other primary grain sizes. I defined the facies by grain size classifications, which included sand, gravel, sandy gravel, and bedrock. These methods defaulted to visual identification of grain sizes where the bed was visible. In areas where light did not penetrate the water column sufficiently to see the bed, I used a 10-foot length of ¼-inch rebar to probe the substrate (herein termed “probe”). Areas where the probe responded to the substrate with dull or gritty sound, or by sinking into the substrate, or by moving through the substrate sluggishly, were mapped as sand. Areas where the rebar probe responded to the substrate with a sharp, bright, or chirping sound, with varying depths to bottom, and where individual grains could be moved with the probe, were mapped as gravel. Areas with both previous characteristics were mapped as sandy gravels. Areas where the rebar probe responded to the substrate with a sharp, bright, and chirping sound, with smooth or even depths to bottom, and where the probe slid easily across the bed, were mapped as bedrock. An exception to the bedrock mapping, was in areas where volcanic tuff was exposed on the river bottom; tuff typically exhibited a sticky clay texture that held on to the rebar as it was probed. To calibrate the feel of the rebar probe’s response to substrate textures, substrate was probed in areas where the river was shallow enough to see the bed.

I used the depth of surficial sand to classify the primary grain size of an area. For example, an area with a thin veneer of sand overlying bedrock would have been classified as bedrock, or bedrock with sand. In many of these areas, the overlying sand volume was not enough to quantify using the rebar probe method.

The river depth increases beyond the reach of the rebar rod about 1,000 feet downstream from Friant Dam. In this area, the bed was not sampled or probed, but was viewed by lowering a waterproof camera attached to a 30-foot telescoping rod. Bicycle headlights were attached to the rod to illuminate the bed. I videoed the river bottom in August 2021 and November 2023, at approximately 200-foot increments downstream, for a total of 6 locations. I also videoed the bed of the downstream pool at Friant Cove where the river shallows and widens, for comparison. I mapped the river facies throughout the 9-mile study reach in fall seasons of 2021, 2022, and 2023. Fall 2021 represents the baseline in-channel geomorphic conditions of my thesis, being the second consecutive low-flow year following a very high-flow 2019; fall 2022 represents in-channel geomorphic conditions after a four-month period of elevated Contractor Flow Releases of up to 1,600 cfs; and fall 2023 represents the in-channel geomorphic conditions after very high flood flow releases of up to 10,000 cfs. I digitized each of these facies maps to show the presence and extent of the most prominent in-channel sand plumes. I then superimposed the sand plume maps to show how their presence and extent changed between each major flow regime.

### ***In-channel Sand Volume***

I established fifty transects perpendicular to the river flow between Friant Dam and Owl Hollow. I traversed these transects to collect information about the depth of water and sand across the river width. I traversed by wading or by boat where the river was too deep to wade. I used the rebar probe to measure the depth of water and the depth of sand at approximately three-foot intervals where the river was less than 200 feet wide, and at approximately six-foot intervals where greater than 200 feet wide. I measured the depth of in-channel sand by pushing the rebar into the sand until refusal, and recorded as the difference in water depth and total refusal depth.

In areas where only the gravel was mapped, I did not penetrate the rebar into the substrate because that would have biased sand content high. In the mapping events of September 2021, 2022, and 2023, stream flow discharge in the San Joaquin River was similar enough that river stage was not visibly different, and therefore allowed the transect widths to be based on river stage. I measured the river width by stretching a survey tape across the channel and used an inflatable boat where the channel was too deep to wade. I used Google Earth tools to measure river width where the channel was too broad for the survey tape.

I used the  $V^*$  method (Hilton and Lisle 1993) as guidance for measuring in-channel sand storage, however, I modified it to accommodate a larger river and greater spatial extent. Hilton and Lisle described their method for small streams that relies on knowing the downstream riffle crest elevation to calculate residual sand volume throughout the adjacent upstream pool; that was not feasible in this study, so I instead relied only on measurements of sand depth throughout each pool. To calculate sand volume from depth of sand measured with the probe, I calculated the cross-sectional area of sand across each channel transect and multiplied that by half of the distance to the next cross section. Using the standard error of a representative transect and 95 percent confidence interval, I calculated the margin of error to be  $\pm 9$  percent.

It should be noted that while I mapped the presence and extent of the major in-channel sand plumes, I did not measure the depth or calculate the volume of all backwater sand storage locations. I focused my efforts on areas of the channel where the dominant flow direction is downstream. The amount of sand stored in backwater areas likely comprise a large portion of the total amount of surficial sand coverage throughout the study reach; however, my observation of those areas is that they were relatively stable throughout my study period.

### ***Sand Grab Samples***

I collected discrete samples from sand sources both in and outside of the channel for grain size characterization. I then dried the samples and sieved them using California Test 202 (Transportation 2010) methods to determine their grain size distribution. From the cumulative grain size plots, grain size statistics were calculated to show the median grain sizes from each sample, and then compared to other samples based on their proximity to the tributaries, other sand sources, and Friant Dam. The purpose of measuring grain sizes at these sites was not to determine the grain size statistics of each location for fingerprinting purposes, but was instead to gain a basic understanding of the sand size ranges at various storage sites. I think this method was a reasonable approximation based on my observations of general uniformity of grain sizes within each sand source.

### ***Bank Erosion***

The river-right bank on the south end of Ledger Island has shown signs of erosion since 2011 (Figure 26 and Figure 27). To estimate the volume of sediment sourced from this location, I surveyed the bank to measure the amount of lateral bank erosion occurring with time. I installed twelve wooden survey stakes into the horizontal ground surface at intervals of 12.5 paces along the actively eroding 370-foot section of the 600-foot-long bank. I chose wooden stakes because

they would degrade with time if the bank eroded beyond their placement, causing them to fall into the river. The stakes were installed between two and four meters back from the edge in the direction perpendicular to the bank's vertical face. I measured and recorded the azimuth, so that repeat measurements could be made along the same path in the future. I measured the horizontal distance from the bank to the stakes using a 2-meter-long polyvinyl chloride (PVC) pipe, graduated in 10-centimeter (cm) intervals. I then measured the vertical height of the eroding bank from the top of the bank crest down to the highest point of repose where sand sloughing off of the bank collected below.

I also used Google Earth to view the horizontal amount of bank erosion that occurred between different time periods. Google Earth released imagery from April 2021 and October 2023, which are both within one month of the first and last dates of my field reconnaissance. I used Google Earth tools to delineate the bank crest in both of these imagery dates and combined them into a single polygon to measure the area between both delineations. I then used the bank height measurements described above to calculate the total volume of bank sediment that eroded into the river within that time frame. I then calculated the weight of sand (in tons) to more easily compare with sediment transport rates, which herein are referred to in tons/day. To calculate the weight, I first measured the density of the sand by measuring the mass of the sand held in a square tablespoon. I used a yeast scale to measure mass to the nearest 0.01 gram, to then convert the eroded volume of the bank into weight.

## Results

The results of the sand mapping, in-channel volumes, and grain size distributions are presented sequentially downstream, as described below. An index map is provided in Figure 18 to show the extent of each area mapped with significant in-channel sand storage. Annual bed sand storage volumes from 2021 to 2023 throughout the 9-mile reach are presented in Figure 19 and Table 5.

### *Cottonwood Creek confluence to Friant Cove*

Cottonwood Creek meets the San Joaquin River about 1,000 feet downstream of Friant Dam (Figure 20). During low flows in the San Joaquin River, there is a slight backwater into Cottonwood Creek that inundates about 70 feet of channel before a wall of trees is encountered. This channel is mostly scoured to bedrock with large angular boulders and a sandy veneer. Outside of this channel, the bed drops sharply into the San Joaquin River channel where river depths quickly reach 20 to 30 feet.

In August 2021, the backwater area held 7.9 cubic yards of sand. From a grab sample, the median grain size ( $D_{50}$ ) was 0.91 mm, and 92.3 percent of the sample was finer than 2 mm. It is unknown when this sand was deposited, however, operators at Friant Dam stated that the creek flowed in February of 2021. The creek was said to be turbid and was compared to the color of chocolate milk, indicating sediment entrainment. Because Friant Dam releases never exceeded 334 cfs, it is likely bedload would have encountered a backwater, and deposited within the backwater area or shortly thereafter. An August 2021 video of the San Joaquin River bed at the confluence showed mostly coarse gravel and cobble heavily covered in an algal mat, with trace

amounts of clean coarse sand and fine gravel. Video logging of the deep channel downstream of the confluence showed similar substrate (Figure 21), however the area lacks an algal mat and includes some zones of bedrock.

Cottonwood Creek did not flow between February 2021 and the next mapping event in September 2022; however, Friant Dam released flows of up to 1,600 cfs for several months between pulse flow and Contractor flow releases. Sand volume in the backwater area was 10.4 cubic yards, a 32 percent increase since 2021. While I would have expected sand content to have decreased, it is possible that sand could have been transported into the backwater area from Cottonwood Creek and the San Joaquin River's shared floodplain during the increased releases from Friant Dam, or that these calculated sand volumes reflect the error of the probing method.

Cottonwood Creek experienced multiple significant flow events in early 2023, during which bedload sampling demonstrated that significant amounts of sand and fine gravel were transported (see Chapter 2). Sand mapping in August 2023 revealed that all sand and fine gravel had been scoured from the confluence backwater area. A grab sample from the now-dry bedload sampling location showed that the median grain size ( $D_{50}$ ) was 0.83 mm, and 85.3 percent of the sample was finer than 2 mm, slightly larger than the median bedload grain size and slightly smaller than 2021 backwater area grab sample. A November 2023 video of the San Joaquin River bed in the deep channel downstream of Cottonwood Creek showed mostly bedrock, coarse gravel, and cobble. All substrate was covered in a thin layer of a fine material that clouded the water column when disturbed by the camera. No sand was found on the bed of the deep channelized chute (Figure 21).

### ***Friant Cove***

The Friant Cove area that I mapped starts at the end of the deep bedrock chute and ends at the North Fork Bridge (Figure 22). The upstream end of this area starts as a broad and deep pool lined with sandy gravel and cobble, and dense aquatic vegetation cover. The flow is bifurcated around two islands, around which there is significant in-channel sand storage in the center and river-left side.

In 2021, in-channel sand storage was 3,518 cubic yards, and increased to 4,415 cubic yards in 2022 after a peak flow of 1,810 cfs. This indicates that sand content increased 26 percent at this site even though there was no additional sand supplied from upstream in that period. It is possible that sand was transported from the deep upstream pool into this area, which would indicate a plausible limitation of the facies mapping due to the water depth. It is also possible that this is a reflection of the error of the probing method, since a similar sand content percent increase was seen in that time period upstream at Cottonwood Creek. Figure 22 shows a 2022 sand lens trailing on the river-left side of the downstream island that was not mapped in 2021 or 2023; while this additional area of sand might account for the sand increase discrepancy, there were no transects in that area that would have factored into the calculation.

Sand volume in 2023 dropped 48 percent from 2022, to 2,279 cubic yards. This decrease is commensurate with the sand extent mapping, since a significant area previously covered by sand and aquatic vegetation was now primarily gravel and cobble. It appears that the flood flows from earlier that year (peak flow of 10,400 cfs) may have flushed sand from the area. Video

surveying from November 2023 showed that the upstream pool was primarily gravel and cobble with sand present in trace amounts within the gravel interstices.

### ***North Fork Bridge to Lower Lost Lake***

This mapping area covers approximately 2.25 miles from the North Fork Bridge crossing to the downstream end of Lost Lake Park. This section is very straight and wide with deep pockets throughout. This section is primarily sandy gravel and cobble and has scoured to bedrock in many places. Sand was only mapped in a backwater midway through a riffle complex at the upstream end of this section, downstream of a broken bridge (Figure 23). Although sand extent only appeared to change here in 2023, sand depths were not measured here due to the backwater nature of the area.

In all years, it was common to find thin veneers of sand overlying bedrock near the banks of Lost Lake Park. These veneers were typically less than 2.5 cm thick and I did not map them or calculate their volumes because they were insignificant compared to the other plumes of in-channel sand. It is likely that small amounts of sand trickle in from the banks due to the high-use park. It was also common to find picnic tables and park infrastructure within channel near the banks, indicating near-channel land disturbance. Mapping in 2023 revealed that many banks within Lost Lake experienced minor erosion from the flood flows earlier that year.

### ***In-channel Gravel Pits***

This mapping area covers a 1-mile section from the downstream-most riffle at Lost Lake Park to the upstream end of Ledger Island (Figure 24). This reach is generally very deep and scoured to bedrock, other than two square sandy pools that appear to be abandoned in-channel mining pits. Video logging of the deep upstream section revealed bedrock and gravel with no sand. This area leads into a straight chute that features an igneous and metasedimentary bedrock contact running down the center channel, where only a thin sand veneer lines the river-right bank. Downstream, both of the square pools have significant sand content, but are intermixed with fine gravels. Because they are not completely sand bedded and the channel width is very broad, it is likely that these pools are relatively stable and will not scour to bedrock like the straight and narrow chutes on the upstream and downstream ends of this section. There is a grassy floodplain on the river-right between these pools with very clean, white sand that was present after the flood flows of 2023. The sand appeared to be deposited in a lens about 15 cm deep on the floodplain during the flood, had a median grain size diameter of 0.87 mm, and 88.2 percent of the sample was finer than 2 mm.

In 2021, the total sand content in this area was 37,131 cubic yards. In 2022, that volume decreased 15.3 percent to 31,815 cubic yards, and then decreased an additional 16 percent to 28,232 cubic yards in 2023. This indicates that the pulse, contractor, and flood flows might have been effective at evacuating sand from this section; however, chapter 1 of this thesis investigated bedload 1 mile downstream of these pools and found only trace sand in transport at 1,500 cfs during the pulse flows. If sand did mobilize in these pools during the pulse flows, it likely did not propagate downstream to the east end of Ledger Island. Alternative hypotheses are that: the sand needed longer than the pulse flow duration to transport that far; the sand became trapped in the deep pool upstream of Ledger Island; it is an error in the probing method; or that the heavy

organic debris present during the pulse flows effectively clogged the sampler device mesh and prevented the sampler from intaking sand due to upstream backpressure.

Figure 24 shows that the in-channel gravel pit #2 sand extent doubled from 2021 to 2022, despite the listed volume decreasing. This is most likely a mapping discrepancy resulting from a change in floating aquatic vegetation coverage on the river-right, in which more riverbed became exposed after the contractor release flows of 2022 flushed macrophyte from the area.

### ***Ledger Island and Sumner Peck Ranch***

This mapping area covers a section about 0.5 miles along the southeastern end of Ledger Island, adjacent to the Sumner Peck Ranch winery (Figure 25). Its downstream boundary is the Ledger Island bridge 5.4 miles downstream of Friant Dam. The area is characterized by a long sweeping right-hand bend in the river that begins deep and shallows downstream. In 2021, the total sand content in this area was 18,670 cubic yards with channel wide coverage down to the boat launch at Sumner Peck Ranch. At that point, the river shallows to wadable depths (at flows below 400 cfs) and is mostly sandy gravel down to the riffle crest about 400 feet upstream of the bridge, at which point bed substrate becomes mostly gravel and deepens to the bridge.

In 2022, sand content decreased 29.4 percent to 13,180 cubic yards and was mostly stored on the inside of the bend. Sand content and coverage in 2023 remained virtually unchanged, measuring 13,165 cubic yards. This trend implies that sand may have flushed from this area during increased flows in 2022, however, Chapter 1 of this thesis shows from bedload sampling in February 2022 that only trace amounts of sand were observed in bedload 0.35 miles upstream of this area. Figure 25 shows the sand coverage extent increased downstream along the inside bank after 2021; it is likely that this sand was there in 2021, however, may it have been covered by floating vegetation.

### ***Eroding Bank***

The eroding bank at Ledger Island begins 400 feet downstream of the bridge and continues for an addition 600 feet downstream along the river-right side (Figure 25). The bank being eroded is shaped like a trapezoidal prism, with its long axis running parallel to the river and separating it from an abandoned mine pit. Several pipes and electrical lines emanate from the vertical bank face and drop into the river as they break under gravity. One large rusty pipeline juts out from the bank toward a metal corrugated culvert lying submerged in the pool beneath, which is attached to a pump motor. Upon examination of the vertical bank face, it is apparent that the bank was formed by sequentially deposited uniform layers of silt, clay, and fine sand, each layer about 12 inches thick (Figure 26). Several of these layers make up the consolidated bank face that overlies unconsolidated sand, forming low angle sluff at the river's edge. The vertical bank face strata lacks sedimentary structures that would indicate alluvial processes; however, the upstream end of the bank below the elevation of the vertical face shows alluvial sedimentary structures including thin laminar bedding of varying thicknesses, and a load cast resembling a drop stone. The bank has shown evidence of erosion since the high-water year of 2011 (Figure 27) when vegetation was scoured from the bank. Subsequently, lateral erosion of the bank has been propagating toward the abandoned mine pit at about eight feet/year.

In 2021, the bank had eroded an average of 71 feet since 2011. At that time, the pool at the toe of the bank appeared to hold a significant amount of sand, with total volume measuring 3,080 cubic yards. The following year, the bank laterally eroded an additional 3.4 feet on average (maximum of 10.4 feet) between March and August, and sand content in the pool decreased 48.4 percent to 1,589 cubic yards. In 2023, the bank eroded beyond the survey stakes I placed, so I was not able to use them to calculate erosion distance; however, the maximum amount of sediment that could have been measured with the survey stake configuration was 2,356 cubic yards, so they still provided a minimum amount of sediment supplied during that time. Using Google Earth imagery, I calculated the amount of additional bank erosion between 2022 and 2023 was about 10.5 feet on average. The sand volume in the pool increased in 2023 by 22 percent, to 1,944 cubic yards. In total between 2021 and 2023, the bank eroded an average of 13.9 feet laterally and a volume of about 2,700 cubic yards (about 4,000 tons). Because more sediment eroded from the bank than was measured in storage in the pool below, it is evident that sand is being mobilized downstream.

The bank tends to erode by calving off large blocks of consolidated sediment, as compared to winnowing away gradually (Figure 26). At low flows, the bank is protected by a flow eddy that keeps the main current off the sandy sluff at the base of the vertical bank. The river is shifting its path to the north here as it continuously bends into the bank and away from the gravel point bar on the river left. This bend seems to be forming by means of bank-pull instead of by bar-push, since the river left gravel bar does not appear to be growing and the eroding bank exhibits a series of fissures extending parallel to the eroding bank face. The changing residual sand volume within the pool below appears to be dependent on the flows; while bedload sampling described in Chapter 1 of this thesis was not able to demonstrate sand transporting at Ledger Island at 1,500 cfs, it is evident that sand was flushed from this pool during the time that flows were as high as 1,600 cfs.

The vertical bank face is comprised mostly of silt and finer grains and was not sieved. The unconsolidated sand unit at the base of the vertical face had a median grain size diameter of 0.57 mm and 97 percent of the sample was finer than 2 mm.

### ***Ledger Island to Riffle 40***

This mapping area covers a section about 0.5 miles long between Ledger Island and Riffle 40 (Figure 28). The channel here is wide and too deep to wade at low flows. The bed is scoured to bedrock in many spots, and otherwise is largely composed of gravel with lenses of sand stretching downstream. I measured sand content here in 2021 to be 10,780 cubic yards. In 2022, sand content decreased by 6.3 percent to 10,103 cubic yards, and decreased an additional 58 percent in 2023 to 4,283 cubic yards. While the extent of sand coverage did not change substantially between most years, the biggest difference was a thin veneer of sand covering the channel at the pool tail-out near approaching riffle 40. It is worth noting that bedrock outcrops in the channel here at low flows revealing a lahar, where a volcanic matrix once entrained river gravels in the paleo San Joaquin River, forming a conglomerate bedrock not seen in any other section of this study reach.

### ***Riffle 40 to Riffle 38***

This mapping area covers a section about 0.8 miles long between three prominent riffles in the study reach (Figure 29). Riffle 40 contains mostly gravel and cobble substrate with small pockets of sand in protected areas. The run immediately downstream of riffle 40 contains cobble and gravel substrate that was covered in a thick algal mat in 2021 and 2022, but was washed clean after the flood flows of 2023. At low flows, riffle 39 forms a distinct right bend where the mainstem San Joaquin River meets a confining bluff and the confluence of a secondary channel that only activates during high mainstem flows. This confluence marks a sand depositional environment where sand was measured up to 2 m deep (with a median grain size diameter of 0.58 mm and 95 percent of the sample finer than 2 mm). Downstream, outcrops of the Friant Tuff are exposed within the river-right half of the channel which form flat slabs, resembling concrete. The tuff is weathering to clay and exhibits a sticky texture when probed. This unit forms the base of the channel for at least 1,000 feet and is largely overlain by alluvial sand and gravel.

In 2021, I measured 22,896 cubic yards of sand in this area. This was the largest volume of sand I measured throughout the study reach in all three mapping seasons. This volume decreased 28.5 percent in 2022 to 16,366 cubic yards, which is also reflected in the sand mapping in Figure 29. After the flood flows in 2023, sand content decreased an additional 12 percent to 14,338 cubic yards. This change is reflected mostly in the sand storage at the downstream confluence of the secondary channel, where it appears that the channel's activation flushed out sand that was being deposited there in an eddy during low flows. The straight chute downstream of the bend at riffle 39 appears to have sand stored against the low flow inside bend, even though this was the center channel during 2023 flood flows when the river swelled to 560 feet wide here.

### ***Little Dry Creek Confluence***

The area where Little Dry Creek meets the mainstem San Joaquin River is almost entirely gravel with some outcrops of Friant tuff (Figure 30). Traveling upstream into Little Dry Creek, the substrate was almost entirely scoured to Friant Tuff bedrock in 2021 with the exception of some gravel and a protected area at the bank with very coarse sand. This sand was the coarsest that I encountered throughout all three mapping seasons, with a median grain size diameter of 1.56 mm and 64 percent of the sample finer than 2mm. Mapping was not performed here in 2022, however, a small sand pocket was deposited near the confluence in 2023 with more gravel than in 2021. While there was no sand delta at the confluence, in-channel sand content increased 500 feet upstream in Little Dry Creek. A grab sample had a median grain size diameter of 1.52 mm with 64 percent finer than 2 mm, nearly identical to the previous sample from two years prior. Ultimately, this area shows signs that sand does transport this far down Little Dry Creek, albeit only during exceptionally high flows such as 2023.

Six-hundred feet downstream of the Little Dry Creek confluence is a large backwater area where the channel bifurcates. The right channel flows to the north end of Rank Island during high flows, and the left channel marks the mainstem San Joaquin River. The backwater area holds a significant amount of sand, however, I did not measure the sand volume here because it

appeared to be protected from flows. The upstream end of this backwater has an outlet where a secondary channel rejoins the mainstem at high flows. Even though this secondary channel activated during high flows of 2023, it was not apparent through sand mapping if there was a change in stand storage or a flux of sand movement through this area.

### ***Donaghy/Rank Island***

This mapping area covers approximately 0.5 miles where sand was stored near a riverside mansion south of Rank Island (Figure 31). The channel here is wide and has a thalweg about 10 feet deep through a pool near the left bank, but shallows toward the inside bend where I observed sand in all three mapping seasons. Near the downstream end of the mansion lawn lies a distinct trapezoidal gravel bar that traverses the channel perpendicular to flow; it is suspected to be bed material stockpiled from the artificially constructed and maintained 10 ft deep pool upstream.

In 2021, this area contained 10,117 cubic yards of sand with coverage reaching from mid-channel to the river right bank. Sand depths increased toward the right bank, and mid-channel sand plumes exhibited distinct ripples. In 2022, sand content decreased 31 percent to 6,975 cubic yards while simultaneously increasing the amount of coverage across the channel. It is possible that the previously existing sand plumes were spread more evenly by the increased flows of 2022, while also flushing some from the area. A year later, sand volume decreased again by 54 percent to 3,219 cubic yards, with sand coverage limited mostly to the river-right side third of the channel. A distinct break in the 2023 sand coverage can be seen in Figure 31 where the previously mentioned gravel bar crosses the channel. Downstream from the mansion area, the channel bed is mostly sandy gravel with some sand plumes stored in protected areas of the inside bend, which were not accounted for in these volumes.

### ***Vulcan Chute***

This mapping area covers an area approximately 0.67 miles long adjacent to historic mining and Vulcan mining properties. The upstream area is a deep gravel bedded pool bracketed by two riffles, which leads into a narrow and straight chute. The chute is deep at the upstream end (greater than 10 feet deep) and shallows downstream to wading depths at low flows. This area exhibited some sand coverage in 2021 amounting to 1,076 cubic yards. The next year, sand coverage was limited mostly to long lenses extending downstream, however increasing 26 percent to 1,355 cubic yards; I did not map the sand coverage in this season. By 2023, all of the sand had flushed out of this reach and showed no surface coverage. It appears that this chute area has high transport capacity and is probably capable of flushing most of the sand that is supplied to it.

The very downstream end of the chute terminates in a left bend where flow is concentrated against the right bank, and it is actively eroding into the fine-grained bank in a similar manner as the eroding bank at Ledger Island. A stakeholder has applied rip-rap broken concrete blocks to the bank in an attempt to prevent erosion. About 200 feet downstream of the head of erosion, the right bank begins to display dense gravel deposits that the river is eroding and depositing up to 400 feet downstream at the head of Owl Hollow Pool.

### ***Owl Hollow***

This mapping area covers about 1,000 feet and is the downstream-most end of my study reach (Figure 32). Owl Hollow features a wide pool bracketed by two riffles. Owl Hollow pool is a mix of sand and gravel bedded zones, the boundaries of which have migrated since I began mapping in 2021. Sand storage in 2021 was 5,751 cubic yards and mostly limited to the upper half of the pool and the pool tail-out of the lower right channel. A grab sample from this sand plume had a median grain size diameter of 0.81 mm, with 92 percent of the sample finer than 2 mm. In 2022, the sand-to-gravel facies boundary migrated downstream about 200 feet. Although the sand coverage extent appears to have increased, the storage volume decreased 22 percent to 4,477 cubic yards. Chapter 1 of this thesis showed that sand was only found to transport through this pool in trace amounts at 1,500 cfs, however, it is evident that sand was mobilized through this pool at some point during the increased flows of 2022.

The following year, in 2023, the sand-to-gravel boundary shifted again, with coverage extent reduced from 2022, and mostly limited to the upper and right half of the channel. Additionally, the sand storage was removed from the pool tail-out of the lower right channel. Sand storage volume in 2023 reduced 18 percent from 2022, to 3,670 cubic yards. A grab sample from the sand plume had a median grain size diameter of 0.90 mm with 83 percent finer than 2 mm, slightly coarser than the grab sample from 2021. While these measurements indicate that sand was largely flushed from Owl Hollow pool over the last two years with increased flows, it should be noted that a large sand plume now exists at the head of the pool. As current enters the pool from the upstream riffle, it appears to scour away at a small eroding bank in the floodplain at the pool head. The current is concentrated toward the bank at low flows, possibly winnowing away material into the pool, and likely flushes it downstream as higher flows pass directly over the floodplain as observed in 2023.

### ***Total In-channel Sand Storage***

Total sand volume stored in-channel within the nine-mile reach was highest in 2021 and decreased each consecutive year thereafter (Figure 19). The total in-channel sand storage during late summer of 2021, 2022, and 2023 was  $113,000 \pm 10,000$  cubic yards,  $90,300 \pm 8,000$  cubic yards, and  $71,100 \pm 6,400$  cubic yards, respectively. Most of the sand storage areas experienced a decrease in sand storage between September 2021 and September 2022, except for the Cottonwood Creek confluence, Friant Cove, and the Vulcan Chute, which all increased their sand storage by 25 to 32 percent. Similarly, most areas had a decrease in sand storage from September 2022 to August 2023 except for gravel pit #2, the Sumner Peck Ranch area, and the Ledger Island eroding bank pool. Gravel pit #2 and the Sumner Peck Ranch area remained stable in sand storage, but the eroding bank pool had a 22 percent increase (533 tons). In total between 2021 and 2023, the bank eroded an average of 13.9 feet laterally and a volume of about 2,700 cubic yards (about 4,000 tons). Because more sediment eroded from the bank than was measured in storage in the pool below, it is evident that sand is being mobilized downstream.

Between September of 2021 and August of 2023, the in-channel sand storage within the study reach decreased 37 percent, and all sites experienced decreases in sand storage. Sand volume estimates at each site are provided in Figure 19 and Table 5.

### ***Grain Size Distribution***

The cumulative grain size distributions of the grab samples are shown in Figure 33. Figure 33 shows that the grab samples are distinguishable in three different groups where median grain sizes tend to cluster. The eroding bank at Ledger Island is the finest grained sand source in the study reach, which has nearly the same median grain size diameter as the riffle 39 sand plume, but has finer end members above the 80<sup>th</sup> percentile and below the 30<sup>th</sup> percentile. The coarsest site was Little Dry Creek, where sand was collected between 200 and 500 feet upstream of its confluence with the San Joaquin River.

The remaining five grab samples' (Cottonwood Creek, Owl Hollow, and the floodplain near in-channel gravel pit #2) median grain size diameter varied by 0.15 mm, but were more distinguishable above the 60<sup>th</sup> percentile and below the 40<sup>th</sup> percentile. At the 90<sup>th</sup> percentile, the pool at Owl Hollow in 2023 was the coarsest sample, followed by Cottonwood Creek at the cataraft transect site, the gravel pit floodplain, Owl Hollow pool in 2023, and the mouth of Cottonwood Creek; these five samples varied by about 1.5 mm at the 90<sup>th</sup> percentile.

### **Discussion**

#### ***Bedload Flux Through the Study Reach***

Sand mapping and volume measurements show that in-channel sand storage decreased within the study reach after several months of contractor flows in 2022. While bedload transport sampling during the 1,500 cfs pulse flows was only able to confirm that trace amounts of sand transported through Ledger Island and Owl Hollow, Figure 12 illustrates that other researchers have measured sand transport at moderate and low flows within the study reach. Additionally, Figure 19 shows that in-channel sand storage decreased significantly at the sites immediately upstream and downstream of the Ledger Island sample site, and that sand volume decreased in the Owl Hollow pool, indicating sediment transport there.

Conversely, Figure 24 shows that the in-channel gravel pit #2 sand extent doubled from 2021 to 2022. This is most likely a mapping discrepancy resulting from a change in floating aquatic vegetation coverage on the river-right of the channel, in which more riverbed became visible after the contractor release flows of 2022 flushed macrophyte from the area. Similarly, Figure 32 shows that the area of sand coverage at Owl Hollow pool increased from 2021 to 2022 despite a 22 percent decrease in sand volume measured by the probing method. Although these results might seem contradictory, it is possible that the sand stored within Owl Hollow pool was redistributed to cover a greater area while some sand flushed from the pool. While the sand mapping and probing methods are not perfect, they improve our understanding of sand mobility through the study reach when they are interpreted together and not in isolation.

## Conclusions

I set out to answer the question “how is sand transported and stored within a 9-mile reach of the San Joaquin River, directly downstream of Friant dam at flows ranging between 220 and 10,000 cfs?” Chapter 1 of this thesis shows that sand has very low bedload transport rates at low flow rates (up to 600 cfs) and likely occurs infrequently and discontinuously at discrete locations. Other studies have shown that moderate flows (about 1,300 cfs) are capable of transporting sand in bedload where there is ample bed shear stress and sand supply; however, only trace amounts of sand bedload transport were measured at Ledger Island and Owl Hollow when we sampled there at 1,500 cfs. This suggests that sand transport at moderate flows is discontinuous throughout the reach due to low shear stress “bottlenecks” where the sand deposits on the bed, typically in pools. High flow bedload sampling at Ledger Island and Owl Hollow confirmed that a 6,000 to 7,000 cfs flow release is capable of mobilizing the size ranges of sand that we measured in storage on the bed. Order of magnitude differences in bedload transport rate at these sites show that more sand is exiting the study reach than passes through the halfway point, thus suggesting increasing sediment supply downstream, which is an opportunity for additional research.

We then showed in Chapter 2 that Cottonwood Creek delivers sand (and gravel) at the top of the study reach during infrequent flows as low as 160 cfs. We estimate that Cottonwood Creek supplied about 50 tons of sand during a storm in March 2023, and about 450 tons to the San Joaquin River throughout the study period. High flow releases from Friant Dam are capable of transporting the episodic sand deliveries by Cottonwood Creek downstream beyond the deep bedrock chasm between the dam and North Fork bridge, the bottom of which is almost entirely gravel, cobble, and bedrock.

Chapter 3 then showed that the sand supplied by Cottonwood Creek, the eroding bank at Ledger Island, and other minor near-channel sediment sources was flushed through the study reach, and further suggests a 37 percent decrease in sand content since my initial mapping in 2021. I estimate that in-channel surficial sand content was as high as 170,000 tons in August 2021, and then decreased after an extended bankfull flow event in 2022 and a 12.5 year recurrence high flow to 107,000 tons in August 2023. The results of this thesis indicate from multiple methods that in-channel sand storage within the study reach is decreasing, despite episodic sand contributions from tributaries and near-channel sources.

## Figures and Tables

**Figure 1. Map of the 9-mile study reach of the San Joaquin River between Friant Dam and Owl Hollow, in Fresno and Madera counties, near the city of Friant California. Blue markers indicate the number of miles downstream from Friant Dam. The inset map shows the San Joaquin River's westward flow to the Pacific Ocean and its highlighted drainage area. The star marks the approximate study reach near Fresno, California.**

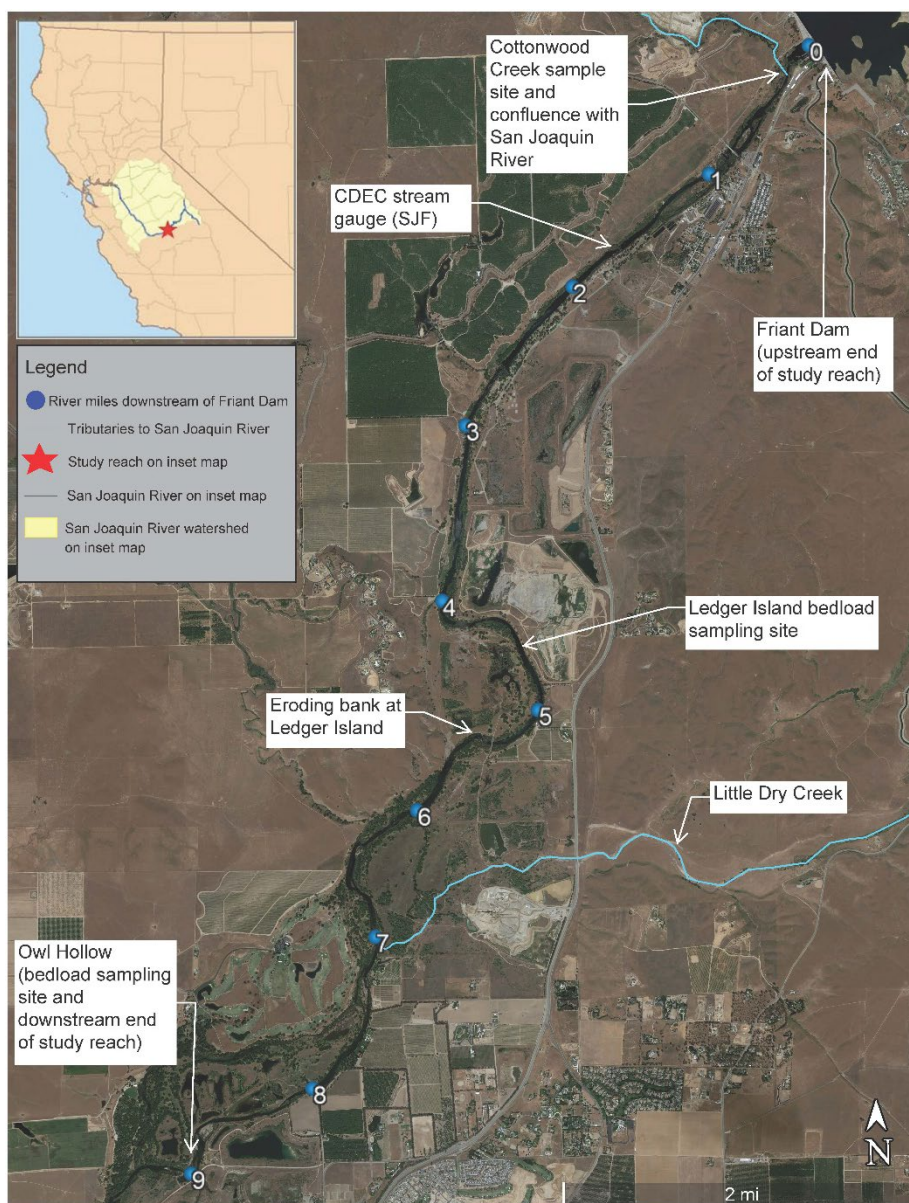


**Figure 2. Hydrograph of the San Joaquin River at USGS stream gauge 11251000 San Joaquin River below Friant (SJF) showing hydrology during the study period. The blue boxes indicate the approximate time of bed sand storage mapping. The pink box shows the approximate time of increased flows for San Joaquin River Exchange Contractor deliveries, and the red circles show the approximate timing of bedload transport sampling events at bankfull (moderate flows) and high flow events.**

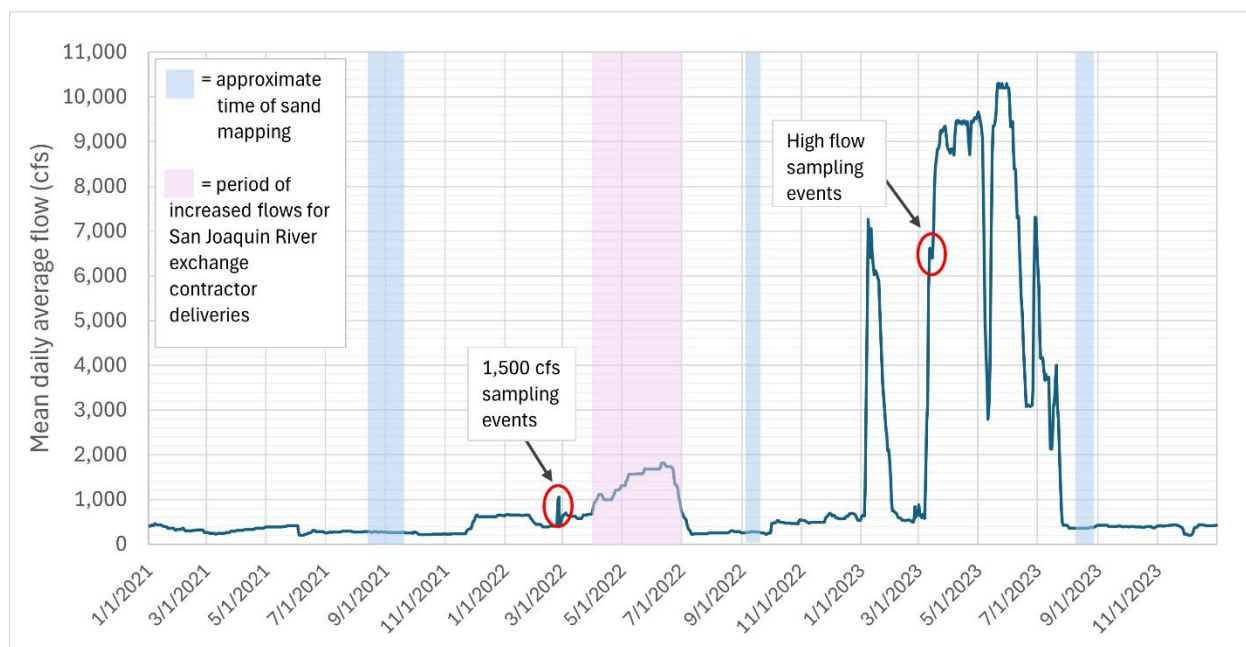


**Figure 3. Helley-Smith bedload sampler at low flows within sandy gravel substrate at the downstream Owl Hollow riffle. The cobble was placed on top to ensure that the sampler entrance remained flush on the bottom plate. River flow is from right to left, and sand is present on the bed.**

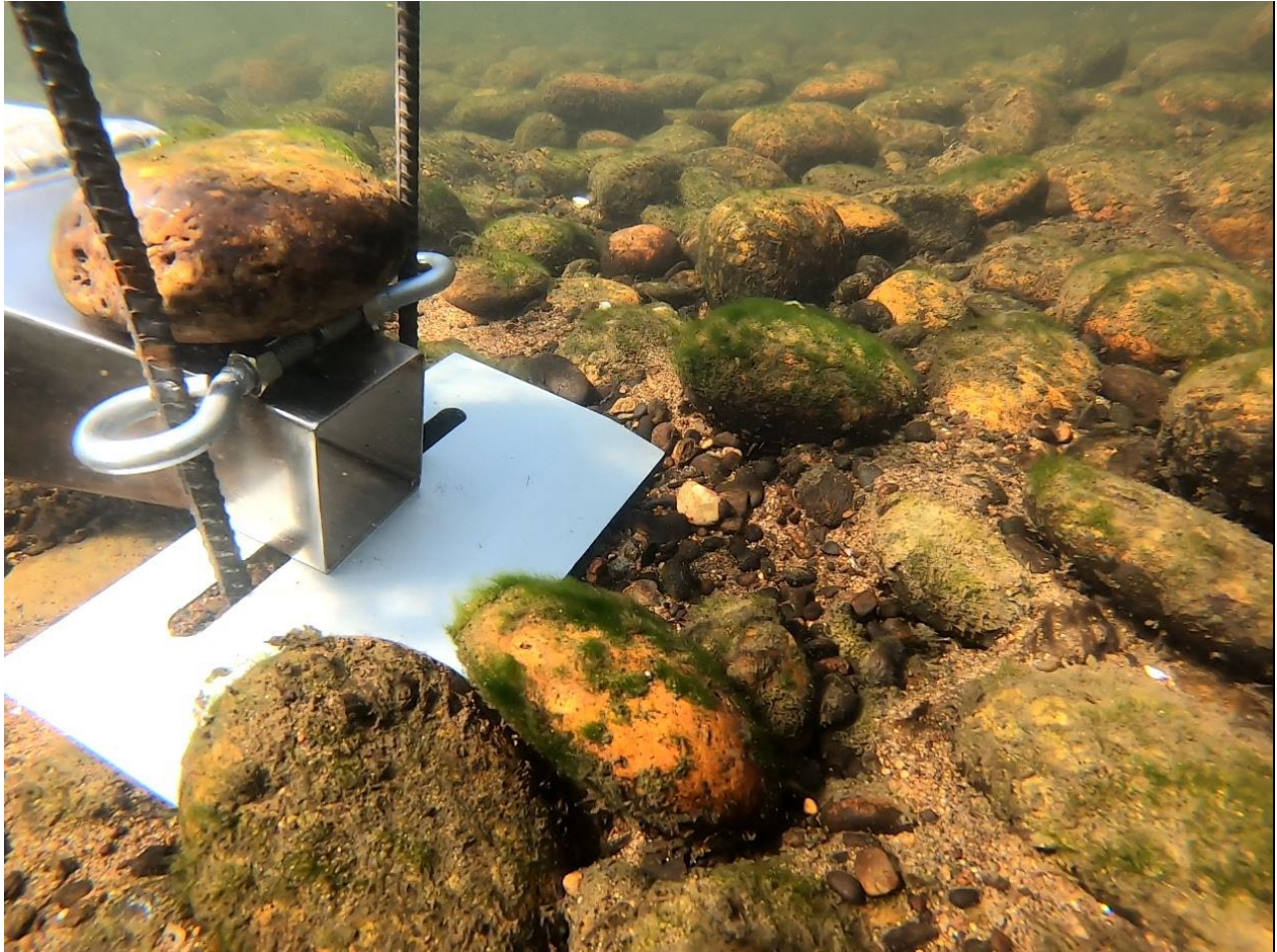


**Figure 4. Low-flow bedload transport rates measured with Helley-Smith bedload sampler, organized by downstream location.**

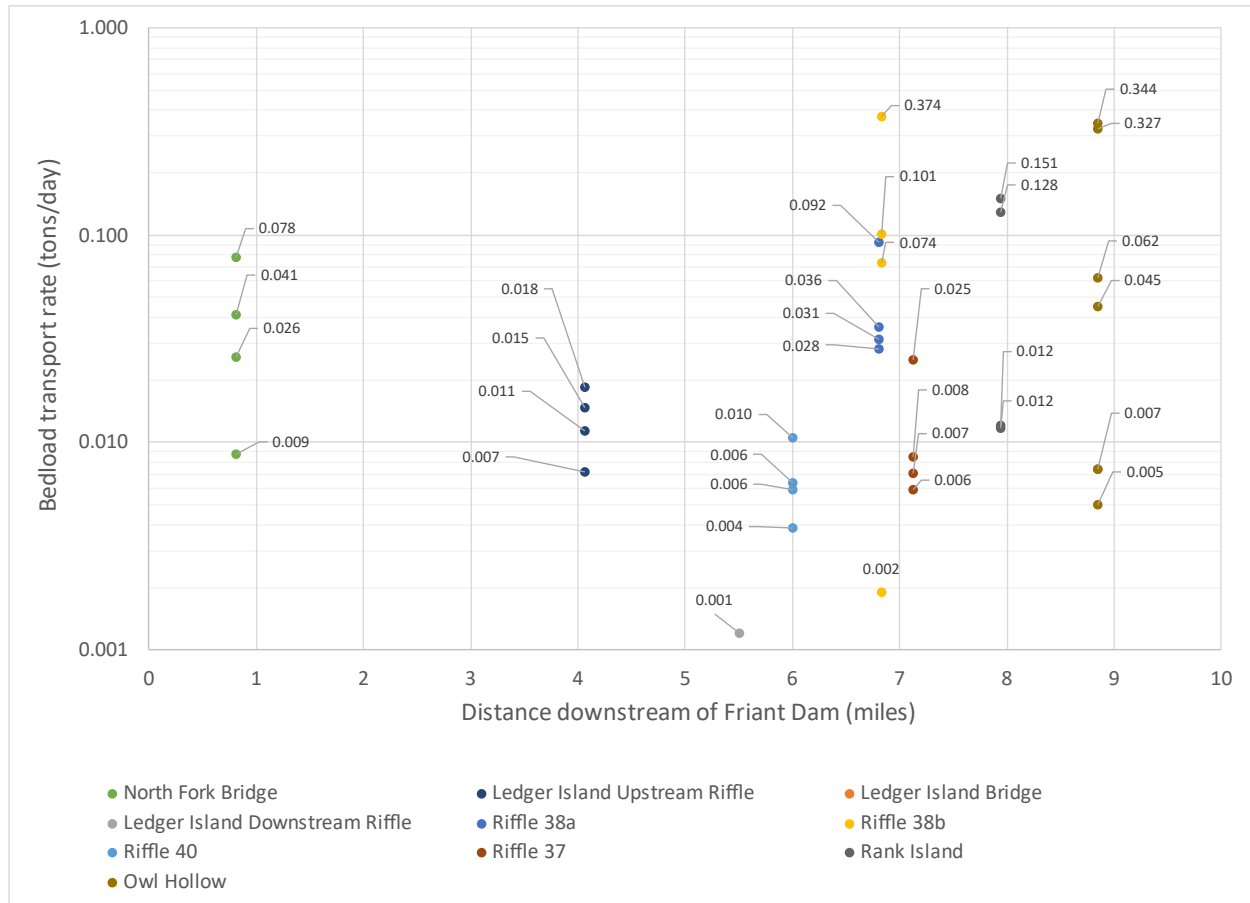


**Figure 5. Mean low-flow bedload transport rates, organized by downstream location.**

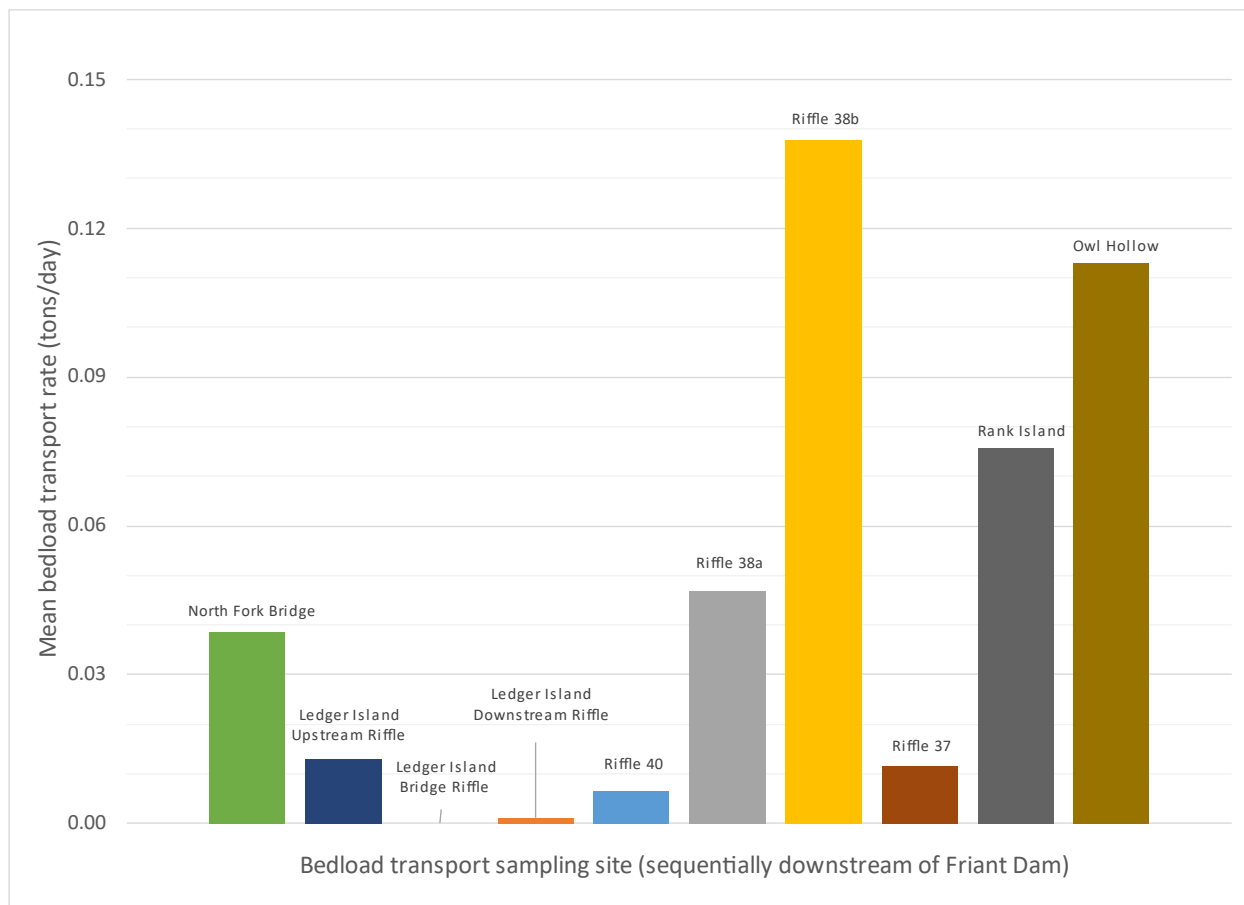


**Figure 6. Hydrograph from California Data Exchange Center stream gage San Joaquin River Below Friant (SJF), illustrating two pulse flow releases from Friant Dam.**

**The red squares indicate the approximate times when bedload samples were collected. Because this stream gaguge is several miles upstream of the sample locations, peak flows during sampling were lower than shown on the hydrograph. Acoustic Dopplar Channel Profiler data confirmed that river discharge was about 1,500 cfs during sampling.**

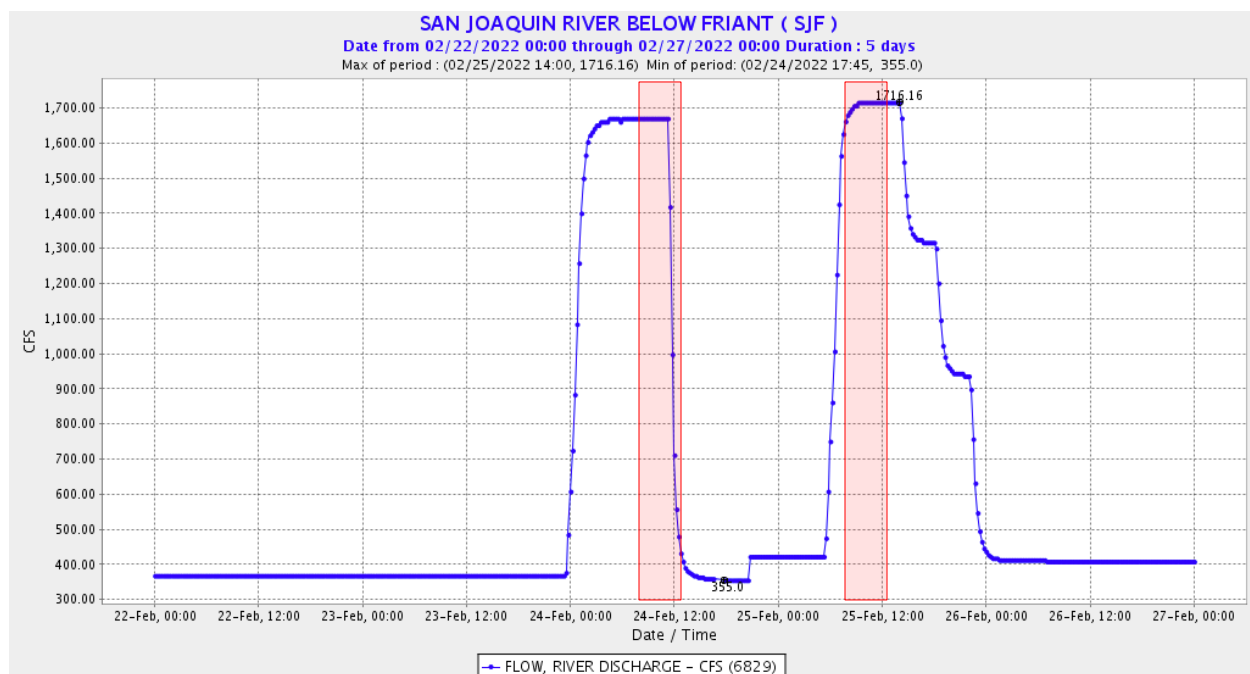


**Figure 7. Large amounts of organic debris and trace amounts of sand were collected in bedload transport sampling at 1,500 cfs during the pulse flows in February 2022.**



**Figure 8. Trace amounts of sand were collected in bedload transport sampling during the pulse flows of 1,500 cfs in February 2022. The mesh size of the TR-2 sampler is 0.5 mm.**



**Figure 9. Stream flow hydrograph and associated timing of bedload transport sampling during high flows of spring 2023.**

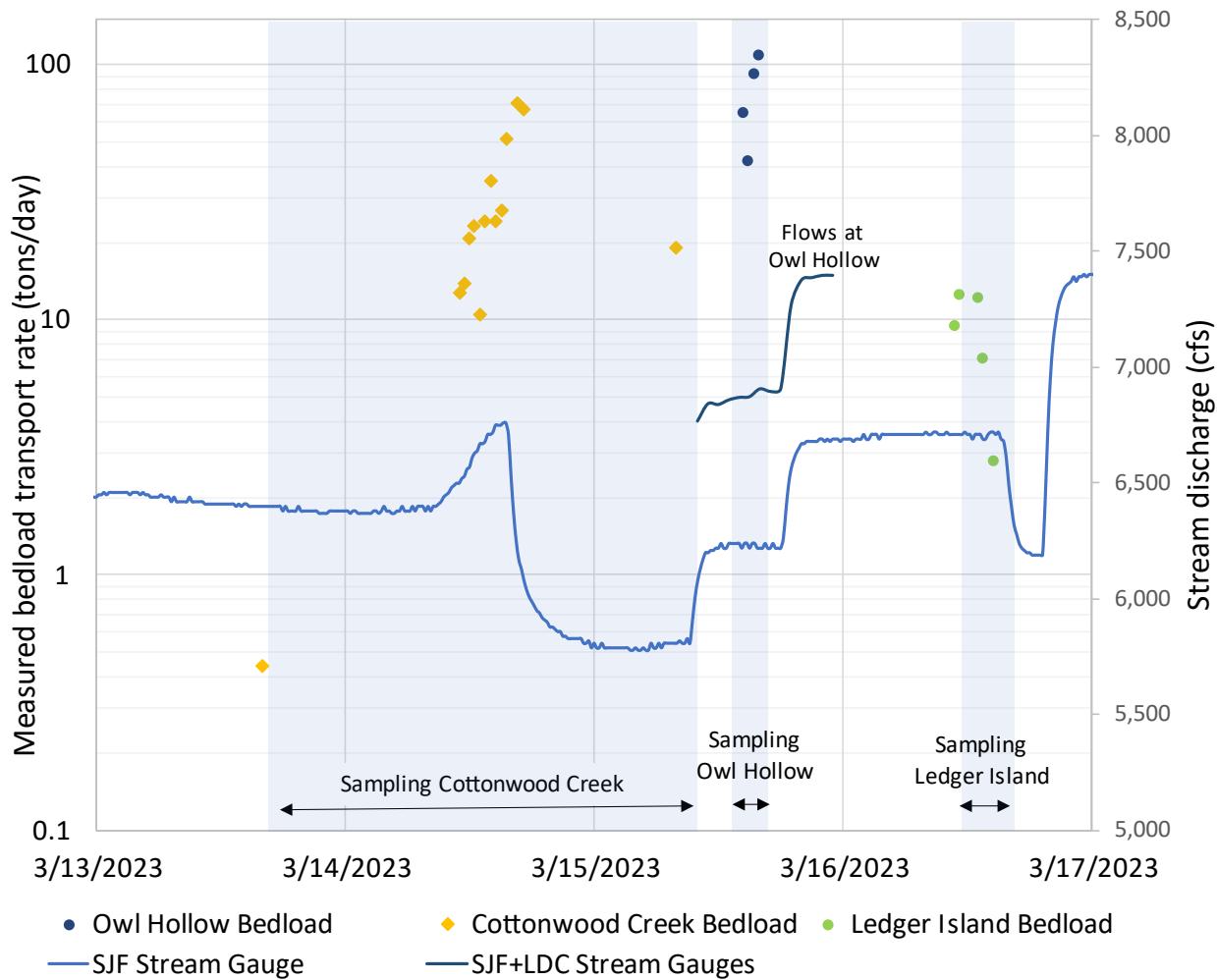


**Figure 10. Calculated bedload transport rates from samples collected by San Francisco State University in March 2023. The majority of sediment in transport at flows of 6,400 cfs and 6,900 cfs at Ledger Island and Owl Hollow, respectively, is comprised of sand sized particles. Gravel was measured in transport; however, it made up a small fraction of the bedload samples. Bedload transport rates were about an order of magnitude higher at Owl Hollow than at Ledger Island.**

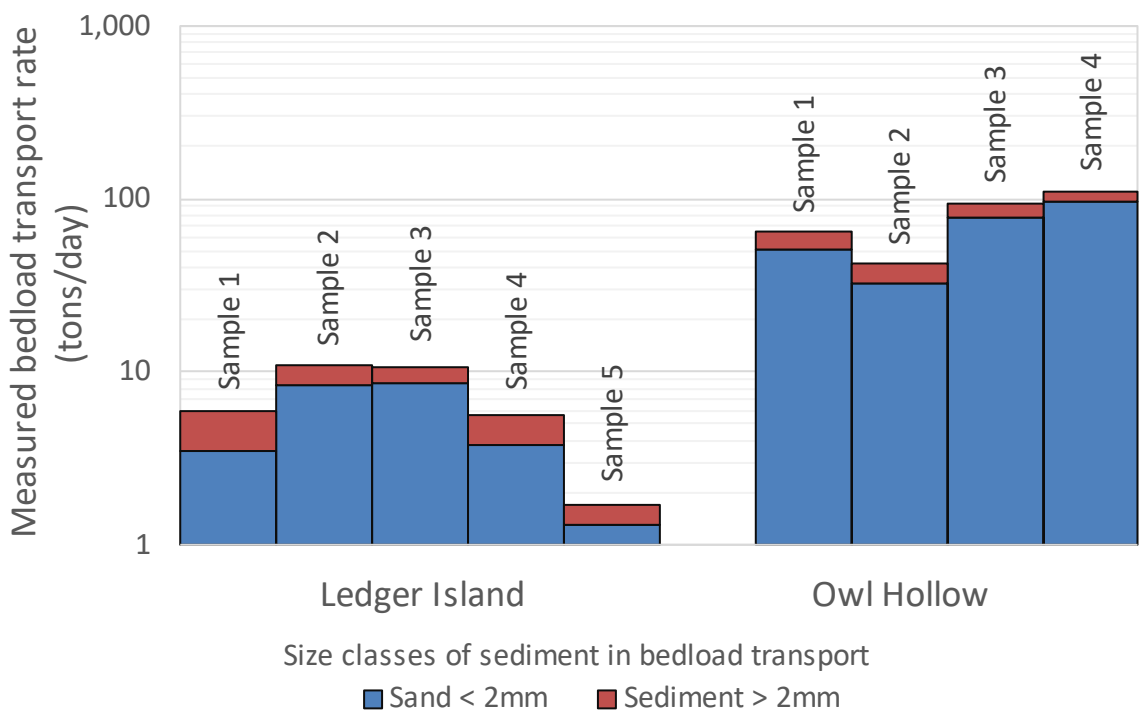


**Figure 11. Box and whisker plot comparing grain sizes between bedload samples (blue boxes) and bed material (brown boxes). Samples were collected from Cottonwood Creek, the mainstem San Joaquin river at Ledger Island and Owl Hollow, the eroding bank at Ledger Island, and the mouth of Little Dry Creek.**

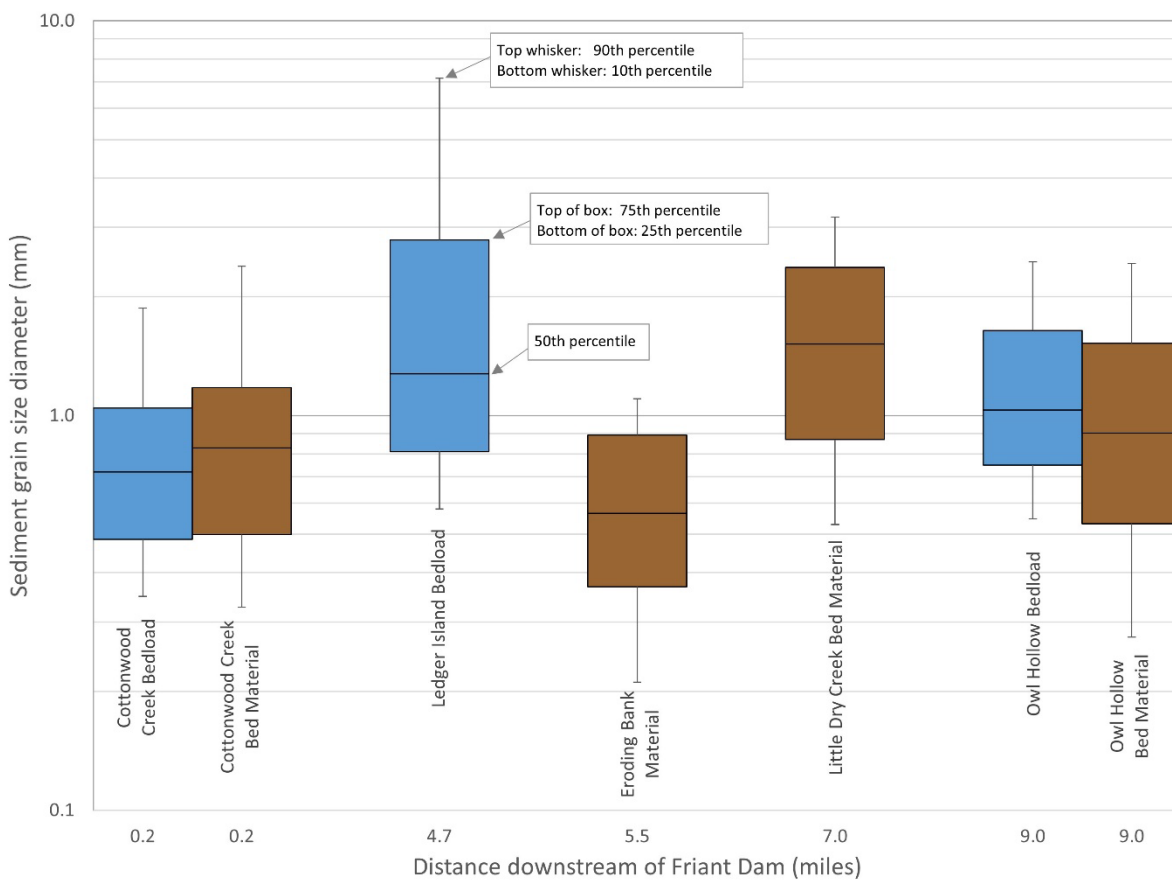


**Figure 12. Bedload transport rates measured on the San Joaquin River from multiple studies at different locations. All measurements were conducted within my study reach except for U.S. Geological Survey which were about 12 miles downstream of Friant Dam. The top panel shows that the ranges of bedload transport rates measured in my thesis are within the rates measured by other studies. The bottom panel shows modeled estimates of bed shear stress at corresponding bedload measurement sites. SFSU = San Francisco State University.**

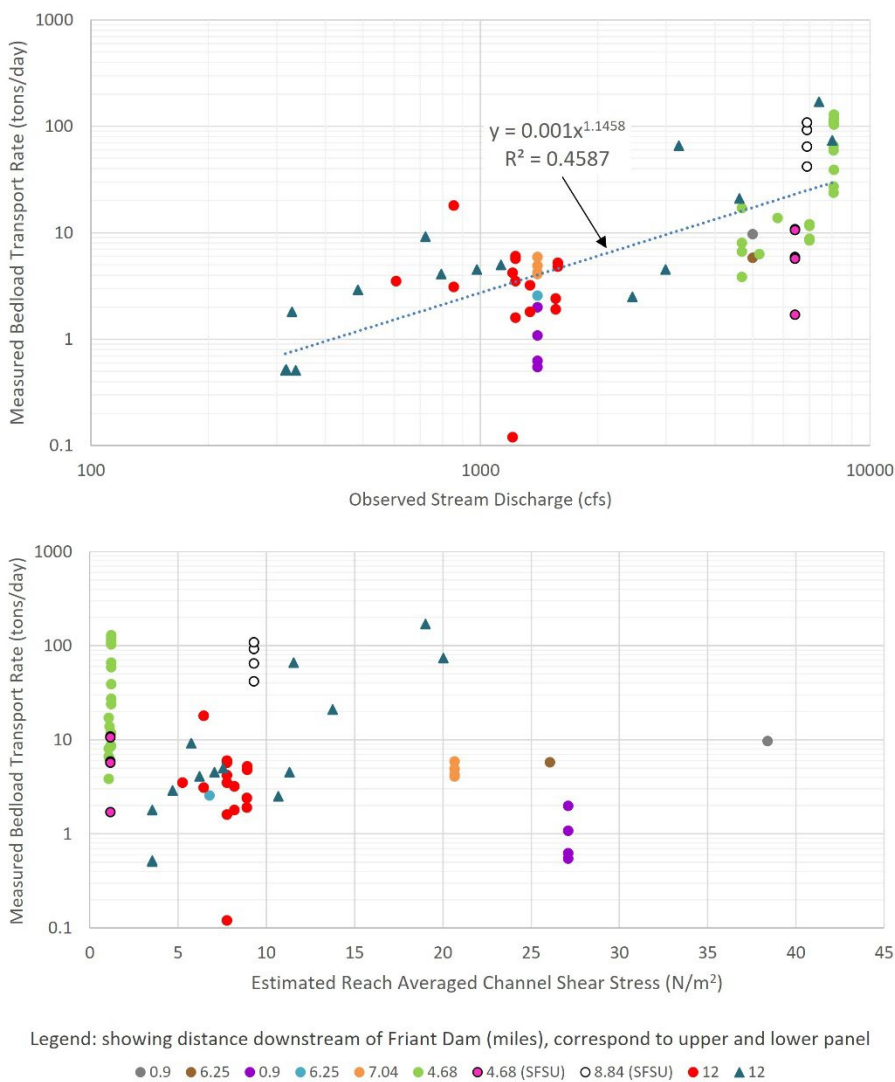


**Figure 13. HEC-RAS model transect locations near the bedload sampling locations at Ledger Island. The model transect locations in the aerial image correspond with the predicted shear stresses (color corresponding) across a range of flows shown in the inset plot.**

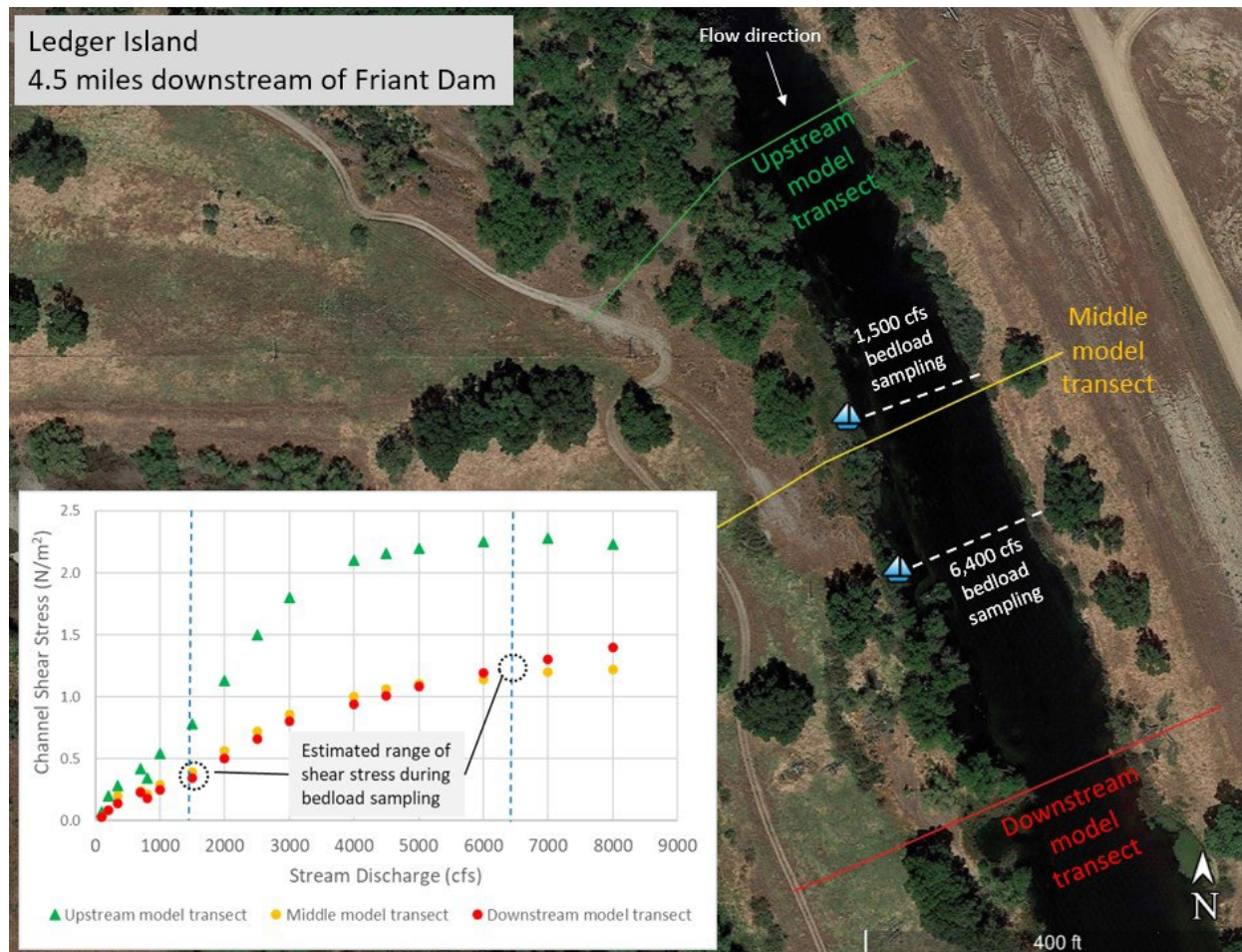


**Figure 14. HEC-RAS model transect locations near the bedload sampling locations at Owl Hollow. The model transect locations in the aerial image correspond with the predicted shear stresses (color corresponding) across a range of flows shown in the inset plot.**

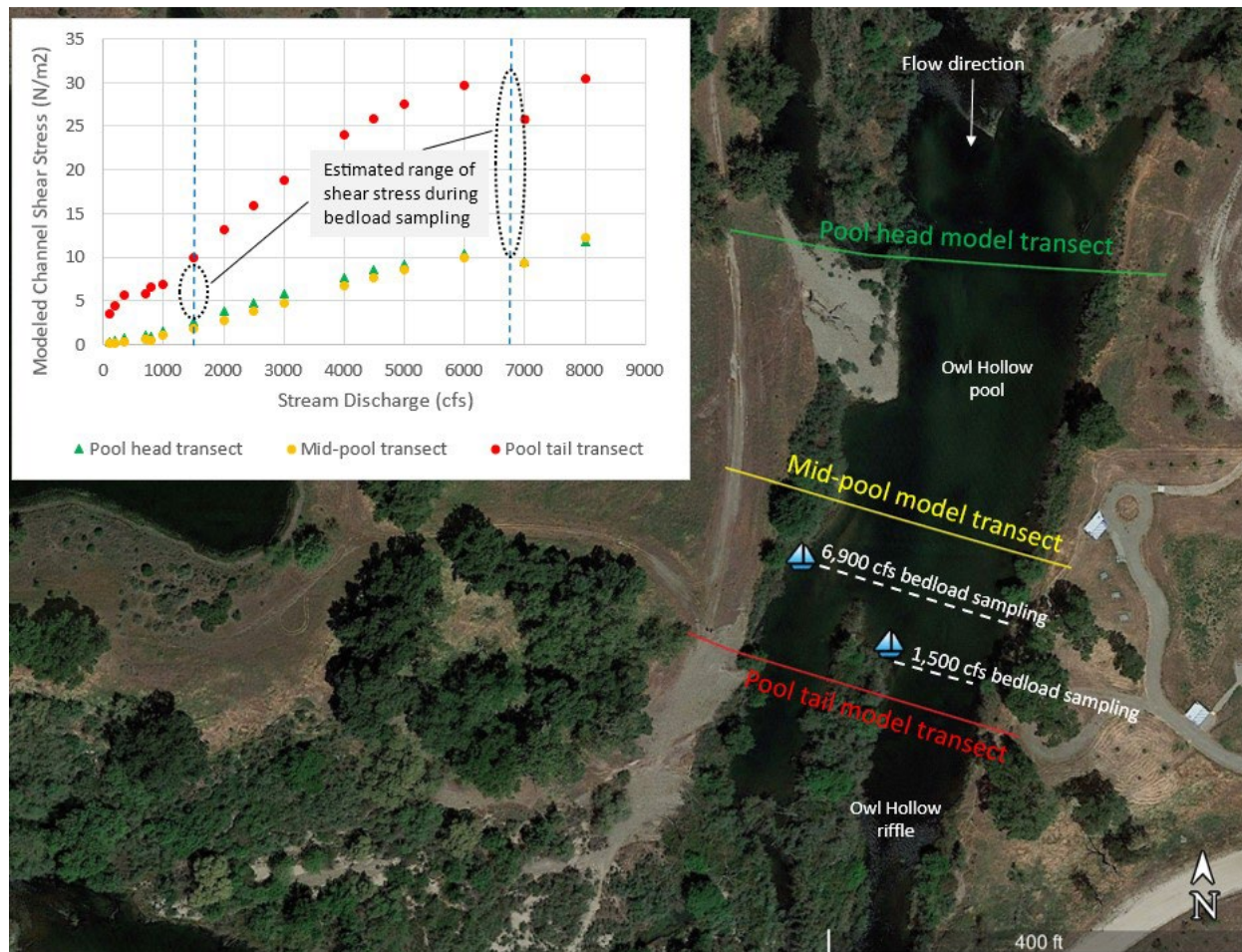


**Figure 15. Bedload rating curve at Ledger Island. The green data, trendline, and function represent data collected by Graham Mathews Associates in 2011, and the pink data represent bedload transport measurements collected by SFSU and McBain Associates at Ledger Island during high flows in 2023. The brown data, trendline, and function are representative of the average bedload transport rate at each corresponding stream flow rate.**

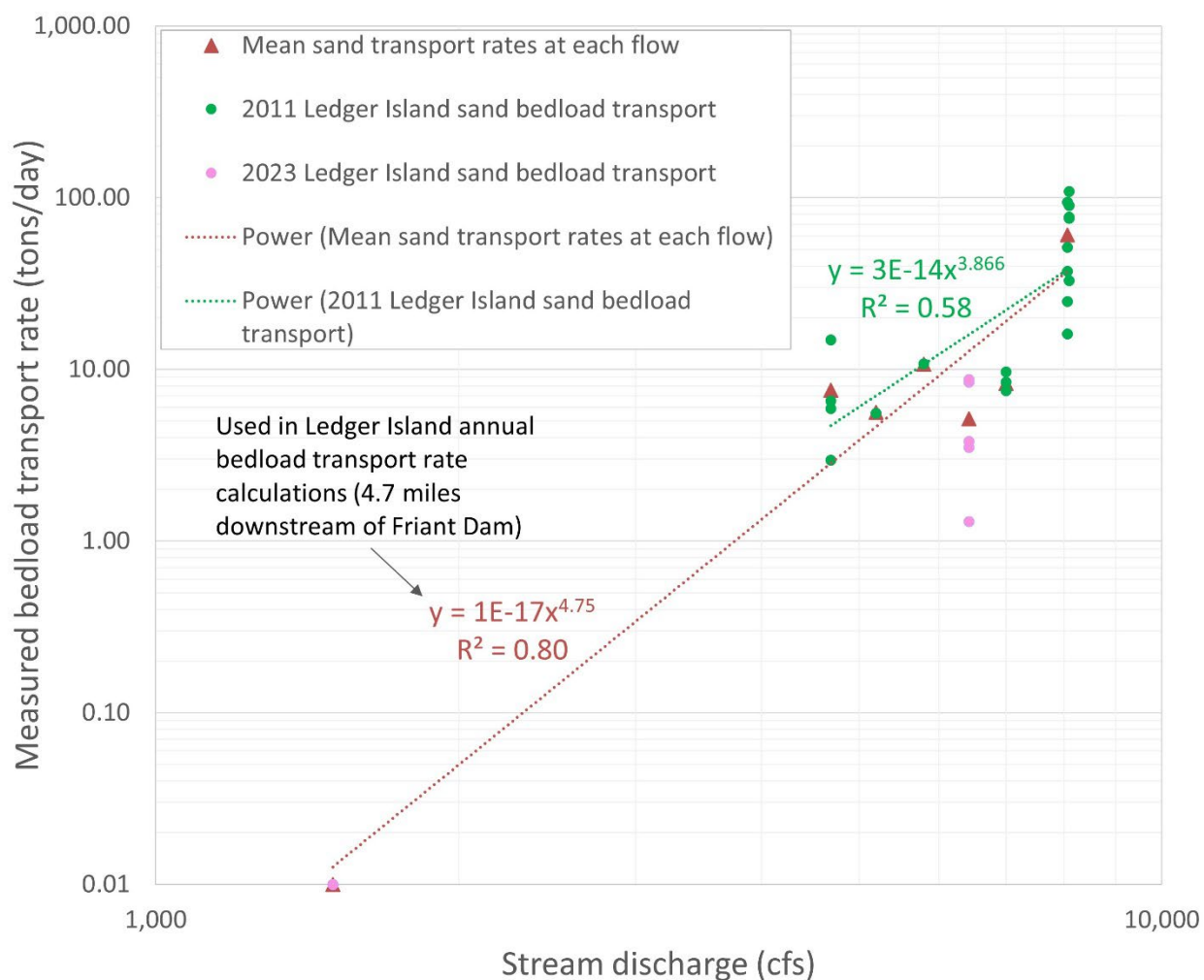


**Figure 16. Subsurface sand content shown as a percentage of substrate bulk composition in riffles downstream of Friant Dam, data from (Resources 2010).**

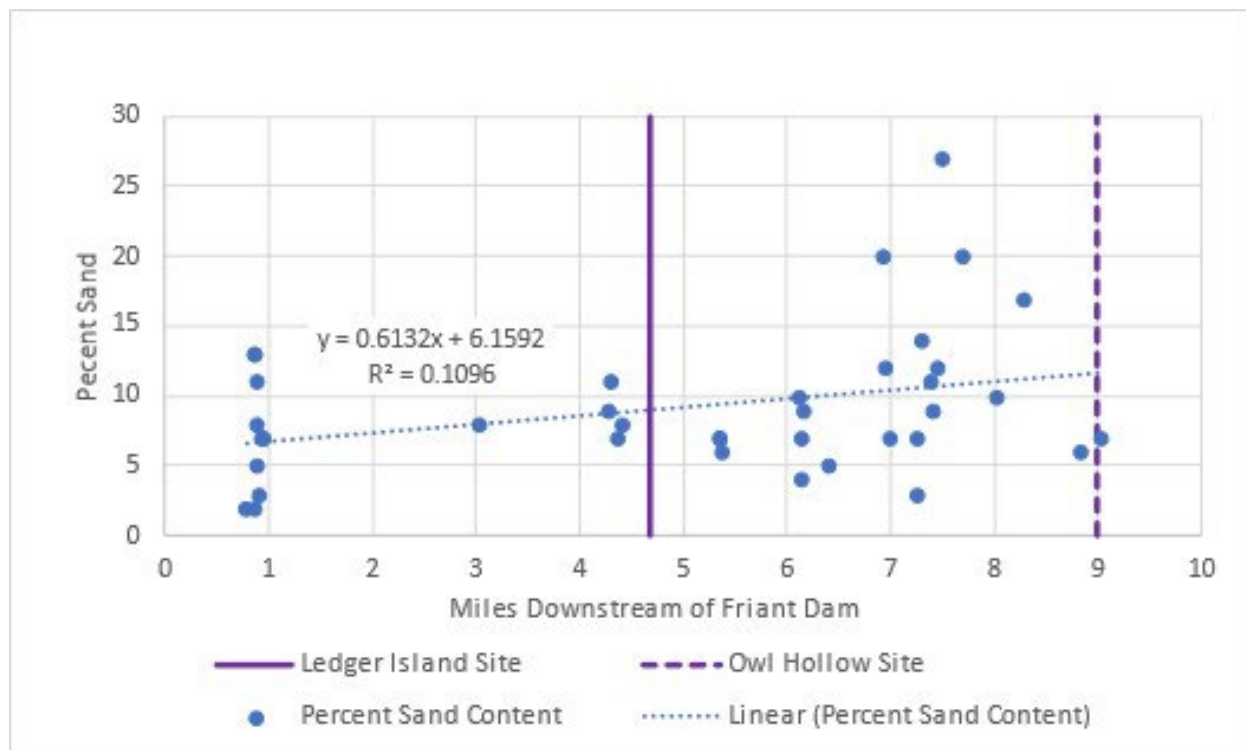


**Figure 17. Cottonwood Creek sedigraph showing the measured bedload transport rates and the estimated continuous transport rates during the sampling period in spring 2023.**

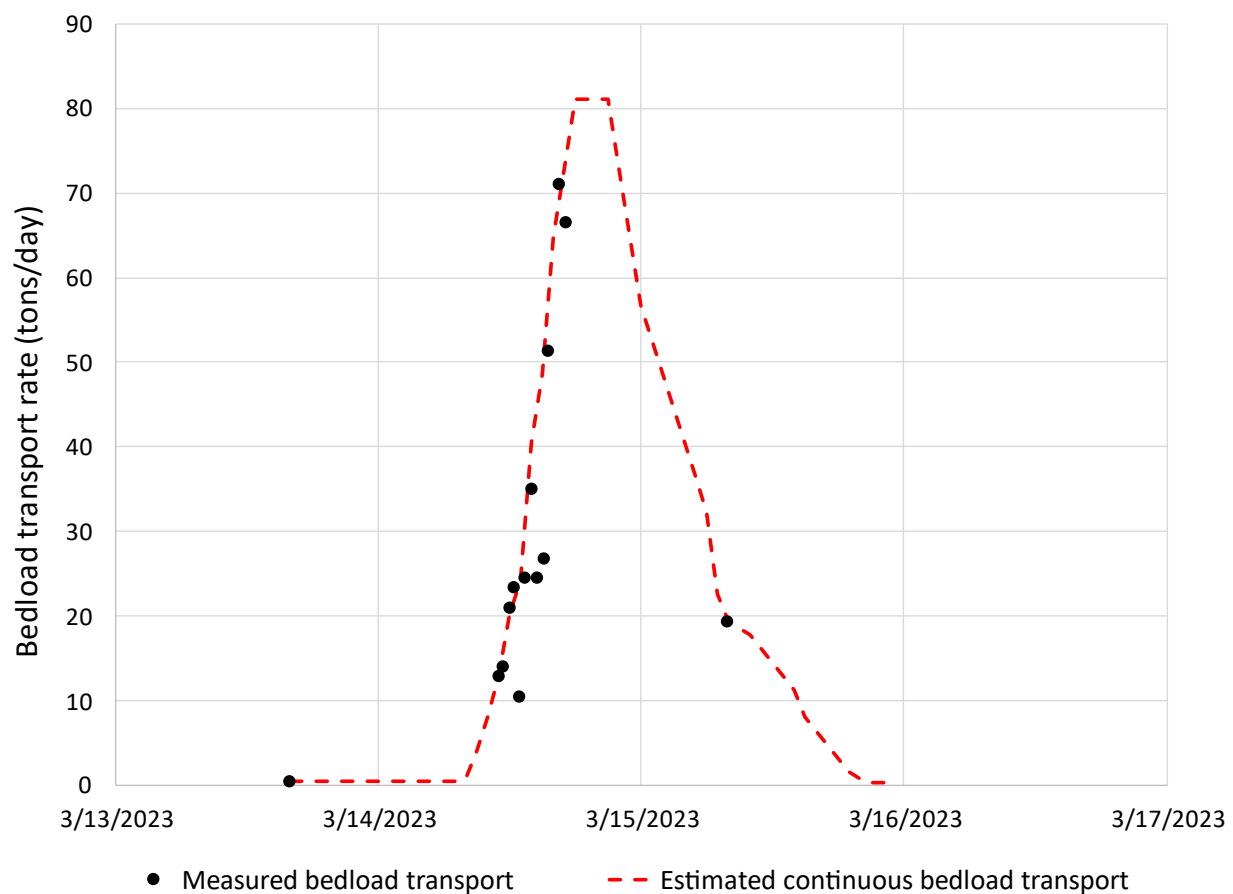


**Figure 18. Index map showing the locations of mapping areas with significant in-channel sand storage.**

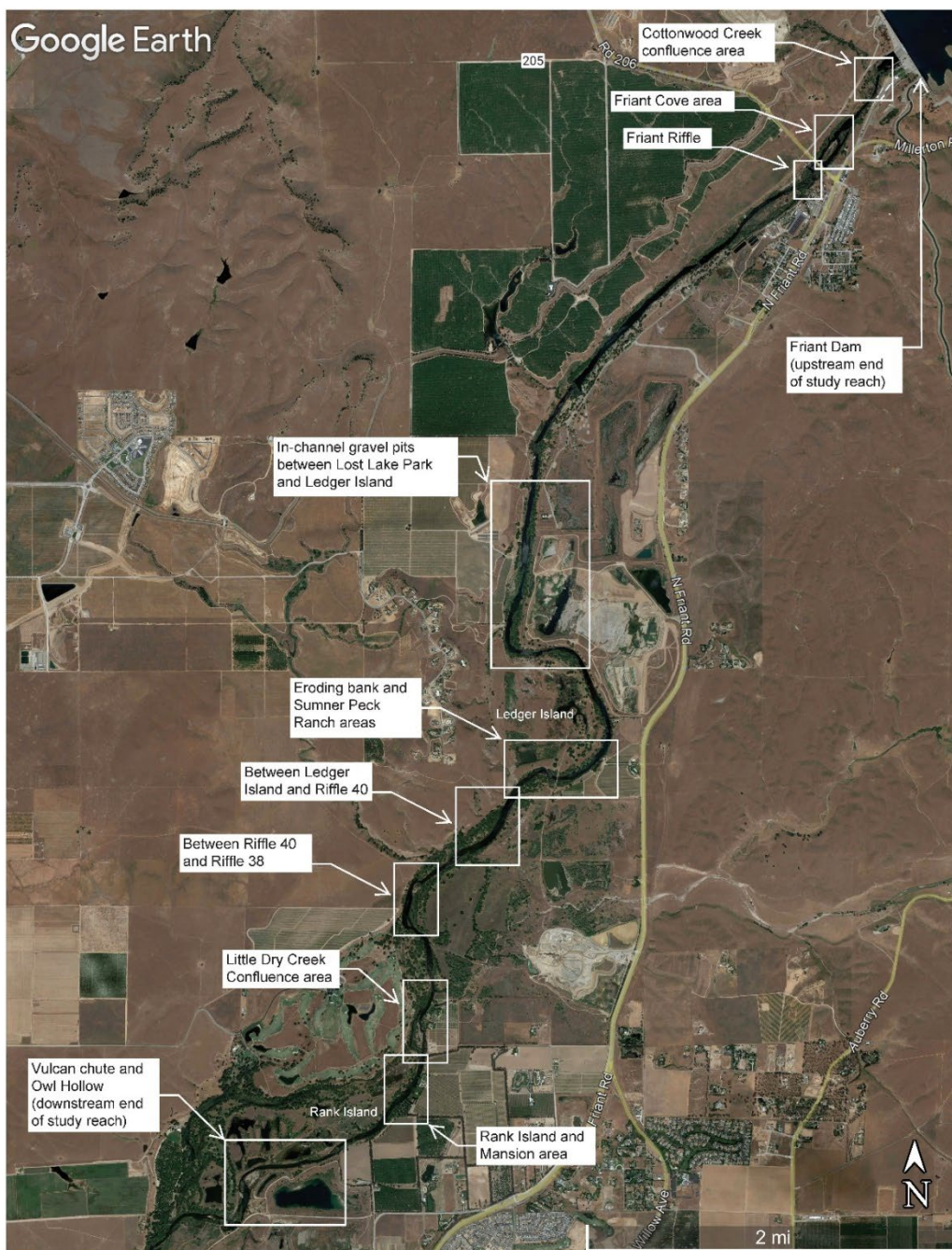


**Figure 19. Study period changes of in-channel sand storage content by site and date.**  
**The three years of data presented below represent dry and wet year conditions. The top panel presents sand storage in tons and the bottom panel presents sand storage in cubic yards. The values correspond with Table 5. Vertical dashed lines correspond to locations of interest in my study reach.**

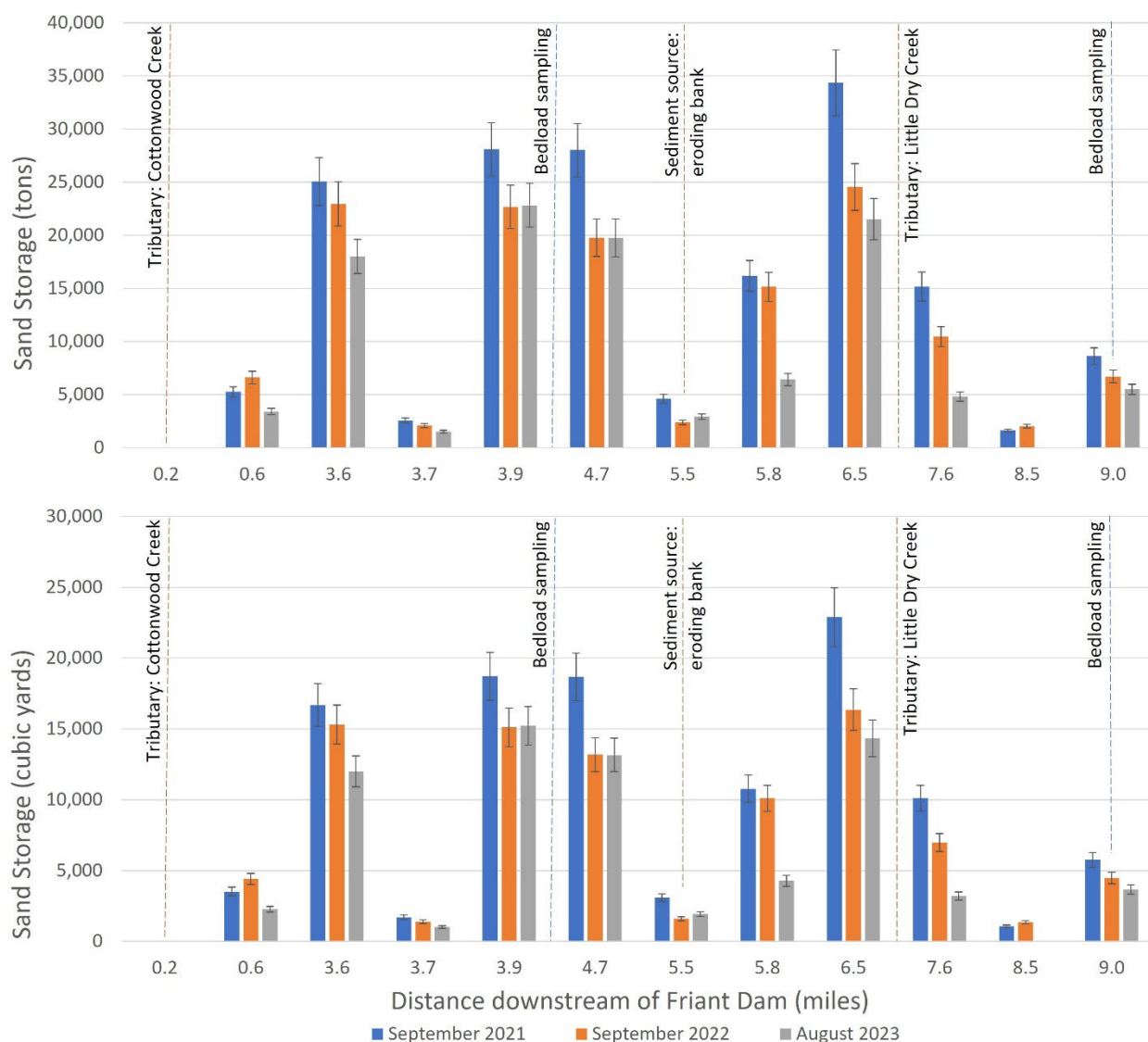


**Figure 20. Sand storage at the confluence of Cottonwood Creek and the San Joaquin River, approximately 1,000 feet downstream of Friant Dam.**



**Figure 21. Bed substrate of the San Joaquin River deep channel downstream of the Cottonwood Creek confluence. Top image shows trace amounts of sand present in 2021.**

**Bottom image shows no sand present in 2023.**

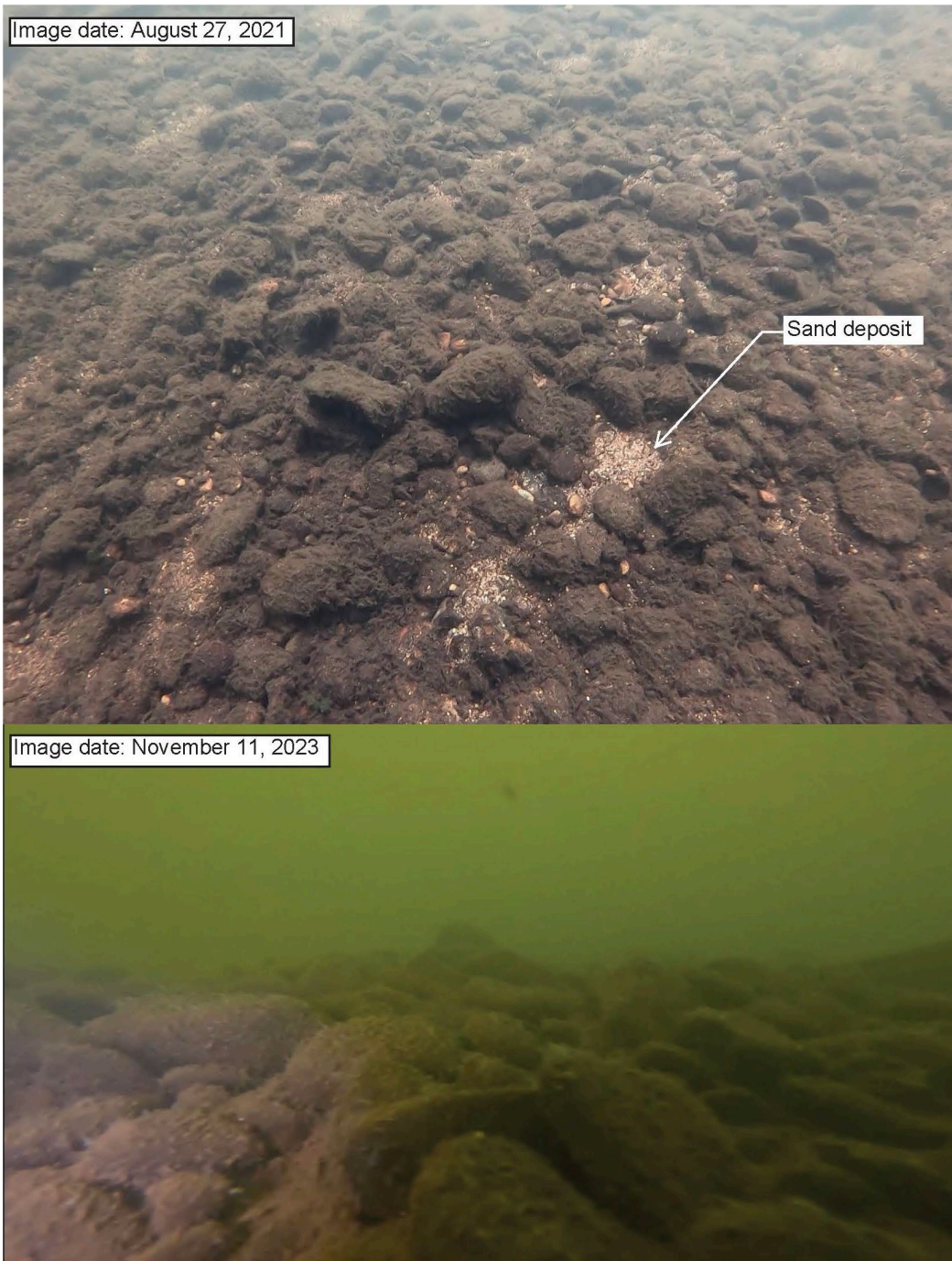


Figure 22. Sand storage at the Friant Cove area.



**Figure 23. Sand storage at the Friant Riffle.**



**Figure 24. Sand storage between Lost Lake Park and Ledger Island.**



**Figure 25. Sand storage at the south end of Ledger Island.**



**Figure 26. Eroding bank at Ledger Island. Top left image shows the bank height relative to the author (6 feet/1.8 meters); the paddle is 5 feet (1.5 meters) long. The top right image shows a fissured block of bank material in a slow calving process; the rod is 2 meters long, graduated in 0.1 meter intervals. The bottom image shows sluff at the base of the eroding bank, pipes (1.5 inch/3.8 cm outside diameter) emanating from the vertical bank face, and multicolored strata indicating the individual lifts this bank was constructed in.**



**Figure 27. Bank edge delineations showing erosion propagation at Ledger Island. The top image shows conditions in 2011 during flood flows and projections of future bank edges in 2021 and 2023. The bottom image shows conditions in 2023 and the previous extents of the bank edge. The bank edge is defined here as the crest at the top of the vertical face. Erosion is propagating toward the abandoned mine pit.**



**Figure 28. Sand storage between Ledger Island and Riffle 40.**

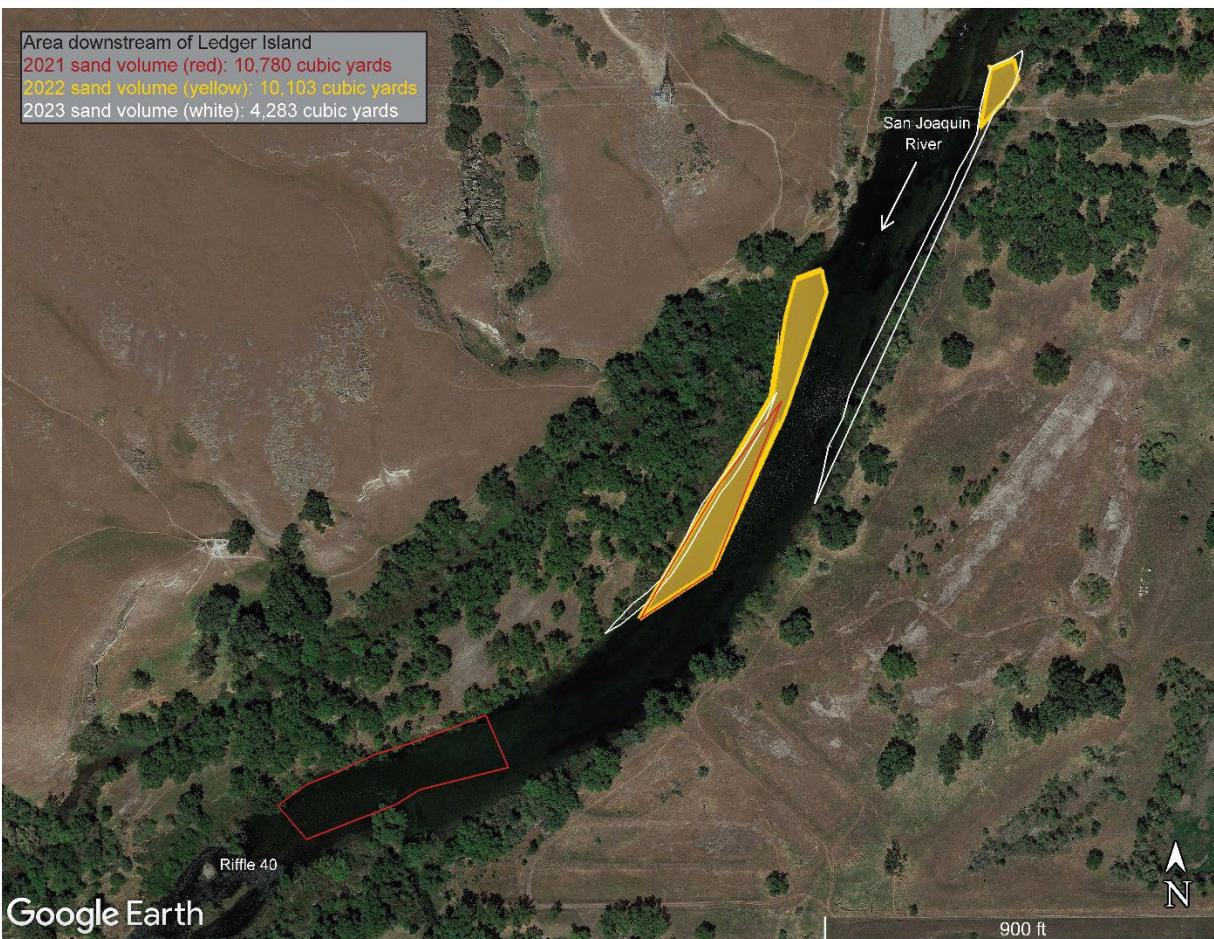


**Figure 29. Sand storage between Riffle 40 and Riffle 38.**



**Figure 30. Sand storage near the confluence of Little Dry Creek and the San Joaquin River.**



**Figure 31. Sand storage at Rank Island near a large mansion.**



**Figure 32. Sand storage at a narrow chute near the Vulcan property and at Owl Hollow.**



**Figure 33. Cumulative grain size distributions of grab samples collected in 2021 and 2023.**

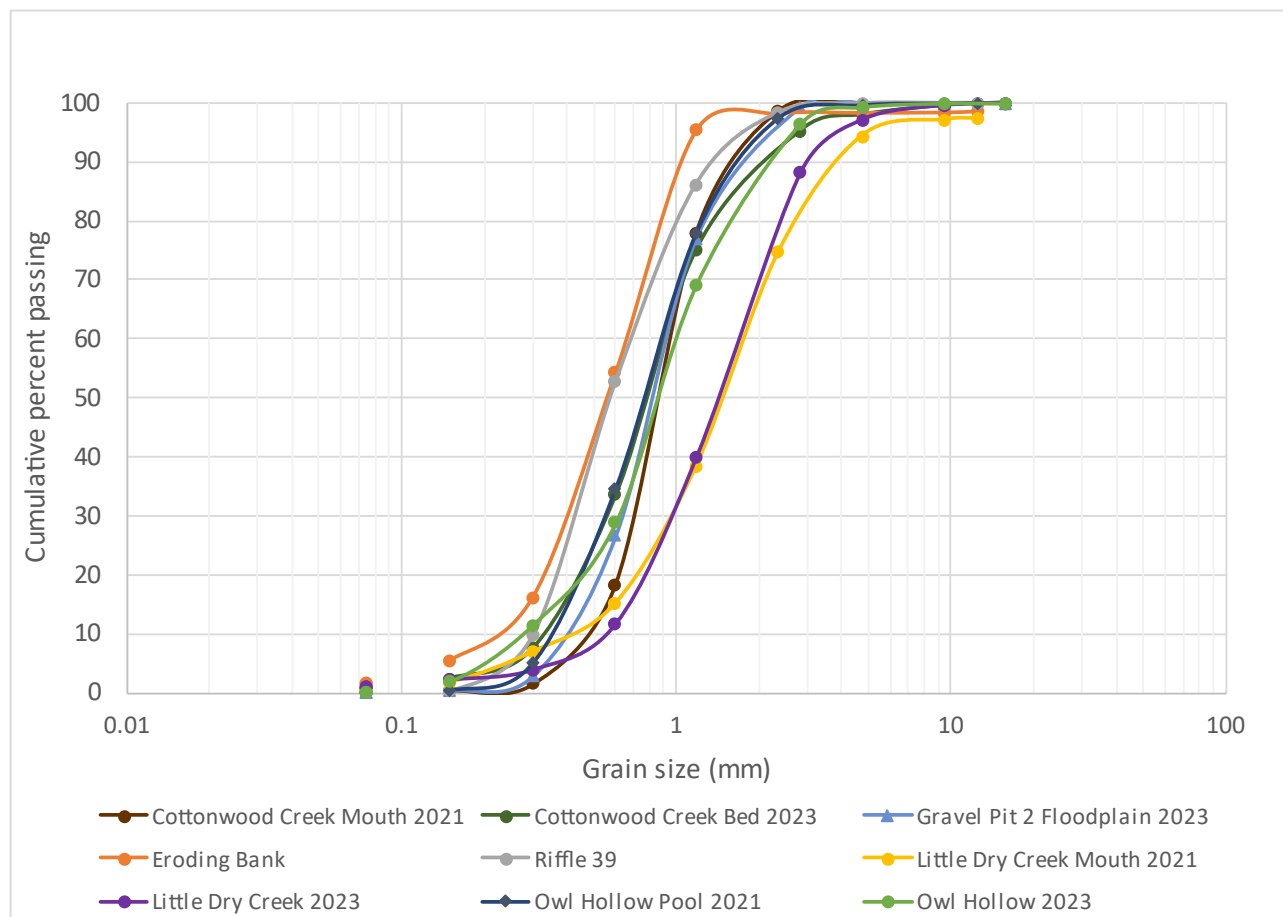


**Table 1. Significant features within the study reach and their distance downstream of Friant Dam.**

<b>Feature or Site</b>	<b>Distance Downstream of Friant Dam (river miles)</b>
Friant Dam, upstream end of study reach	0.0
Cottonwood Creek confluence	0.2
Friant Riffle low-flow bedload sample site	0.81
USGS gaging station 11251000/CDEC SJF gage	1.6
Upstream Ledger Island low-flow bedload sample site	4.07
Ledger Island moderate- and high-flow sample site	4.68
Ledger Island bridge	5.4
Ledger Island bridge low-flow bedload sample site	5.4
Eroding bank at Ledger Island	5.5
Ledger Island downstream low-flow bedload sample site	5.6
Riffle 40 low-flow bedload sample site	6.2
Riffle 38 low-flow bedload sample site	6.83
Little Dry Creek confluence	7.0
Vulcan area low-flow bedload sample site	7.94
Owl Hollow downstream riffle low-to-high flow bedload sample site; end of study reach	8.84

**Table 2. Summary of bedload transport rates sampled at Owl Hollow, Ledger Island, and Cottonwood Creek between March 13 and 17, 2023.**

	Owl Hollow	Ledger Island	Cottonwood Creek
<b>Total Bedload</b>			
Maximum (tons/day)	109.1	10.8	67
Minimum (tons/day)	41.8	1.7	0.1
Mean (tons/day)	77.0	6.9	22.3
Standard Deviation (tons/day)	29.9	3.8	20.3
Maximum grain size diameter (mm)	21	40	24
<b>&gt; 2mm Bedload</b>			
Maximum (tons/day)	14.1	2.4	8.4
Minimum (tons/day)	9.0	0.4	0.0
Mean (tons/day)	12.4	1.8	2.2
Standard Deviation (tons/day)	2.3	0.8	2.5
<b>&lt; 2mm Bedload</b>			
Maximum (tons/day)	95.6	8.7	59.5
Minimum (tons/day)	32.7	1.3	0.1
Mean (tons/day)	64.4	5.1	20.1
Standard Deviation (tons/day)	28.0	3.2	17.9

**Table 3. Ledger Island modeled values for channel shear stress and associated Meyer-Peter Muller bedload transport rates. Observed bedload transport rates are provided for comparison.**

HEC-RAS Cross Section: 761250		Dimensionless Shields values for Qb calcs using MP-M equation								Observed Mean Qb <2 mm (tons/day)	Observed Mean Qb total (tons/day)
Discharge (cfs)	HEC-RAS Channel Shear Stress (N/m <sup>2</sup> )	0.03	0.031	0.032	0.033	0.034	0.035	0.036	0.037		
1,500	0.39	0	0	0	0	0	0	0	0	0	0
6,000	1.14	11	8	6	4	2	0	0	0	5.1*	6.9*
7,000	1.20	17	14	11	8	5	3	2	0	5.1*	6.9*

\* Qb values were observed at approximately 6,400 cfs

**Table 4. Owl Hollow modeled channel shear stress and associated Meyer-Peter Muller bedload transport rates. Observed bedload transport rates are provided for comparison.**

Owl Hollow HEC-RAS Cross Section: 739058		Dimensionless Shields values for Qb calcs using MP-M equation			Observed Mean Qb <2 mm (tons/day)	Observed Mean Qb total (tons/day)
Discharge (cfs)	HEC-RAS Channel Shear Stress (N/m <sup>2</sup> )	0.034 Qb (tons/day)	0.035 Qb (tons/day)	0.047 Qb (tons/day)		
1,500	1.83	173	161	47	0	0
6,000	10.00	8240	8195	7662	64*	77*
7,000	9.30	7316	7273	6760	64*	77*
* Qb values were observed at approximately 6,900 cfs						

**Table 5. Calculated in-channel sand storage along 9-mile study reach between Friant Dam and Owl Hollow. The top section presents values in tons and the bottom section presents values in cubic yards. Values correspond with Figure 19.**

Location	September 2021 Volume (tons)	September 2022 Volume (tons)	August 2023 Volume (tons)	Percent Difference Sept 2021 to Sept 2022	Percent difference Sept 2022 to Aug 2023	Percent difference Sept 2021 to Aug 2023
Cottonwood Ck mouth	11.8	15.6	0.0	32%	-100%	-100%
Friant Cove area	5,277	6,623	3,419	26%	-48%	-35%
Gravel Pit #1	25,052	22,955	18,005	-8%	-22%	-28%
Connecting chute	2,565	2,094	1,517	-18%	-28%	-41%
Gravel Pit #2	28,080	22,674	22,827	-19%	1%	-19%
Sumner Peck Ranch area	28,006	19,770	19,748	-29%	0%	-29%
Eroding Bank (Ledger Island)	4,620	2,383	2,916	-48%	22%	-37%
Ledger Island to Riffle 40	16,169	15,155	6,424	-6%	-58%	-60%
Riffle 39 to Riffle 38	34,344	24,549	21,507	-29%	-12%	-37%
Rank Island/mansion area	15,175	10,462	4,828	-31%	-54%	-68%
Vulcan chute	1,614	2,032	0	26%	-100%	-100%
Owl Hollow pool	8,627	6,715	5,505	-22%	-18%	-36%
<b>Sum along 9-mile reach (tons):</b>	<b>169,540</b>	<b>135,427</b>	<b>106,696</b>	<b>-20%</b>	<b>-21%</b>	<b>-37%</b>

Location	September 2021 Volume (Yrd <sup>3</sup> )	September 2022 Volume (Yrd <sup>3</sup> )	August 2023 Volume (Yrd <sup>3</sup> )	Percent Difference Sept 2021 to Sept 2022	Percent difference Sept 2022 to Aug 2023	Percent difference Sept 2021 to Aug 2023
Cottonwood Ck mouth	7.9	10.4	0.0	32%	-100%	-100%
Friant Cove area	3,518	4,415	2,279	26%	-48%	-35%
Gravel Pit #1	16,701	15,304	12,003	-8%	-22%	-28%
Connecting chute	1,710	1,396	1,011	-18%	-28%	-41%
Gravel Pit #2	18,720	15,116	15,218	-19%	1%	-19%
Sumner Peck Ranch area	18,670	13,180	13,165	-29%	0%	-29%
Eroding Bank (Ledger Island)	3,080	1,589	1,944	-48%	22%	-37%
Ledger Island to Riffle 40	10,780	10,103	4,283	-6%	-58%	-60%
Riffle 39 to Riffle 38	22,896	16,366	14,338	-29%	-12%	-37%
Rank Island/mansion area	10,117	6,975	3,219	-31%	-54%	-68%
Vulcan chute	1,076	1,355	0	26%	-100%	-100%
Owl Hollow pool	5,751	4,477	3,670	-22%	-18%	-36%
<b>Sum along 9-mile reach (Yrd<sup>3</sup>):</b>	<b>113,027</b>	<b>90,285</b>	<b>71,131</b>	<b>-20%</b>	<b>-21%</b>	<b>-37%</b>

## Appendices

## Appendix A: Flood Frequency Analysis

This section provides results from a flood frequency analysis that I conducted. I used the USGS PeakFQ<sup>1</sup> software package with annual peak flow data at the stream gauge San Joaquin River below Friant (SJF, USGS gauge 11251000<sup>2</sup>) between years 1950 and 2023. I conducted this analysis to gain an understanding of the approximate recurrence interval of the flows that were observed throughout my study period to help define “moderate” and “high” flows. I chose a dataset beginning in 1950 because I wanted to include the longest period of record that could reasonably represent the flow regime after the construction of Friant Dam in 1942. By beginning my data set in 1950, a seven-year buffer is provided to pad inconsistencies in dam operations that might have occurred after its recent construction, such as upstream reservoir filling or downstream channel morphology adjustments near the stream gauge. Figure A- 1 shows the annual peak flows for the period of record (1908 – 2023, count = 114 years), which suggests that no major floods occurred between 1942 and 1950 that would have a major impact on the flood frequency curve.

The results of this flood frequency analysis are illustrated in Figure A- 2, a plot generated by the USGS PeakFQ software package. I used a multiple Grubbs-Beck analysis within the software, which identifies Potentially Influential Low Flows (PILFs) that impact the upper end of the flood frequency curve; these low flows were identified by PeakFQ as those at and below 465 cfs, which coincidentally is the peak flow that occurred in 2021, the first year of my study period. PeakFQ identified 26 PILFs out of the 114-year sample, which are identified in Figure A- 2 as hollow circle data points. The reader should keep in mind that as these data points affect the upper end of the frequency curve, it is possible that higher flows have a less-frequency recurrence interval than what is represented, especially those listed in Table A- 1 that represent the measured data and not the Log-Pearson Type III distribution. Because of this uncertainty, *it is imperative that this flood frequency analysis or its results are not used by others beyond the scope of this thesis.* A range of estimated flood frequency values are provided by comparing Figure A- 2 and Table A- 1.

I annotated Figure A- 2 to show the flows (and corresponding recurrence intervals) during my bedload sampling events, which provide the definition of moderate (bankfull) and high flows. Bedload transport sampling at 1,500 cfs in February 2022 fall on the flood frequency curve (Figure A- 2) at approximately the 2-year recurrence interval. Bankfull flows typically recur about 1.5 – 2 years, so this it is reasonable to classify this bedload sampling event as moderate flows at about bankfull flow discharge. It is important to understand that bankfull flow discharges are usually considered over a range of flows, can vary spatially throughout a river, and can vary temporally if there are major changes in hydrologic or sediment supply regimes.

The high flow bedload sampling event indicator line intersects the data in Figure A- 2 near a knick-point just below where the data trend flattens and deviates from the trend line. This implies that dam operations tend to curtail the high flows of most years below about 10,000 cfs.

---

<sup>1</sup> <https://water.usgs.gov/software/PeakFQ/>

<sup>2</sup> [https://nwis.waterdata.usgs.gov/usa/nwis/peak/?site\\_no=11251000](https://nwis.waterdata.usgs.gov/usa/nwis/peak/?site_no=11251000)

The high flow sampling event indicator line intersects the trendline between about the 6-8 year recurrence interval, which seems reasonable for classifying high flows downstream of Friant Dam. Similarly, the 2023 peak flow of 10,400 cfs aligns closely with the Figure A- 2 trendline and has a recurrence interval of 12.5 years as indicated by Table A- 1. While San Francisco State University did not measure bedload transport rates during this peak flow, I performed sand mapping within the study reach to quantify the changes after the flow occurred.

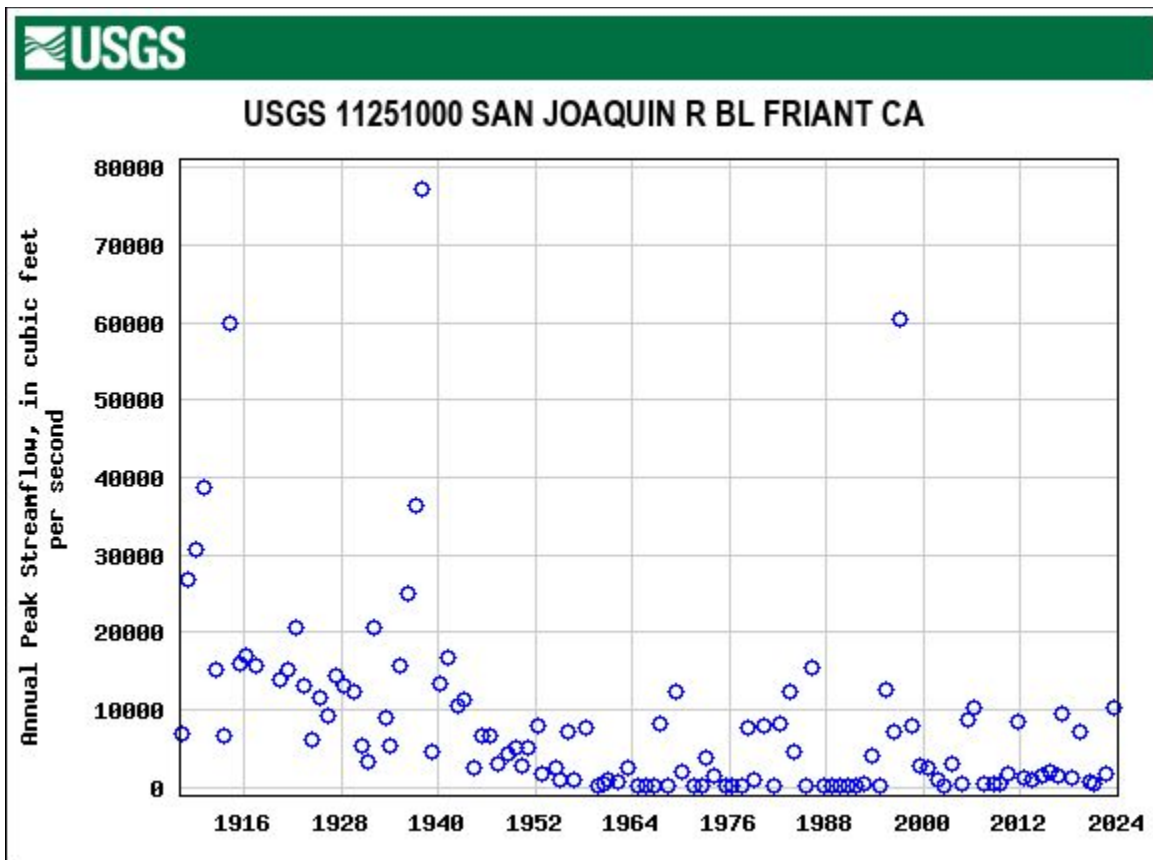


Figure A- 1: annual peak flows on San Joaquin River as measured at the USGS stream gauge 11251000 for the entire period of record (1908 – 2023, count = 114 years).

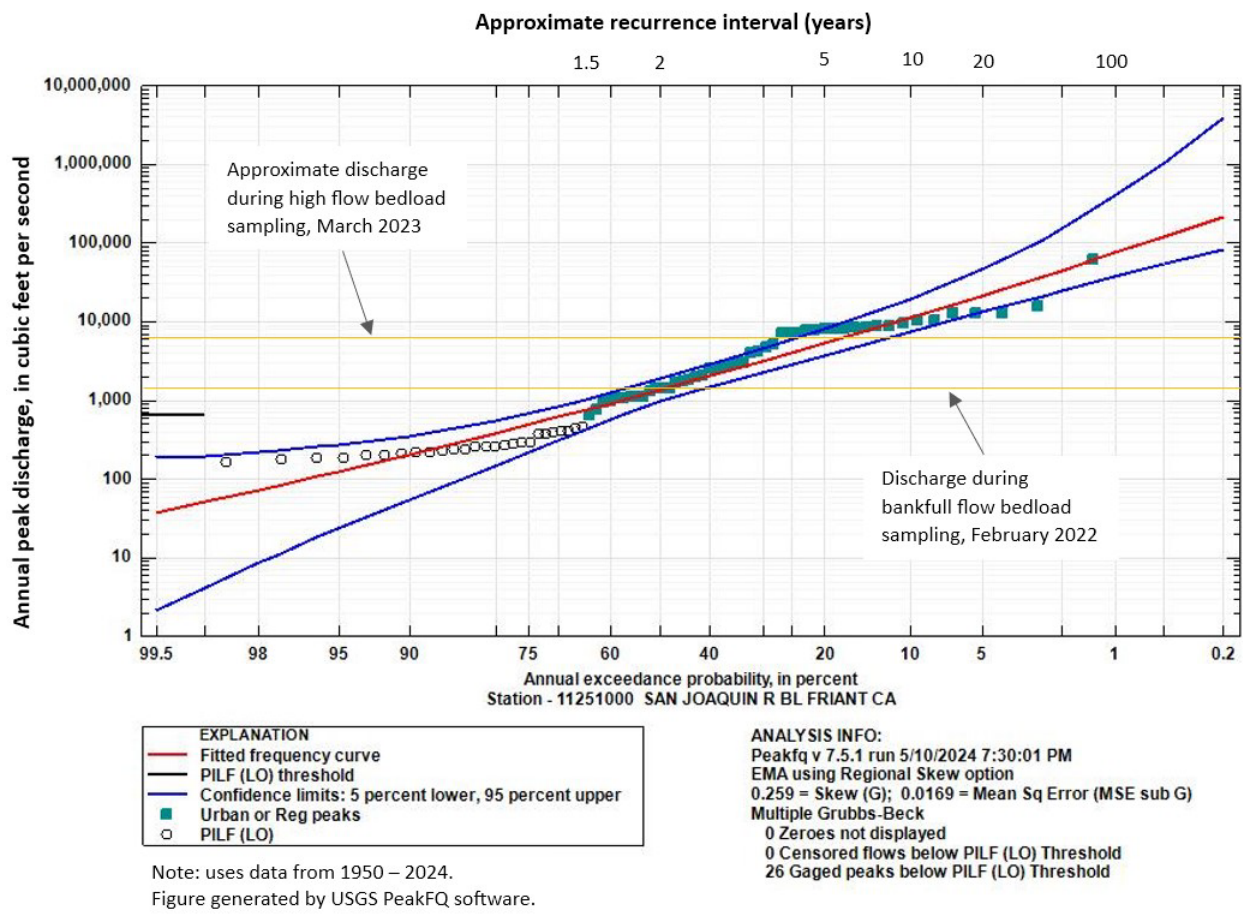


Figure A- 2: Flood frequency analysis plot using post-dam peak flow data from 1950 to 2024 at USGS stream gauge 11251000 San Joaquin River below Friant. The horizontal lines show the flows that were sampled for bedload transport rates by the Bray Rivers Lab at San Francisco State University. The statistics and figure were generated using USGS PeakFQ software.

<b>USGS PeakFQ - EMPIRICAL FREQUENCY CURVES HIRSCH-STEDINGER PLOTTING POSITIONS (1950 - 2024)</b>			
Water Year	Ranked Discharge (cfs)	EMA Estimate of Annual Exceedance Probability	Recurrence Interval (years)
1997	60300	0.0133	75.2
1986	15500	0.0266	37.6
1995	12500	0.04	25.0
1969	12400	0.0533	18.8
1983	12300	0.0666	15.0
2023	10400	0.08	12.5
2006	10300	0.0933	10.7
2017	9580	0.1066	9.4
2005	8750	0.12	8.3
2011	8560	0.1333	7.5
1982	8250	0.1466	6.8
1967	8230	0.16	6.3
1980	8060	0.1733	5.8
1952	8000	0.1866	5.4
1998	7960	0.2	5.0
1978	7640	0.2133	4.7
1958	7570	0.2266	4.4
1956	7120	0.24	4.2
1996	7100	0.2533	3.9
2019	7090	0.2666	3.8
1951	5050	0.28	3.6
1984	4660	0.2933	3.4
1993	4070	0.3067	3.3
1973	3900	0.32	3.1
2003	2940	0.3333	3.0
1999	2800	0.3467	2.9
1950	2750	0.36	2.8
2000	2590	0.3733	2.7
1954	2510	0.3867	2.6
1963	2500	0.4	2.5
2015	2020	0.4133	2.4
1970	1960	0.4267	2.3

2022	1810	0.44	2.3
2010	1740	0.4533	2.2
1953	1640	0.4667	2.1
2016	1410	0.48	2.1
2014	1400	0.4933	2.0
1974	1380	0.5067	2.0
2018	1300	0.52	1.9
2012	1100	0.5333	1.9
1957	1090	0.5467	1.8
2013	1070	0.56	1.8
1979	1040	0.5733	1.7
1955	1030	0.5867	1.7
1961	973	0.6	1.7
2001	911	0.6133	1.6
1962	764	0.6267	1.6
2020	649	0.64	1.6
*2021	465	0.6533	1.5
*2004	437	0.6667	1.5
*1960	407	0.68	1.5
*1992	398	0.6933	1.4
*2009	385	0.7067	1.4
*2008	373	0.72	1.4
*2007	369	0.7334	1.4
*1976	287	0.7467	1.3
*2002	284	0.76	1.3
*1994	273	0.7734	1.3
*1971	270	0.7867	1.3
*1991	260	0.8	1.3
*1959	254	0.8134	1.2
*1990	253	0.8267	1.2
*1977	233	0.84	1.2
*1981	232	0.8534	1.2
*1989	225	0.8667	1.2
*1968	220	0.88	1.1
*1965	215	0.8934	1.1
*1972	208	0.9067	1.1
*1987	196	0.9334	1.1
*1988	196	0.92	1.1
*1964	183	0.9467	1.1

*1975	182	0.96	1.0
*1985	180	0.9734	1.0
*1966	161	0.9867	1.0

\*Denotes potentially  
influencing low flows (PILF,  
LO)

*Table A- 1: Flood frequency analysis results at San Joaquin River Below Friant stream gauge (11251000) using USGS PeakFQ software package for years 1950 to 2024. These results correspond to actual annual peak flows measured and do not represent the Log-Pearson Type-III distribution fitted curve in Figure A- 2. The Estimated Moments Analysis (EMA) method was used. Study period years are highlighted in yellow.*

The following is a print-out of the USGS PeakFQ results from my flood frequency analysis.

```

1
  Program PeakFq          U. S. GEOLOGICAL SURVEY          Seq.002.000
  Version 7.5.1          Annual peak flow frequency analysis      Run Date /
Time                      3/ 4/2024                      05/10/2024
19:27

```

--- PROCESSING OPTIONS ---

```

Plot option              = Graphics device
Basin char output       = None
Print option            = Yes
Debug print             = No
Input peaks listing     = Long
Input peaks format      = WATSTORE peak file

```

Input files used:

```

  peaks (ascii) -
C:\Users\tsher\Downloads\PEAK_1950-2024
  specifications -
C:\Users\tsher\Downloads\PKFQWPSF.TMP

```

Output file(s):

```

  main - C:\Users\tsher\Downloads\PEAK_1950-
2024.PRT

```

\*\*\* User responsible for assessment and interpretation of the following analysis \*\*\*

1

```

  Program PeakFq          U. S. GEOLOGICAL SURVEY          Seq.001.001
  Version 7.5.1          Annual peak flow frequency analysis      Run Date /
Time                      3/ 4/2024                      05/10/2024
19:27

```

Station - 11251000 SAN JOAQUIN R BL FRIANT CA

TABLE 1 - INPUT DATA SUMMARY

Number of peaks in record	=	74
Peaks not used in analysis	=	0
Gaged peaks in analysis	=	74
Historic peaks in analysis	=	0
Beginning Year	=	1950

```

Ending Year = 2023
Historical Period Length = 74
Skew option = REGIONAL
Regional skew = 0.259
    Standard error = 0.130
    Mean Square error = 0.017
Gage base discharge = 0.0
User supplied high outlier threshold = --
User supplied PILF (LO) criterion = --
Plotting position parameter = 0.00
Type of analysis = EMA
PILF (LO) Test Method = MGBT
Perceptible Ranges:
    Start Year End Year Lower Bound Upper Bound
        1950 2023 0.0 INF
DEFAULT
Interval Data = None Specified

```

## TABLE 2 - DIAGNOSTIC MESSAGE AND PILF RESULTS

```

1 *WCF151I-17B WEIGHTED SKEW REPLACED BY USER OPTION. 0.245 0.259
WCF002J-CALCS COMPLETED. RETURN CODE = 2
EMA002W-CONFIDENCE INTERVALS ARE NOT EXACT IF HISTORIC PERIOD > 0

```

## MULTIPLE GRUBBS-BECK TEST RESULTS

```

MULTIPLE GRUBBS-BECK PILF THRESHOLD 649.0
NUMBER OF PILFS IDENTIFIED 26
CLASSIFICATION OF PILFS:
    NUMBER OF ZERO FLOWS 0
    NUMBER OF CENSORED FLOWS 0
    NUMBER OF GAGED PEAKS 26
    GAGED PEAKS AND CORRESPONDING P-VALUES
        161.0 (0.9999)
        180.0 (0.9998)
        182.0 (0.9988)
        183.0 (0.9942)
        196.0 (0.9904)
        196.0 (0.9688)
        208.0 (0.9534)
        215.0 (0.9174)
        220.0 (0.8549)
        225.0 (0.7673)
        232.0 (0.6713)

```

233.0	(0.5136)
253.0	(0.4962)
254.0	(0.3392)
260.0	(0.2313)
270.0	(0.1605)
273.0	(0.0848)
284.0	(0.0508)
287.0	(0.0212)
369.0	(0.0868)
373.0	(0.0420)
385.0	(0.0223)
398.0	(0.0111)
407.0	(0.0044)
437.0	(0.0028)
465.0	(0.0016)

## Kendall's Tau Parameters

	TAU	P-VALUE	MEDIAN SLOPE	No. of PEAKS
GAGED PEAKS	0.093	0.245	4.600	74

1

Program PeakFq	U. S. GEOLOGICAL SURVEY	Seq.001.002
Version 7.5.1	Annual peak flow frequency analysis	Run Date /
Time		
3/ 4/2024		05/10/2024
19:27		

Station - 11251000 SAN JOAQUIN R BL FRIANT CA

TABLE 3 - ANNUAL FREQUENCY CURVE PARAMETERS -- LOG-PEARSON TYPE III

	LOGARITHMIC		
	MEAN	STANDARD DEVIATION	SKEW
EMA WITHOUT REG SKEW	3.0345	0.8877	-0.853
EMA WITH REG SKEW	3.1545	0.6802	0.259
EMA ESTIMATE OF MSE OF SKEW WITHOUT REG SKEW			0.1300
EMA ESTIMATE OF MSE OF SKEW W/GAGED PEAKS ONLY (AT-SITE)			0.1300

TABLE 4 - ANNUAL FREQUENCY CURVE -- DISCHARGES AT SELECTED EXCEEDANCE PROBABILITIES

ANNUAL EXCEEDANCE PROBABILITY	<- EMA ESTIMATE ->		<- FOR EMA ESTIMATE WITH REG SKEW -> LOG VARIANCE OF EST.	<-CONFIDENCE LIMITS->	
	WITH REG SKEW	WITHOUT REG SKEW		5.0% LOWER	95.0% UPPER
0.9950	37.0	1.1	0.2732	2.1	180.9
0.9900	50.4	2.7	0.2009	4.1	194.7
0.9500	122.5	24.7	0.0756	23.2	268.7
0.9000	201.3	70.3	0.0409	53.6	348.6
0.8000	376.0	222.4	0.0183	143.2	534.7
0.6667	689.4	584.5	0.0094	377.6	922.1
0.5000	1334.	1443.	0.0070	952.4	1857.0
0.4292	1766.	2033.	0.0071	1295.0	2503.0
0.2000	5208.	6219.	0.0100	3662.0	7989.0
0.1000	11040.	11500.	0.0148	7292.0	19180.0
0.0400	25330.	19990.	0.0265	15160.0	59760.0
0.0200	44040.	27120.	0.0412	24140.0	147900.0
0.0100	73270.	34540.	0.0620	36360.0	383000.0
0.0050	117800.	42030.	0.0896	52450.0	1028000.0
0.0020	212200.	51720.	0.1374	80850.0	3863000.0

\*Note: If Station Skew option is selected then EMA ESTIMATE WITH REG SKEW will

display values for and be equal to EMA ESTIMATE WITHOUT REG SKEW.

1

Program PeakFq	U. S. GEOLOGICAL SURVEY	Seq.001.003
Version 7.5.1	Annual peak flow frequency analysis	Run Date /
Time		
3/ 4/2024		05/10/2024
19:27		

Station - 11251000 SAN JOAQUIN R BL FRIANT CA

TABLE 5 - INPUT DATA LISTING

WATER UPPER BOUND)	PEAK VALUE	PEAKFQ CODES	FLOW INTERVALS (WHERE LOWER BOUND NOT = LOWER BOUND UPPER BOUND REMARKS		
YEAR					
1950	2750.0	K			
1951	5050.0	K			
1952	8000.0	K			

1953	1640.0	K
1954	2510.0	K
1955	1030.0	K
1956	7120.0	K
1957	1090.0	K
1958	7570.0	K
1959	254.0	K
1960	407.0	K
1961	973.0	K
1962	764.0	K
1963	2500.0	K
1964	183.0	K
1965	215.0	K
1966	161.0	K
1967	8230.0	K
1968	220.0	K
1969	12400.0	K
1970	1960.0	K
1971	270.0	K
1972	208.0	K
1973	3900.0	K
1974	1380.0	K
1975	182.0	K
1976	287.0	K
1977	233.0	K
1978	7640.0	K
1979	1040.0	K
1980	8060.0	K
1981	232.0	K
1982	8250.0	K
1983	12300.0	K
1984	4660.0	K
1985	180.0	K
1986	15500.0	K
1987	196.0	K
1988	196.0	K
1989	225.0	K
1990	253.0	K
1991	260.0	K
1992	398.0	K
1993	4070.0	K
1994	273.0	K
1995	12500.0	K
1996	7100.0	K
1997	60300.0	K
1998	7960.0	K
1999	2800.0	K
2000	2590.0	K
2001	911.0	K
2002	284.0	K

2003	2940.0	K
2004	437.0	K
2005	8750.0	K
2006	10300.0	K
2007	369.0	K
2008	373.0	K
2009	385.0	K
2010	1740.0	K
2011	8560.0	K
2012	1100.0	K
2013	1070.0	K
2014	1400.0	K
2015	2020.0	K
2016	1410.0	K
2017	9580.0	K
2018	1300.0	K
2019	7090.0	K
2020	649.0	K
2021	465.0	K
2022	1810.0	K
2023	10400.0	K

Explanation of peak discharge qualification codes

PeakFQ CODE	NWIS CODE	DEFINITION
D	3	Dam failure, non-recurrent flow anomaly
G	8	Discharge greater than stated value
X	3+8	Both of the above
L	4	Discharge less than stated value
K	6 OR C	Known effect of regulation or urbanization
O	0	Opportunistic peak
H	7	Historic peak
- Minus-flagged discharge -- Not used in computation -8888.0 -- No discharge value given		
- Minus-flagged water year -- Historic peak used in computation		

1

Program PeakFq	U. S. GEOLOGICAL SURVEY	Seq.001.004
Version 7.5.1	Annual peak flow frequency analysis	Run Date /
Time		
3/ 4/2024		05/10/2024
19:27		

Station - 11251000 SAN JOAQUIN R BL FRIANT CA

TABLE 6 - EMPIRICAL FREQUENCY CURVES -- HIRSCH-STEDINGER PLOTTING POSITIONS

WATER UPPER BOUND)	RANKED DISCHARGE	EMA ESTIMATE	FLOW INTERVALS (WHERE LOWER BOUND NOT = UPPER BOUND)	
YEAR			LOWER BOUND	UPPER BOUND
1997	60300.0	0.0133		
1986	15500.0	0.0266		
1995	12500.0	0.0400		
1969	12400.0	0.0533		
1983	12300.0	0.0666		
2023	10400.0	0.0800		
2006	10300.0	0.0933		
2017	9580.0	0.1066		
2005	8750.0	0.1200		
2011	8560.0	0.1333		
1982	8250.0	0.1466		
1967	8230.0	0.1600		
1980	8060.0	0.1733		
1952	8000.0	0.1866		
1998	7960.0	0.2000		
1978	7640.0	0.2133		
1958	7570.0	0.2266		
1956	7120.0	0.2400		
1996	7100.0	0.2533		
2019	7090.0	0.2666		
1951	5050.0	0.2800		
1984	4660.0	0.2933		
1993	4070.0	0.3067		
1973	3900.0	0.3200		
2003	2940.0	0.3333		
1999	2800.0	0.3467		
1950	2750.0	0.3600		
2000	2590.0	0.3733		
1954	2510.0	0.3867		
1963	2500.0	0.4000		
2015	2020.0	0.4133		
1970	1960.0	0.4267		
2022	1810.0	0.4400		
2010	1740.0	0.4533		
1953	1640.0	0.4667		
2016	1410.0	0.4800		
2014	1400.0	0.4933		
1974	1380.0	0.5067		
2018	1300.0	0.5200		
2012	1100.0	0.5333		

1957	1090.0	0.5467
2013	1070.0	0.5600
1979	1040.0	0.5733
1955	1030.0	0.5867
1961	973.0	0.6000
2001	911.0	0.6133
1962	764.0	0.6267
2020	649.0	0.6400
* 2021	465.0	0.6533
* 2004	437.0	0.6667
* 1960	407.0	0.6800
* 1992	398.0	0.6933
* 2009	385.0	0.7067
* 2008	373.0	0.7200
* 2007	369.0	0.7334
* 1976	287.0	0.7467
* 2002	284.0	0.7600
* 1994	273.0	0.7734
* 1971	270.0	0.7867
* 1991	260.0	0.8000
* 1959	254.0	0.8134
* 1990	253.0	0.8267
* 1977	233.0	0.8400
* 1981	232.0	0.8534
* 1989	225.0	0.8667
* 1968	220.0	0.8800
* 1965	215.0	0.8934
* 1972	208.0	0.9067
* 1987	196.0	0.9334
* 1988	196.0	0.9200
* 1964	183.0	0.9467
* 1975	182.0	0.9600
* 1985	180.0	0.9734
* 1966	161.0	0.9867

\* DENOTES PILF (LO)

1

Program PeakFq	U. S. GEOLOGICAL SURVEY	Seq.001.005
Version 7.5.1	Annual peak flow frequency analysis	Run Date /
Time		
3/ 4/2024		05/10/2024
19:27		

Station - 11251000 SAN JOAQUIN R BL FRIANT CA

TABLE 7 - EMA REPRESENTATION OF DATA

```

<----- USER-ENTERED -----
><----- FINAL ----->
  WATER <----- OBSERVED -----><----- EMA -----><- PERCEPTIBLE RANGES -
><- PERCEPTIBLE RANGES ->
  YEAR      Q_LOWER    Q_UPPER    Q_LOWER    Q_UPPER    LOWER
UPPER      LOWER        UPPER
  1950      2750.0      2750.0      2750.0      2750.0      0.0      INF
649.0      INF
  1951      5050.0      5050.0      5050.0      5050.0      0.0      INF
649.0      INF
  1952      8000.0      8000.0      8000.0      8000.0      0.0      INF
649.0      INF
  1953      1640.0      1640.0      1640.0      1640.0      0.0      INF
649.0      INF
  1954      2510.0      2510.0      2510.0      2510.0      0.0      INF
649.0      INF
  1955      1030.0      1030.0      1030.0      1030.0      0.0      INF
649.0      INF
  1956      7120.0      7120.0      7120.0      7120.0      0.0      INF
649.0      INF
  1957      1090.0      1090.0      1090.0      1090.0      0.0      INF
649.0      INF
  1958      7570.0      7570.0      7570.0      7570.0      0.0      INF
649.0      INF
  1959      254.0       254.0       0.0         649.0       0.0      INF
649.0      INF
  1960      407.0       407.0       0.0         649.0       0.0      INF
649.0      INF
  1961      973.0       973.0       973.0       973.0       0.0      INF
649.0      INF
  1962      764.0       764.0       764.0       764.0       0.0      INF
649.0      INF
  1963      2500.0      2500.0      2500.0      2500.0      0.0      INF
649.0      INF
  1964      183.0       183.0       0.0         649.0       0.0      INF
649.0      INF
  1965      215.0       215.0       0.0         649.0       0.0      INF
649.0      INF
  1966      161.0       161.0       0.0         649.0       0.0      INF
649.0      INF
  1967      8230.0      8230.0      8230.0      8230.0      0.0      INF
649.0      INF
  1968      220.0       220.0       0.0         649.0       0.0      INF
649.0      INF
  1969      12400.0     12400.0     12400.0     12400.0     0.0      INF
649.0      INF
  1970      1960.0      1960.0      1960.0      1960.0      0.0      INF
649.0      INF

```

1971	270.0	270.0	0.0	649.0	0.0	INF
649.0	INF					
1972	208.0	208.0	0.0	649.0	0.0	INF
649.0	INF					
1973	3900.0	3900.0	3900.0	3900.0	0.0	INF
649.0	INF					
1974	1380.0	1380.0	1380.0	1380.0	0.0	INF
649.0	INF					
1975	182.0	182.0	0.0	649.0	0.0	INF
649.0	INF					
1976	287.0	287.0	0.0	649.0	0.0	INF
649.0	INF					
1977	233.0	233.0	0.0	649.0	0.0	INF
649.0	INF					
1978	7640.0	7640.0	7640.0	7640.0	0.0	INF
649.0	INF					
1979	1040.0	1040.0	1040.0	1040.0	0.0	INF
649.0	INF					
1980	8060.0	8060.0	8060.0	8060.0	0.0	INF
649.0	INF					
1981	232.0	232.0	0.0	649.0	0.0	INF
649.0	INF					
1982	8250.0	8250.0	8250.0	8250.0	0.0	INF
649.0	INF					
1983	12300.0	12300.0	12300.0	12300.0	0.0	INF
649.0	INF					
1984	4660.0	4660.0	4660.0	4660.0	0.0	INF
649.0	INF					
1985	180.0	180.0	0.0	649.0	0.0	INF
649.0	INF					
1986	15500.0	15500.0	15500.0	15500.0	0.0	INF
649.0	INF					
1987	196.0	196.0	0.0	649.0	0.0	INF
649.0	INF					
1988	196.0	196.0	0.0	649.0	0.0	INF
649.0	INF					
1989	225.0	225.0	0.0	649.0	0.0	INF
649.0	INF					
1990	253.0	253.0	0.0	649.0	0.0	INF
649.0	INF					
1991	260.0	260.0	0.0	649.0	0.0	INF
649.0	INF					
1992	398.0	398.0	0.0	649.0	0.0	INF
649.0	INF					
1993	4070.0	4070.0	4070.0	4070.0	0.0	INF
649.0	INF					
1994	273.0	273.0	0.0	649.0	0.0	INF
649.0	INF					
1995	12500.0	12500.0	12500.0	12500.0	0.0	INF
649.0	INF					

1996	7100.0	7100.0	7100.0	7100.0	0.0	INF
649.0	INF					
1997	60300.0	60300.0	60300.0	60300.0	0.0	INF
649.0	INF					
1998	7960.0	7960.0	7960.0	7960.0	0.0	INF
649.0	INF					
1999	2800.0	2800.0	2800.0	2800.0	0.0	INF
649.0	INF					
2000	2590.0	2590.0	2590.0	2590.0	0.0	INF
649.0	INF					
2001	911.0	911.0	911.0	911.0	0.0	INF
649.0	INF					
2002	284.0	284.0	0.0	649.0	0.0	INF
649.0	INF					
2003	2940.0	2940.0	2940.0	2940.0	0.0	INF
649.0	INF					
2004	437.0	437.0	0.0	649.0	0.0	INF
649.0	INF					
2005	8750.0	8750.0	8750.0	8750.0	0.0	INF
649.0	INF					
2006	10300.0	10300.0	10300.0	10300.0	0.0	INF
649.0	INF					
2007	369.0	369.0	0.0	649.0	0.0	INF
649.0	INF					
2008	373.0	373.0	0.0	649.0	0.0	INF
649.0	INF					
2009	385.0	385.0	0.0	649.0	0.0	INF
649.0	INF					
2010	1740.0	1740.0	1740.0	1740.0	0.0	INF
649.0	INF					
2011	8560.0	8560.0	8560.0	8560.0	0.0	INF
649.0	INF					
2012	1100.0	1100.0	1100.0	1100.0	0.0	INF
649.0	INF					
2013	1070.0	1070.0	1070.0	1070.0	0.0	INF
649.0	INF					
2014	1400.0	1400.0	1400.0	1400.0	0.0	INF
649.0	INF					
2015	2020.0	2020.0	2020.0	2020.0	0.0	INF
649.0	INF					
2016	1410.0	1410.0	1410.0	1410.0	0.0	INF
649.0	INF					
2017	9580.0	9580.0	9580.0	9580.0	0.0	INF
649.0	INF					
2018	1300.0	1300.0	1300.0	1300.0	0.0	INF
649.0	INF					
2019	7090.0	7090.0	7090.0	7090.0	0.0	INF
649.0	INF					
2020	649.0	649.0	649.0	649.0	0.0	INF
649.0	INF					

2021	465.0	465.0	0.0	649.0	0.0	INF
649.0	INF					
2022	1810.0	1810.0	1810.0	1810.0	0.0	INF
649.0	INF					
2023	10400.0	10400.0	10400.0	10400.0	0.0	INF
649.0	INF					

1

End PeakFQ analysis.

Stations processed :	1
Number of errors :	0
Stations skipped :	0
Station years :	74

Data records may have been ignored for the stations listed below.  
 (Card type must be Y, Z, N, H, I, 2, 3, 4, or \*.)  
 (2, 4, and \* records are ignored.)

For the station below, the following records were ignored:

FINISHED PROCESSING STATION: 11251000 USGS SAN JOAQUIN R BL FRIANT  
 CA

For the station below, the following records were ignored:

FINISHED PROCESSING STATION:

## References

- Andrews, E. D. (1983). "Entrainment of gravel from naturally sorted riverbed material." Geological Society of America Bulletin 94: 1225-1231.
- Associates, G. M. (2011). San Joaquin River Bedload Sampling WY 2011: 10.
- Bjornn, T. C. (1969). Embryo survival and emergence studies. B. Idaho Department of Fish and Game, Idaho.
- Bjornn, T. C. and D. W. Reiser (1991). "Habitat Requirements of Salmonids in Streams." American Fisheries Society Special Publication 19;83-138;1991: 56.
- Bray, E. N. and T. Dunne (2017). "Observations of bedload transport in a gravel bed river during high flow using fiber-optic DTS methods." Earth Surface Processes and Landforms 42: 15.
- Bunte, K. and S. R. Abt (2009). Transport relationships between bedload traps and a 3-inch Helley-Smith sampler in coarse gravel-bed streams and development of adjustment functions. 3909 Halls Ferry Rd. Vicksburg, MS 39180, Federal Interagency Sedimentation Project.
- Bunte, K., K. W. Swingle, R. Ettema, S. R. Abt and D. A. Cenderelli (2019). Bedload Traps and Helley-Smith Sampler Collect Different Rates and Particle Sizes of Gravel Bedload. 11th Federal Interagency Sedimentation and 6th Hydrologic Modeling Conference. Reno, NV. USA: 15.
- Cain, J. R., Jr. (1997). Hydrologic and Geomorphic Changes to the San Joaquin River between Friant Dam and Gravely Ford and Implications for Restoration of Chinook Salmon (Oncorhynchus tshawytscha). Master of Landscape Architecture, University of California, Berkeley.
- Curran, J. C. and P. R. Wilcock (2005). "Effect of Sand Supply on Transport Rates in a Gravel-Bed Channel." Hydraulic Engineering 131(11): 961-967.
- Harrelson, C. C., C. L. Rawlins and J. P. Potyondy (1994). Stream Channel Reference Sites: An Illustrated Guide to Field Technique. U. S. D. o. A. F. Service: 67.
- Haight, D. R. W., M. D. Marinuea, J. T. Minear, S. A. Wright and J. V. Lopez (2023). Sediment transport in two tributaries to the San Joaquin River immediately Below Friant Dam - Cottonwood Creek and Littel Dry Creek, California. U.S. Geological Survey Scientific Investigations Report 2023-5023. U.S. Geological Survey, Reston, Virginia: 2023, U.S. Geological Survey: 34.
- Hilton, S. and T. E. Lisle (1993). Measuring the Fraction of Pool Volume Filled with Fine Sediment. U. S. D. o. Agriculture. Pacific Southwest Research Station: 12.
- Kondolf, G. M. and P. R. Wilcock (1996). "The flushing flow problem: defining and evaluating objectives." Water Resources Research 32(8): 2589-2599.
- Marinuea, M. D., S. A. Wright and J. V. Lopez (2016). Sediment Transport in Tributary Creeks of the San Joaquin River. 2016 San Joaquin River Restoration Program Science Meeting. Fresno, California.
- Marinuea, M. D., S. A. Wright and J. T. Minear (2015). Sediment-transport monitoring using hydrophones on the San Joaquin River and tributaries. 2015 San Joaquin River Restoration Program Science Meeting. Los Banos, California.

- McBain & Trush, I. (2002). San Joaquin River Restoration Study Background Report.
- Meyer-Peter, E. and R. Muller (1948). Formulas for bed-load transport. 2nd Congress International Association for Hydraulic Research, Stockholm, Sweden.
- Meyers, M. A. (2021). Gravel Mobility Measurements at San Joaquin River Chinook Salmon Spawning Riffles: An Overview of Gravel-Cobble Tracer Monitoring and Force Gauge Surveys. C. D. o. W. Resources: 91.
- Milhous, R. T. (1994). Sediment Balance and Flushing Flow Analysis: Trinity River Case Study. Hydrology Days, Colorado State University Fort Collins, Colorado, Hydrology Days Publications 57 Selby Lane, Atherton, California 94027-3926 USA.
- Nelson, S. M. and G. K. Reed (2011). Observations on the hyporheic environment along the San Joaquin River below Friant Dam. U. S. D. o. t. I. B. o. R. D. Colorado: 57.
- Program, S. J. R. R. (2017). Fisheries Framework: Spring-run and Fall-run Chinook Salmon: 107.
- Reclamation (2014). "Sediment Budget Analysis of the San Joaquin River for Water Years 2010 through 2012." Prepared for San Joaquin River Restoration Program, Mid-Pacific Region US Bureau of Reclamation, Technical Service Center, Denver, CO.(SRH-2015-18).
- Resources, C. D. o. W. (2010). San Joaquin River Riffle Particle Size Composition Survey Interim Report River Miles 247 - 267: 74.
- Resources, C. D. o. W. (2019). Artificial redd study: the effect of sand accumulation on incubation habitat quality.
- Shields, I. A. (1936). Application of Similarity Principles and Turbulence Research to Bed-Load Movement. Pasadena, CA, California Institute of Technology. No. 167: 47.
- Survey, U. S. G. (2008). "Scientific Investigations Report 2008-5093." from <https://pubs.usgs.gov/sir/2008/5093/table7.html>.
- Survey, U. S. G. (2019). "The StreamStats program, online at <https://streamstats.usgs.gov/ss/>." Retrieved January 2, 2024.
- Tetra Tech, I. (2012). DRAFT San Joaquin River: Evaluation of Sand Supply, Storage, and Transport in Reaches 1A and 1B, Prepared for the California Department of Water Resources: 72.
- Tetra Tech, I. (2018). DRAFT San Joaquin River 2014 and 2017 Sediment-Transport Sampling, Prepared for the California Department of Water Resources: 73.
- Tetra Tech, I. (2018). DRAFT San Joaquin River Reach 1A Sand Study, Prepared for the California Department of Water Resources: 41.
- Transportation, D. o. (2010). Method of Tests for Sieve Analysis of Fine and Coarse Aggregates: California Test 202. D. o. E. Services: 21.
- Wilcock, P., J. Pitlick and Y. Cui (2009). Sediment transport primer: estimating bed-material transport in gravel-bed rivers: 78.
- Willis, C. M. and G. B. Griggs (2003). "Reductions in Fluvial Sediment Discharge by Coastal Dams in California and Implications for Beach Sustainability." The Journal of Geology 111:167-182.

Kristin Bunte and Steven R. Abt. Transport relationships between bedload traps and a 3-inch Helley-Smith Sampler in coarse gravel-bed streams and development of adjustment functions. Engineering Research Center. Colorado State University, Fort Collins, CO. December 2009.